SISSA
Scuola
Internazionale
Superiore di
Studi Avanzati

Physics Area - PhD course in
Theoretical Particle Physics

Stochastic Minimization in the Conformal Bootstrap

Candidate:
Uriel Adrian
Luviano Valenzuela

Advisors:
Marco Serone
Alessandro Laio
Co-advisors:
Andrea Cappelli (INFN, Firenze)
Antonio Rago (Plymouth Univ.)
Michele Caselle (Univ. Torino)
Marcello Dalmonte (ICTP, Trieste)

Academic Year 2021-2022

Abstract

Stochastic optimization algorithms are a fundamental tool in many areas of physics. They allow to characterize complicated landscapes populated with several minima where deterministic approaches are of limited utility. In this thesis we explore their applicability to the numerical bootstrap of the $4-$point function of identical scalars in a Conformal Field Theory in $d = 2, 3, 4$. We find minima compatible with known examples of CFTs such as the critical Ising model in $d = 2, 3$ and the Generalized Free Theory. We also identify several interesting features of the landscape and propose possible candidates that could explain them.

The thesis is based on the following paper:

[1] Alessandro Laio, Uriel Luviano Valenzuela, and Marco Serone. Monte carlo approach to the conformal bootstrap. Phys. Rev. D, 106:025019, Jul 2022.

Acknowledgements

This thesis, being the culmination of 4 years of work would clearly have been impossible without the help and support of numerous people who I will now try to acknowledge. I apologize beforehand to anyone that might be left out.

Due to a simple causality argument, I must thank first and foremost my family. I must recognize my mother's strength and patience and my father's unwavering commitment for kindling my curiosity and answering all my questions without ever being condescending. I thank my siblings for being such a source of pride, joy, support and understanding, and for giving me a reason to persevere in this path.

I must thank all the friends from my hometown and my extended family, for their support and all the good times we had together. I thank Cristian for all the dreams we chased together.

I must also acknowledge the dear friends and colleagues with whom I shared classrooms and gardens in my alma mater. Christian, Felipe, Andrés, Claudio et al. I must thank specially Prof. Saul Ramos for being an example of dedication and critical thought.

In Trieste I found a second home, and as such I must thank my second family. All the people from the office, Ale[3], Paolo, Shani, my musical friends from the choir, and the people from 431 will be forever in a very special place in my heart.

I must thank Alfredo for all the dinners and the music we shared. I must also thank Etien for feeding my creative mind and helping me find new roads to beauty.

I finally thank my advisors for their guidance and patience, and my opponents for the time dedicated to reading this dissertation.

Contents

Chapter 1

Introduction and Overview

It is hard to pinpoint the moment in which symmetry became a core principle of physical research. However, it is clear that during the last 100 years or so it has been crucial to our understanding of physics. Even outside particle physics, the symmetries of a problem are considered to be highly informative and are often used to distinguish the best method to solve it. In Quantum physics they are of particular importance because they determine the structure of the Hilbert Space of the theory.

In Quantum Field Theories two important distinctions can be done. One one hand we have internal symmetries, which relate several fields with the same properties, for example Global symmetries. On the other hand space-time symmetries act on the underlying geometric space where the QFT is defined. Most of our microscopic understanding of nature is based upon theories with Poincaré symmetry, but interesting extensions have been studied in the last 70 years. One of these proposals is Supersymmetry, where fermionic generators are introduced, with the effect of relating fields with different statistics. In this thesis we will discuss the symmetry obtained when the Poincaré group is extended with scale transformations, arriving at the so called Conformal Group.

Conformal Field Theories are fundamentally different from theories with Poincaré-symmetry that one cannot speak of particles anymore, and thus the scattering matrix is no longer a well defined observable. Instead, one focuses mostly on the correlation functions of fields with well-defined scaling properties. As all symmetries do, Conformal symmetry restricts the shape of physical observables. In particular, the correlation function of four different fields will have to satisfy a set of constraints that when combined with other general assumptions impose restrictions on the spectrum of the theory. This program is known as conformal bootstrap and its ultimate goal is to fully solve a CFT by using only the requirements derived from Conformal Invariance.

The effect of conformal symmetry was first analyzed in a field theoretical language some 50 years ago (e.g. [2, 3, 4]). Since then it has sustained the growth of a rich area of scientific research, ranging from condensed matter to high energy physics. For one, the special case of two-dimensional Conformal Field Theories is of special interest to String Theorists. Since the worldsheet of a string defines a two-dimensional manifold and the theory defined thereupon should be invariant under reparametrizations of said manifold, one can show that it has to be indeed a CFT [5].Another setting where CFT arises naturally is in the boundary theory in the AdS/CFT correspondence[6].

More generally, studying the effect of the renormalization group (RG)[7] on the parameters that define a generic QFT shows the existence of fixed points where the RG flow effectively slows down to a halt. At these special points the couplings of the QFT stop "running" with respect to the scale and thus the physics of such a theory should be invariant under scale transformations. Moreover, it is widely believed and in some cases proved that scale invariant QFTs are invariant under the bigger group of conformal transformations (see e.g. [8]). This means that CFTs effectively give reference points in the space of QFTs and in many cases can help compute physical quantities in theories nearby (a concrete example can be seen in Conformal Perturbation Theory [9]). Another important application appears due to the scale invariance of critical phenomena. More precisely, it was shown by Wilson [10] that a second order phase transition can be described by the fixed point of a RG flow.

This last topic allows us to segue into what will be the other building block of this thesis: numerical methods. Numerical methods are crucial for the study of statistical physics, specially in $d > 2$ where analytical solutions are not available in general. One of the most renowned approaches is the family of techniques known as Monte Carlo methods. These are particularly useful for studying complex systems because they allow to efficiently compute thermodynamical properties by sampling the state space of the system even when it is large and complex.

The main proposal of this dissertation is to apply these methods to the parameter space that determines the CFT. This has the potential for making a step forward with respect to analytic treatments but, as will be shown in the chapters of this thesis, it also entails specific challenges that were overcome only after painstaking work.

1.1 Introduction

The roots of the bootstrap philosophy date more than 50 years. They were first applied to the $S-$matrix of local theories, where it was expected that Poincaré symmetry would be enough for constraining the form of these functions. In the

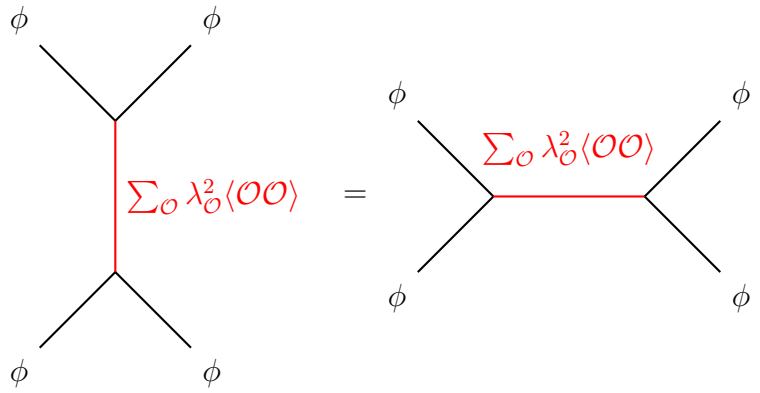

Figure 1.1: Schematic representation of the crossing equations for the 4−pt function $\langle \phi\phi\phi\phi \rangle$. Here $\lambda_{\mathcal{O}}$ are the OPE coefficients and the sum runs over all the operators of the theory.

case of CFTs the bootstrap manifests itself most clearly in the analysis of a given 4−point function. Under reasonable assumptions the Operator Product Expansion in a CFT allows to rewrite the product of two nearby operators as a convergent series over all the operators of the theory. Conformal invariance moreover fixes the functional form of this expansion up to a countable number of coefficients (the so called OPE coefficients). Thus, any given 4−point function can be written as a sum of 2−point functions (which are completely fixed by conformal symmetry). The additional assumption of OPE associativity implies that the different ways of expanding this function should be equivalent, which finally leads us to the crossing equations. We show a pictorial representation of this idea for the 4−point function of identical scalars in fig. 1.1.

The modern numerical bootstrap approach approach (that which will be most relevant for this work) was kindled by the pioneering work of [11], where it was shown that assuming crossing symmetry of the correlator of 4 identical scalars ϕ led to a constraint on the scaling dimension of the lightest scalar exchanged in the OPE $\phi \times \phi$. This was achieved by using the fact that in an unitary theory the OPE coefficients should be real, and thus the constraints of crossing symmetry could be rephrased as a linear programming problem that could be efficiently solved via numerical methods.

This approach was quickly adapted to other settings and improved to deal with systems of multiple correlators. This led eventually to the *rigorous* determination of the scaling dimensions of the leading scalars of the critical 3d Ising model (see [12]) to an unprecedented accuracy. Additionally, interesting results have been found for other theories like the critical $O(N)$ models[13], SCFTs[14] and fermionic theories [15], just to name a few.

The state of the art is represented by the Semidefinite Programming Bootstrap (SDPB), introduced in [16] and further optimized in [17]. In these programs, the user inputs a series of assumptions on the possible spectrum of a CFT and then the code determines whether it is possible or not to solve the crossing equations within sad assumptions. If not, such a spectrum is rigorously ruled out. Otherwise the point is said to be allowed at the given precision. In this way the parameter space is divided into "allowed" and excluded regions.

The great wealth of algorithms and techniques developed have had great success but are limited mostly to the so-called extremal theories, i.e. theories that lie on the border of the aforementioned excluded region. In these cases an algorithm (due to [18]) can give approximate values for several tenths of operators, albeit with less rigour than the results discussed above. This approach, called the *extremal functional*, is one of the most powerful tools that the bootstrap provides for obtaining quantitative information about CFTs. Summarizing, we see that the numerical bootstrap can study extremal theories to an outstanding degree of precision, but a robust method for exploring the rest of the parameter space is missing.[1]

We seek to propose an alternative approach that can find approximate (in a way that we will make precise later on) CFTs away from the extremal region. To this end we explore in this thesis a method based on stochastic optimization that for a truncated spectrum (determined by the number of operators at each spin and the maximum scaling dimension Δ^*) explores the "landscape" of theories compatible with these assumptions on the spectrum and finds the regions where the crossing equations are best satisfied. The object of the optimization is a function of the crossing equations designed so that it has a minimum in such regions. It is clear that not every minimum will be related to a valid solution to crossing.

In order to identify the most relevant minima we must sample the parameter space extensively. The crossing equations are computationally expensive functions of the scaling dimensions and thus a deterministic search cannot be done with full precision without quickly becoming impracticable. We circumvent this problem by carefully approximating the crossing equations with cubic splines and reducing the problem to double precision. This comes with the evident caveat of renouncing to arbitrary accuracy, but as we will show in the main sections of this thesis, it produces sensible results in many settings of interest.

[1] In this respect, the navigator function introduced by [19] might lead to some positive developments, although for now its main results have been mostly confined to the extremal region.

1.2 Overview

The rest of the thesis will be split in 5 chapters. The first two (2 and 3) will deal mostly with background material on CFTs and Numerical optimization, respectively. Then in chapter 4 we will analyze our first attempt at the problem stated above. Using a functional inspired by the work of Gliozzi [20] gave promising results for very sparse settings such as the free theory, but was hard to generalize to other CFTs of interest. It was therefore abandoned in favor of the approach detailed in chapter 5. There, we will discuss the main results of this thesis. We will first describe the protocol that allows us to determine the spectrum of several CFTs in $d = 2, 3$. This protocol is based in a Markov Chain Monte Carlo (see 3.2.2) that explores the parameter space and through several statistical tests determines the points most likely to constitute solutions to crossing. This method is then applied to the space of truncated spectra with $N_{\text{Ops}} \sim 20$ operators, $\ell_{\text{max}} = 10$ and $\Delta < \Delta^* \sim 15$ in $d = 2, 3, 4$, finding good agreement with known CFTs such as the minimal models in $d = 2$ and the critical Ising model in $d = 3$. Moreover, some interesting features of the general landscape are observed and discussed.

We close with chapter 6 where we summarize our conclusions on the topic and present an overview of the work to come.

Chapter 2

Theoretical background

Conformal symmetry is the property of a physical system of being invariant under coordinate transformations that leave intact the angle between two arbitrary vectors. This can be found both in theoretical settings (e.g. String theory) and experimental ones like critical phenomena. In section 2.1 we will briefly review the mathematical underpinning of this symmetry, the structure of a Quantum Field Theory endowed with it and thence the construction of the conformal bootstrap program. Then, in sec. 2.2 we will describe in detail several examples of CFTs, most of which will be of particular relevance to the settings studied in the main work here presented. Finally, in 2.3 we perform a literature review covering both the most successful algorithms and techniques developed since the publication of [11] and the results thus obtained.

2.1 CFT basics

We will review in the following subsections some of the building blocks of conformal field theory. This exposition will be far from thorough, having instead the scope of introducing some concepts and setting the conventions in which the central work will be framed. Our discussion will follow mostly the notation used in [21].

2.1.1 Conformal Group

As said above, a conformal transformation is one where the angle between vectors does not change. This is equivalent to demanding that under a change of coordinates

$$x^\mu \to (x')^\mu$$

the metric transform as

$$g_{\mu\nu}(x) \to \Omega(x) g_{\mu\nu}(x).$$

Let us now specialize to flat metric and consider an infinitesimal transformation $x^\mu \to x^\mu + \epsilon^\mu(x)$. We see that a conformal transformation must satisfy

$$\partial_\mu \epsilon_\nu + \partial_\nu \epsilon_\mu = \omega(x) g_{\mu\nu}. \tag{2.1.1}$$

If we trace both sides we see that $\omega(x) = 2\partial_\nu \epsilon^\nu / d$, where d is the dimensionality of spacetime. Elementary manipulations allow us to show that

$$(2-d)\partial_\mu \partial_\nu \omega(x) = g_{\mu\nu} \partial^2 \omega(x)$$

and thence

$$(d-1)\partial^2 \omega(x) = 0.$$

For $d > 2$ these conditions will restrict the local form of the conformal group. In particular, $\epsilon(x)$ will at most be quadratic in x and thus the group will be finite dimensional. Acting on scalar functions, the generators can be written as

$$P_\mu \equiv -i\partial_\mu \,, \tag{2.1.2}$$
$$M_{\mu\nu} \equiv i(x_\mu \partial_\nu - x_\nu \partial_\mu) \,, \tag{2.1.3}$$
$$D \equiv -i x_\mu \partial^\mu \,, \tag{2.1.4}$$
$$K_\mu \equiv i(x^2 \partial_\mu - 2x_\mu x_\nu \partial^\nu) \,, \tag{2.1.5}$$

which correspond to translations, rotations, dilatations and special conformal transformations (SCTs), respectively.

They satisfy the following commutation relations

$$\begin{aligned}
[D, K_\mu] &= -iK_\mu \,, \\
[D, P_\mu] &= iP_\mu \,, \\
[K_\mu, P_\nu] &= 2i(\eta_{\mu\nu} D - M_{\mu\nu}) \,, \\
[K_\mu, M_{\nu\rho}] &= i(\eta_{\mu\nu} K_\rho - \eta_{\mu\rho} K_\nu) \,, \\
[P_\rho, M_{\mu\nu}] &= i(\eta_{\rho\mu} P_\nu - \eta_{\rho\nu} P_\mu) \,, \\
[M_{\mu\nu}, M_{\rho\sigma}] &= i(\eta_{\nu\rho} M_{\mu\sigma} + \eta_{\mu\sigma} M_{\nu\rho} - \eta_{\mu\rho} M_{\nu\sigma} - \eta_{\nu\sigma} M_{\mu\rho}) \,,
\end{aligned} \tag{2.1.6}$$

with commutators vanishing for the other cases.

Moreover, for a flat metric $g_{\mu\nu} = \eta_{\mu\nu}$ with signature (p, q) it can be shown that the algebra that generates these transformations is isomorphic to $SO(p+1, q+1)$. In the Euclidean case, with which we will mostly be concerned, the generators of the latter are given in terms of the former as

$$\begin{aligned}
L_{\mu\nu} &= M_{\mu\nu} \quad & L_{-1,\mu} &= \frac{1}{2}(P_\mu - K_\mu) \\
L_{-1,0} &= D & L_{0,\mu} &= \frac{1}{2}(P_\mu + K_\mu)
\end{aligned} \tag{2.1.7}$$

We note in passing that this is the cornerstone of the embedding space formalism, which is outside the scope of this review but has been crucial in computing correlators for spinning operators (see e.g. [22]).

On the other hand, for $d = 1$ we see that any function of one variable will trivially be conformal. For $d = 2$ it is clear that any meromorphic function $f(z)$ (where we define $z \equiv x^1 + ix^2$) will satisfy (2.1.1). Thus, in this case the group will be infinite dimensional and some special considerations will apply. In particular, the algebra will split into an holomorphic and an antiholomorphic part with generators given by [1]

$$L_i = -z^{i+1}\partial_z\,, \quad \bar{L}_i = -\bar{z}^{i+1}\partial_{\bar{z}} \tag{2.1.8}$$

that satisfy the following commutation relations

$$[L_i, L_j] = (i-j)L_{i+j}\,, \quad [\bar{L}_i, \bar{L}_j] = (i-j)\bar{L}_{i+j}\,, \quad [L_i, \bar{L}_j] = 0. \tag{2.1.9}$$

It is important to note that the subalgebra $\{L_{-1}\,, L_0\,, L_1\}$ is globally well defined and generates the group $SL(2, \mathbb{C})$.

At the quantum level this algebra admits a central extension given by

$$\begin{aligned} [L_i, L_j] &= (i-j)L_{i+j} + \frac{c}{12}i(i^2-1)\delta_{i+j,0} \\ [\bar{L}_i, \bar{L}_j] &= (i-j)\bar{L}_{i+j} + \frac{c}{12}i(i^2-1)\delta_{i+j,0} \\ [L_i, \bar{L}_j] &= 0 \end{aligned} \tag{2.1.10}$$

known as the Virasoro algebra. Here, the constant c is the central charge and depends on the actual content of the theory.

Irreducible representations

Although the representation theory for non-compact groups is a very interesting topic we will steer away from any technical discussion and define a quasi-primary scalar field[2] to be one that transforms as

$$\phi(x) = \left|\frac{\partial(x')^\mu}{\partial x^\nu}\right|^{\Delta/d} \phi'(x'),$$

under global conformal transformations. In the $d = 2$ case we say that the field is primary only if it transforms in this way also for the full conformal group and not only for the globally defined subgroup. To label these irreducible representations we can use their scaling dimension Δ (i.e. the eigenvalue under the action of D) and the

[1] Not to be confused with the generators of $SO(d+1, 1)$ defined in (2.1.7).

[2] In the following, for $d > 2$ they will also be called primary, since the distinction between the former and the latter is only relevant in $d = 2$.

representation in which they transform under the $SO(d)$ subgroup of the conformal group. In the $d = 2$ we choose L_0 and $\bar{L}_0$ as the maximal subset of commuting generators and use their eigenvalues as the quantum numbers for our operators. Thus, quasiprimary operators are labeled by two real numbers, h and $\bar{h}$, usually called the conformal weights that come from the following eigenvalue equation

$$L_0|\phi\rangle = h|\phi\rangle, \quad \bar{L}_0|\phi\rangle = \bar{h}|\phi\rangle. \tag{2.1.11}$$

The correspondence between the operator ϕ and the vector $|\phi\rangle$ will be made precise in section 2.1.2. For the sake of this discussion it suffices to know that $|\phi\rangle \sim \phi(0)|0\rangle$, where $|0\rangle$ is the vacuum of the theory.

Moreover, the commutation relations in eq. (2.1.6) imply that, wrt. D, K and P behave as annihilation and creation operators, respectively. This means that one can generate the whole representation by acting upon $|\phi\rangle$ with different combinations of P^μ. The states thus obtained are known as *descendants*.

Correlation functions

One of the most important differences between a generic QFT and conformal field theories is that demanding that correlation functions be covariant under conformal transformations fixes their functional form to a great extent. We will now show how conformal symmetry fixes 2−point functions completely and 3−point ones up to a constant. The case of 4− operators will be particularly interesting because there the correlator is only required to be a generic function of some conformally invariant ratios. This function is at the heart of the conformal bootstrap program.

2−point function Conformal symmetry constrains any 2−point function between operators of different scaling dimension Δ to vanish. The functional form is also fixed and in the scalar case reads

$$\langle\phi(x)\phi(y)\rangle = \frac{1}{|x-y|^{2\Delta_\phi}}. \tag{2.1.12}$$

(The numerator can be fixed by normalizing the operators.) The case of spinning operators is the same modulo the appearance of the relevant spin structures in the numerator.

3−point function Conformal invariance constrains the correlator of three scalars (with scaling dimensions Δ_i, Δ_j, Δ_k) to be of the form

$$\langle\phi_i(x)\phi_j(y)\phi_k(z)\rangle = \frac{\lambda_{ijk}}{|x-y|^{\Delta_i+\Delta_j-\Delta_k}|z-y|^{\Delta_k+\Delta_j-\Delta_i}|x-z|^{\Delta_i-\Delta_j+\Delta_k}},$$

where the constant λ_{ijk} is also known as the OPE coefficient and will be discussed in more detail shortly. Moreover, if $\phi_i = \phi_j$ one can show that invariance under $x \to -x$ fixes the third operator to be an even-spin traceless symmetric tensor.

4−point function With 4 points there are 2 independent conformal invariants that can be constructed:

$$u = \frac{x_{12}^2 x_{34}^2}{x_{13}^2 x_{24}^2} = z\bar{z}, \quad v = \frac{x_{14}^2 x_{32}^2}{x_{13}^2 x_{24}^2} = (1-z)(1-\bar{z}), \quad x_{ij} \equiv |x_i - x_j|. \tag{2.1.13}$$

We introduce here the variables $z, \bar{z}$ that will come in handy shortly.

Thus, the 4−point function for identical scalars must be of the form

$$\langle \phi(x_1)\phi(x_2)\phi(x_3)\phi(x_4)\rangle = |x_{12}|^{-2\Delta_\phi}|x_{34}|^{-2\Delta_\phi}\mathcal{G}(u,v).$$

So far, the function $\mathcal{G}$ is completely unconstrained. The main aim of the bootstrap program, as we will see, is to dissect this function and use this knowledge to "solve" the CFT non perturbatively. To do this, we must first discuss one of the key properties of any CFT.

2.1.2 Operator-state correspondence

A crucial element of any QFT is the Hilbert space upon which the operators of the theory act. One of the most notable effects of conformal symmetry at the quantum level is relating the local operators to states (and vice versa) in a very natural way. This would seem strange in principle because states are defined on a whole leaf of the foliation with respect to which we choose to quantize our system, whereas local operators are evaluated on a single point. Intuitively, one can see that symmetry under dilatations can contract any surface to a point, and thus the two spaces should match.

We can make this more precise if we quantize the theory by choosing concentric spheres around the origin (or any other point). Thus, the dilation operator D will be the evolution operator connecting the hilbert space at each sphere. From a path integral quantization approach we can define a state $|\mathcal{O}\rangle$ from an operator $\mathcal{O}(x)$ by its behaviour in correlation functions as

$$\langle \phi_b|\mathcal{O}\rangle \equiv \langle \phi_b|\mathcal{O}(0)|0\rangle = \int_{\phi(r,\mathbf{n})=\phi_b(\mathbf{n}),\, r\leq 1} \mathcal{D}\phi(r,\mathbf{n})\mathcal{O}(x)e^{-S[\phi]}, \tag{2.1.14}$$

where $\mathcal{D}\phi$ is the integration measure inside a ball of radius one with the boundary condition given by the $d-1$ dimensional field.

To show that the construction holds backwards we need only consider eigenstates $|\mathcal{O}_i\rangle$ of the dilation operator $\mathcal{D}$ and define the correlation function

$$\langle \mathcal{O}_1(x_1)\dots\mathcal{O}_n(x_n)\rangle = \int \prod_i \mathcal{D}\phi_{bi}\langle \phi_{bi}|\mathcal{O}_i\rangle \int_{\phi_{\partial i}=\phi_{bi},\, x\notin B_i} \mathcal{D}\phi(x)e^{-S[\phi]} \tag{2.1.15}$$

in which we cut n balls B_i around the operators and integrate over the fields outside the balls with the given boundary conditions.

Restricted to operators $\mathcal{O}(x)$ that are eigenstates of Δ we see that this correspondence will be one to one.

2.1.3 OPE

The Operator-State correspondence has a very important consequence. Let us consider two field insertions $\phi(x)$ y $\phi(0)$ and a ball B containing them. It is clear that these two insertions define a state $\phi(x)\phi(0)|0\rangle$ that –assuming the Hilbert space defined at the surface ∂B is complete– should be expressable as a linear combinations of a basis given by insertions at the origin. Namely,

$$\phi_i(x)\phi_j(0) \sim \sum_k c_{ijk}(x)\phi_k(0),$$

where k runs over all the operators in the theory, both primary and descendants.

Scale invariance fixes the form of c_{ijk} to be

$$c_{ijk}(x,\partial) = \lambda_{ijk}|x|^{\Delta_k-\Delta_j-\Delta_i}(1+\alpha x^\mu\partial_\mu + \beta x^2\partial^2 + \cdots).$$

The coefficients of the derivative expansion, on the other hand, can be determined by demanding invariance under SCTs or by expanding the three point function in $|x|/|y|$ and matching the terms order by order.

The first hints of the bootstrap program appear when we consider a $4-$point function. For example, we can apply the OPE to the following correlator like so (as long as there is a sphere separating $x_{1,2}$ from $x_{3,4}$):

$$\langle\overbrace{\phi(x_1)\phi}(x_2)\overbrace{\phi(x_3)\phi}(x_4)\rangle = \sum_{\mathcal{O}} c_{\phi\phi\mathcal{O}}(x_{12},\partial_2)c_{\phi\phi\mathcal{O}}(x_{34},\partial_4)\langle\mathcal{O}(x_2)\mathcal{O}(x_4)\rangle. \quad (2.1.16)$$

It is useful to sum up the whole contribution of each primary operator and its descendants by introducing the conformal blocks $g_{\Delta,\ell}(u,v)$, with which we can write the previous equation as

$$\langle\phi(x_1)\phi(x_2)\phi(x_3)\phi(x_4)\rangle = \frac{1}{x_{12}^{2\Delta_\phi}x_{34}^{2\Delta_\phi}}\sum_{\mathcal{O}}\lambda^2_{\phi\phi\mathcal{O}}g_{\Delta_\mathcal{O},\ell_\mathcal{O}}(u,v). \quad (2.1.17)$$

Alternatively, we can also do the following OPEs

$$\langle\overbrace{\phi(x_1)\overbrace{\phi(x_2)\phi}(x_3)\phi}(x_4)\rangle = \frac{1}{x_{32}^{2\Delta_\phi}x_{14}^{2\Delta_\phi}}\sum_{\mathcal{O}}\lambda^2_{\phi\phi\mathcal{O}}g_{\Delta_\mathcal{O},\ell_\mathcal{O}}(v,u). \quad (2.1.18)$$

This is equivalent to exchanging $1 \leftrightarrow 3$ (notice the exchange between $u \leftrightarrow v$ in the arguments of g) and can only be done if a sphere separating $x_{2,3}$ from $x_{1,4}$ exists. Assuming that the OPE is associative we have that the two expansions should match, and thus we arrive at the crossing equations, which we now discuss.

Equating (2.1.17) and (2.1.18) gives the following expression:

$$\sum_{\Delta>0,\ell} \lambda^2_{\phi\phi\mathcal{O}_{\Delta_\ell}} \mathcal{F}_{\Delta,\ell}(u,v) = I(u,v), \tag{2.1.19}$$

where we defined

$$\mathcal{F}_{\Delta,\ell}(u,v) = v^{\Delta_\phi} g_{\Delta,\ell}(u,v) - u^{\Delta_\phi} g_{\Delta,\ell}(v,u), \quad I(u,v) = u^{\Delta_\phi} - v^{\Delta_\phi}. \tag{2.1.20}$$

As we can see, this equation will impose conditions on the spectrum of the theory, in particular the operators exchanged in the $\phi \times \phi$ OPE. In order to do so, however, we must obtain explicit expressions for the conformal blocks. Fortunately, during the last 20 years there has been substantial discoveries in this regard. In the next subsection we will review two of the most useful techniques for computing the conformal blocks.

2.1.4 Conformal Blocks

As will become clear in our discussion of the numerical bootstrap, it is paramount to have practical expressions for the conformal blocks $g_{\Delta,\ell}(u,v)$ in order to extract information from the crossing equations. Developing technology for this aim is naturally one of the areas of greater development in the bootstrap community. We will now discuss only two of those approaches, in particular those most relevant to the investigation pursued in this work.

Casimir differential equation

In the early 2000's Dolan and Osborn [23, 24] realized that the conformal block satisfies a differential equation given by the action of the quadratic Casimir of the conformal group. This equation can be solved in terms of hypergeometric functions in $d = 2, 4$.

Schematically, one can insert the quadratic Casimir (cf. eq. (2.1.7) for the definition of L_{ab})

$$C = \frac{1}{2} L_{ab} L^{ab},$$

into the following expression for a conformal conformal block

$$\langle\phi(x_1)\phi(x_2)|P_{\mathcal{O}}|\phi(x_3)\phi(x_4)\rangle = \frac{1}{x_{12}^{2\Delta_\phi}x_{34}^{2\Delta_\phi}}\lambda^2_{\phi\phi\mathcal{O}}g_{\Delta_{\mathcal{O}},\ell_{\mathcal{O}}}(u,v). \tag{2.1.21}$$

.

Here we introduce the projector onto the conformal multiplet of the operator $\mathcal{O}$. The latter being an irreducible representation implies that the action upon it of C should be proportional to the identity. Namely $CP_{\mathcal{O}} = P_{\mathcal{O}}C = c_{\mathcal{O}}P_{\mathcal{O}}$, where the eigenvalue $c_{\mathcal{O}} = \Delta_{\mathcal{O}}(\Delta_{\mathcal{O}} - d) + \ell_{\mathcal{O}}(\ell_{\mathcal{O}} + d - 2)$ depends on the representation to which $\mathcal{O}$ belongs. We thus obtain

$$\langle\phi(x_1)\phi(x_2)|C|P_{\mathcal{O}}|\phi(x_3)\phi(x_4)\rangle = c_{\mathcal{O}}\frac{1}{x_{12}^{2\Delta_\phi}x_{34}^{2\Delta_\phi}}\lambda^2_{\phi\phi\mathcal{O}}g_{\Delta_{\mathcal{O}},\ell_{\mathcal{O}}}(u,v). \tag{2.1.22}$$

.

On the other hand, C also has a representation on the space of functions as a quadratic differential operator. Thus, the conformal blocks must satisfy a second-order linear differential equation. The main achievement of Dolan and Osborn is finding a set of coordinates where said equation is easiest to solve.

Introducing the $z, \bar{z}$ coordinates (defined as in (2.1.13)), Dolan and Osborn showed that the following combinations of hypergeometric functions solve the resulting differential equation:

$$\begin{aligned} g^{2d}_{\Delta,\ell}(z,\bar{z}) &= \frac{2^\ell}{1+\delta_{\ell,0}}\left(k_{\Delta+l}(z)k_{\Delta-l}(\bar{z}) - k_{\Delta+l}(\bar{z})k_{\Delta-l}(z)\right), \\ g^{4d}_{\Delta,\ell}(z,\bar{z}) &= \frac{2^\ell z\bar{z}}{z-\bar{z}}\left(k_{\Delta+l}(z)k_{\Delta-l-2}(\bar{z}) - k_{\Delta+l}(\bar{z})k_{\Delta-l-2}(z)\right), \\ k_\beta(x) &\equiv x^{\beta/2}{}_2F_1\left(\frac{\beta}{2},\frac{\beta}{2},\beta,x\right). \end{aligned} \tag{2.1.23}$$

Where the boundary conditions are set by matching this solution to the $x_{12}, x_{34} \to 0$ limit.

In principle, a closed expression can be found for any even d, whereas for generic d only certain limits or the blocks for a certain spin are known.

Recursion formula

For generic d there are no known closed expressions, although several techniques can give series expansions in some coordinate systems. Another highly fruitful approach is to exploit the meromorphic structure of the conformal blocks as a function of Δ in order to obtain recursion relations for the blocks.

Drawing inspiration on Zamolodchikov's recursion relations for the Virasoro blocks in $d = 2$ [25, 26], Kos et al. showed in [27] that a similar property holds for $g_{\Delta,\ell}(u,v)$.

Namely, the block has poles in Δ below the unitarity bound that allow for a rational approximation.

The existence of these poles is conceptually very clear and can be seen e.g. from eq. (2.1.22). In fact, we can write the projector as a sum over all the descendants of $\mathcal{O}$ like so

$$P_{\mathcal{O}} = \sum_{\alpha,\beta} |\alpha\rangle G^{\alpha\beta} \langle\beta|, \quad G_{\alpha\beta} \equiv \langle\alpha|\beta\rangle, \quad G^{\alpha\gamma} G_{\gamma\beta} = \delta^{\alpha}_{\beta}. \tag{2.1.24}$$

We see that for $\Delta_{\mathcal{O}} > \Delta_\ell$ (the unitarity bound) this matrix will be positive definite. On the other hand for certain values of Δ Below the unitarity bound (denoted by Δ_A in what follows) some vectors might become null. This means that the inverse matrix $G^{\alpha\beta}$ will develop a pole and so will the It can be also shown that the residue of these poles will be proportional to the conformal block with scaling dimension $\Delta = \Delta_A + n_A$.

By identifying the different families of poles and their residues it is possible to write the conformal block as the following recursion formula (in radial coordinates where $\rho = z/(1-\sqrt{1-z})^2$ and $\rho = re^{i\theta}$, $\eta = \cos\theta$)

$$g_{\Delta,\ell}(r,\eta) = (4r)^{\Delta} h_{\Delta,\ell}(r,\eta), \tag{2.1.25}$$

where we factor out the exponential dependence on Δ to obtain a meromorphic function that can thus be characterized fully by its poles and its limit when $\Delta \to \infty$, namely

$$h_{\Delta,\ell}(r,\eta) = h_{\infty,\ell}(r,\eta) + \sum_A \frac{R_A}{\Delta - \Delta_A} (4r)^{n_A} h_{\Delta_A+n_A,\ell_A}(r,\eta) \tag{2.1.26}$$

This approach can be refined by using the Casimir differential equation to extract recursion relations between the coefficients of the series expansions of these blocks. As of today, this is one of the most efficient ways of evaluating the conformal blocks for numerical applications.

2.2 Notable CFTs

We now illustrate the concepts described in the previous section with some examples. They will also be relevant for some of the systems studied in the main text.

2.2.1 2d

The two dimensional setting is much richer than its higher dimensional counter parts. We will start by reviewing the free scalar field which, besides being the simplest example at hand, is also the basis for the Coulomb Gas formalism. The latter will be crucial when presenting the Minimal models later on.

Free scalar

A free scalar ϕ with action

$$S = \frac{g}{2}\int \mathrm{d}^2x\, \partial^\mu\phi(x)\partial_\mu\phi(x) = \frac{g}{2}\int \mathrm{d}z\mathrm{d}\bar{z}\, \partial\phi(z,\bar{z})\bar{\partial}\phi(z,\bar{z}) \tag{2.2.1}$$

defines a CFT. It is important to note, however, ϕ itself has engineering dimension zero and as such cannot be a primary operator but has instead a correlator of the form

$$\langle\phi(z,\bar{z})\phi(w,\bar{w})\rangle \sim -\log(z-w) - \log(\bar{z}-\bar{w}) \tag{2.2.2}$$

in complex coordinates. On the other hand derivatives of ϕ will be primaries of conformal dimension 1.

Another way to construct primary operators is by exponentiation. This way, one can define the so-called *vertex operators*:

$$V_\alpha(z,\bar{z}) \equiv :e^{\sqrt{2}\alpha\phi(z,\bar{z})}: \tag{2.2.3}$$

which have the following correlator

$$\langle V_{\alpha_1}(z_1,\bar{z}_1)V_{\alpha_2}(z_2,\bar{z}_2)\dots V_{\alpha_n}(z_n,\bar{z}_n)\rangle = \prod_{i<j}|z_i-z_j|^{4\alpha_i\alpha_j} \tag{2.2.4}$$

if $\sum\alpha_i = 0$ and zero otherwise. This condition can be seen intuitively by demanding invariance under the $U(1)$ transformation that shifts $\phi \to \phi + a$. More formally, one can compute the Ward identity for this symmetry applied to the correlator in (2.2.4) and see that the sum of the charges α must vanish.

Being the conserved current associated to coordinate transformations, the stress energy tensor T can also be seen as their generator. In that sense, the OPE of an operator $\mathcal{O}$ and T determines the conformal weight of the former. For the action in eq. (2.2.1) the holomorphic component of T is given by

$$T(z) = -\frac{1}{2} :\partial\phi\partial\phi: \tag{2.2.5}$$

where the $:\ :$ notation indicates normal ordering of the fields in the product. This means in practice that any singular terms have been substracted. Computing the respecti OPEs we find that the conformal weights of the vertex operator $V_\alpha(z,\bar{z})$ read $h_\alpha = \bar{h}_\alpha = \alpha^2$.

Minimal models

Minimal models are one of the best examples of the power of Virasoro symmetry to completely solve a CFT (see [28]). There are many ways to study these models, some of them more amenable for critical phenomena or for high energy physics purposes.

In our case we will use the Coloumb Gas Formalism because it gives a very practical way of computing 4−point functions, and we will be using the exact results as a benchmark for some results in the main chapter of this work.

To do this we take the free scalar construction shown above and couple the scalar field to the curvature scalar[3] R like so (cf. eq. (2.2.1))

$$S = \frac{1}{4\pi}\int \mathrm{d}^2x\,\sqrt{g}\left(\partial^\mu\phi(x)\partial_\mu\phi(x) + 2\gamma\phi R\right).$$

Here g is the determinant of the metric and γ is the coupling constant. This manifestly breaks the symmetry given by $\phi \to \phi + a$, under which the action changes by a topological term, i.e. $\delta S = 2a\gamma$. One can see that the Ward identities for the $U(1)$ symmetry will change and the new conservation law for the correlation function

$$\langle V_{\alpha_1}(z_1,\bar{z}_1)V_{\alpha_2}(z_2,\bar{z}_2)\dots V_{\alpha_n}(z_n,\bar{z}_n)\rangle \tag{2.2.6}$$

will be

$$\sum \alpha_i = -i\sqrt{2}\gamma \equiv 2\alpha_0.$$

We note that this implies γ has to be imaginary, which in turn makes the theory non unitary. We will see later on that for certain values of α_0, however, a consistent unitary CFT can be defined.

This will also change the stress energy tensor from eq. (2.2.5) into the following

$$T(z) = -\frac{1}{2} : \partial\phi\partial\phi : + i\sqrt{2}\alpha_0\partial^2\phi \tag{2.2.7}$$

and consequently we will have

$$h_\alpha = \alpha^2 - 2\alpha\alpha_0. \tag{2.2.8}$$

Finally, from the $T(z)T(w)$ OPE we can see that the central charge of this new theory will be

$$c = 1 - 24\alpha_0^2. \tag{2.2.9}$$

We must now pause for a second and consider the two point function $\langle V_\alpha V_\alpha\rangle$. In order to create a sensible theory we would like this correlator not to vanish, but its incompatibility with charge conservation forces it to be zero. On the other hand, since $h_\alpha = h_{2\alpha_0-\alpha}$, it should be equivalent to[4]

$$\langle V_\alpha(z)V_{2\alpha_0-\alpha}(w)\rangle = \frac{1}{(z-w)^{h_\alpha}}. \tag{2.2.10}$$

[3]Although we will work in flat space, this is a useful trick to add a background charge to the theory.

[4]when not prone to generating confusion we will write only the holomorphic components of the fields, bearing in mind that only the product $V(z,\bar{z}) \sim V(z)\bar{V}(\bar{z})$ will be well defined.

The solution for this apparent contradiction is to introduce the screening operators

$$Q_\pm \equiv \oint \mathrm{d}z\, V_\pm(z), \quad V_\pm(z) \equiv e^{i\sqrt{2}\alpha_\pm \phi(z)} \tag{2.2.11}$$

that have charge $\alpha_\pm = \alpha_0 \pm \sqrt{\alpha_0^2 + 1}$. Moreover, being the integral of a vertex operator with $h = 1$ they are invariant under conformal mappings and thus commute with all the Virasoro generators. This means that adding them to any correlation function will not change the conformal properties of the function, only the charge. For example, consider once more the function

$$\langle V_\alpha(z) V_\alpha(w) Q_-^n Q_+^m \rangle \tag{2.2.12}$$

where the charge conservation equation now reads

$$2\alpha + m\alpha_+ + n\alpha_- = 2\alpha_0 = \alpha_+ + \alpha_-. \tag{2.2.13}$$

This means that in order to define a consistent theory 2α must be an integer combination of $\alpha_\pm$.

We will thus define

$$\alpha_{r,s} \equiv \frac{1}{2}(1-r)\alpha_+ + \frac{1}{2}(1-s)\alpha_- \tag{2.2.14}$$

and consequently

$$V_{r,s} \equiv V_{\alpha_{r,s}}. \tag{2.2.15}$$

This convention ensures that the conjugation $\alpha \to 2\alpha_0 - \alpha$ is realized as $(r,s) \to (-r,-s)$ and that

$$h_{r,s} = \frac{1}{4}(r\alpha_+ + s\alpha_-)^2 - \alpha_0^2. \tag{2.2.16}$$

Minimal models can then be defined by two integers p, p', $(p > p')$ and demanding that $\alpha_\pm$ satisfy

$$p'\alpha_+ + p\alpha_- = 0 \tag{2.2.17}$$

which implies a periodicity condition on the charges $\alpha_{r,s} = \alpha_{r+p',s+p}$ and thus can be used to limit one of the dimensions on the (r,s) grid. By computing the appropriate 3−point functions one can show that restricting the indices to lie in a rectangle given by

$$0 \le s \le p' \quad 0 \le r \le p \tag{2.2.18}$$

gives a closed algebra. This CFT will have a central charge given by

$$c = 1 - \frac{6(p-p')^2}{4pp'}. \tag{2.2.19}$$

In the following, we will denote these models by $\mathcal{M}(p,p')$. The 4−point function of $\phi_{2,1}$ will be of particular importance in section 5.3.3, where we will use numerical

methods to determine the spectrum of operators in the OPE of $\phi_{1,2} \times \phi_{1,2}$. We will now show how to obtain this information from the correlator

$$\langle \phi_{1,2}(z_1, \bar{z}_1)\phi_{1,2}(z_2, \bar{z}_2)\phi_{1,2}(z_3, \bar{z}_3)\phi_{1,2}(z_4, \bar{z}_4)\rangle \tag{2.2.20}$$

by studying a particular case of the discussion found in [29].

There are many ways of expressing this correlator in terms of vertex operators, each of them requiring different screening operators. The one that requires the least number of insertions is shown in the following representation of eq. (2.2.20)

$$\oint_C \mathrm{d}v \langle V_{1,2}(z_1)V_{1,2}(z_2)V_{1,2}(z_3)V_{-1,-2}(z_4)V_-(v)\rangle \times \text{c.c.} \tag{2.2.21}$$

where the contour C is not yet specified but must contain all four z_i.

This integral is more tractable if we use conformal symmetry to set $z_1 = 1$, $z_3 = 0$ and $z_4 = \infty$, leaving $z_2 = z$. Neglecting the antiholomorphic components and using (2.2.4)) we have that (2.2.21) can be written as

$$(z(1-z))^{2\alpha_{1,2}^2} \oint_C \mathrm{d}v\, v^{2\alpha_{1,2}\alpha_-}(v-1)^{2\alpha_{1,2}\alpha_-}(v-z)^{2\alpha_{1,2}\alpha_-}. \tag{2.2.22}$$

This integrand has branch cuts at $v = 0, 1, z, \infty$. There are several ways to choose the contour C but they are all equivalent to a combination of one of the following integrals ($a = 2\alpha_{1,2}\alpha_-$)

$$I_1(z;a) \equiv \int_{[1,\infty]} \mathrm{d}v v^a (v-1)^a (v-z)^a = \frac{\Gamma(-1-3a)\Gamma(a+1)}{\Gamma(-2a)} F(z; -a, -3a-1, -2a) \tag{2.2.23}$$

$$I_2(z;a) \equiv \int_{[0,1]} \mathrm{d}v\, v^a (v-1)^a (v-z)^a = \frac{\Gamma(a+1)^2}{\Gamma(2a+2)} z^{1+a+c} F(z; -a, a+1, 2a+2) \tag{2.2.24}$$

where F is the hypergeometric function. With this, we can write the full correlator as

$$\langle \phi_{1,2}(1,1)\phi_{1,2}(z,\bar{z})\phi_{1,2}(0,0)\phi_{1,2}(\infty)\rangle = |z|^{4\alpha_{1,2}^2}|1-z|^{4\alpha_{1,2}^2} Y(z,\bar{z}) \tag{2.2.25}$$

where

$$Y(z,\bar{z}) \equiv X_{ij} I_i(z) I_j(z) \tag{2.2.26}$$

is a quadratic function of the integrals defined above and X is a matrix that we will shortly specify.

In order to fix the entries of X_{ij} we must use the fact that although I_i have non trivial monodromies around $z = 0, 1, \infty$, 2.2.25 should be a well-defined function

of $z, \bar{z}$. In practice, the monodromy around 0 forces X to be diagonal and the one around $z = 1$ implies

$$\frac{X_{11}}{X_{22}} = \frac{s(3a)s(a)}{s(a)^2}, \tag{2.2.27}$$

where $s(x) = \sin(\pi x)$.

The overall factor is fixed by looking at the $z \to 0$ limit, in which the correlator should behave as $1/|z|^{4h_{1,2}}$. This singularity is reproduced by I_2 which means that we can write 2.2.25 as

$$\begin{aligned} \langle \phi_{1,2}(1,1)\phi_{1,2}(z,\bar{z})\phi_{1,2}(0,0)\phi_{1,2}(\infty)\rangle = |z|^{4\alpha_{1,2}^2}|1-z|^{4\alpha_{1,2}^2} \\ \times \frac{1}{s(a)^2}\left(\frac{\Gamma(2a+2)}{\Gamma(a+1)^2}\right)^2 \left[s(a)s(3a)|I_1(z,a)|^2 + s(a)^2|I_2(z,a)|^2\right] \end{aligned} \tag{2.2.28}$$

We can also use this expression to see which other operators appear in the OPE of $\phi_{1,2}$ with itself, besides the identity. For example, looking at the expansion around $z = 0$ we see that the the function I_1 contributes with a term proportional to $1/|z|^{2(2h_{1,2}-h_{1,3})}$, which means that the operator $\phi_{1,3}$ should also appear in this OPE. Moreover, the proportionality constant fixes the OPE coefficient to be

$$\lambda_{12,12,13} = \frac{\Gamma(2-2\rho)}{\Gamma(2\rho)}\left(\frac{\gamma^3(\rho)}{\gamma(3\rho-1)}\right)^{1/2}\frac{\gamma(1-\rho)}{\gamma(2-3\rho)}, \tag{2.2.29}$$

where $\rho \equiv \alpha_-^2$ and $\gamma(x) = \Gamma(x)/\Gamma(1-x)$.

So far we have talked mostly about primary operators in the sense of $2d$ CFTs. However, in numerical bootstrap one is more interested in the global part of the conformal group, which is the one that parallels more closely the kinematics in $d > 2$. Therefore it is important to see how the two operators in the $\phi_{1,2} \times \phi_{1,2}$ OPE, namely the identity and $\phi_{1,3}$, decompose in irreps of the global conformal group in $d = 2$. This is easily done by noting that quasiprimaries belonging to the same Verma module (primary) will have scaling dimensions differing by integer values and then expanding each term in 2.2.28 as a series in z and matching the different terms to the expansion of the $2d$ $SL(2,\mathbb{C})$ blocks reported in (2.1.23).

The above discussion shows that diagonal unitary minimal models of the form $\mathcal{M}(p+1, p)$ always have a set of three fields with the following fusion rules:

$$\phi_{1,2} \times \phi_{1,2} \sim \phi_{1,1} + \phi_{1,3} \tag{2.2.30}$$

for $p = 3, 4, \ldots$. The $p = 3$ case corresponds to the critical Ising model and this motivates to write 2.2.30 in the following terms

$$\sigma \times \sigma \sim \mathbb{I} + \epsilon. \tag{2.2.31}$$

The position of these models on the $\Delta_\sigma - \Delta_\epsilon$ plane (here $\Delta_\mathcal{O} = h_\mathcal{O} + \bar{h}_\mathcal{O}$) describes a line, which raises the question of whether other CFTs exist in between the different minimal models. This was partially answered by [30] who realized realized that a family of 4−point functions interpolate between these unitary models.

Later on, [31] formalized these solutions to crossing and discovered that although the operators exchanged in $\phi_{1,2} \times \phi_{1,2}$ obeyed unitarity the solutions to crossing interpolating between the different MMs were not full fledged unitary CFTs (this was expected since it is known that the only unitary CFTs with $c < 1$ are the minimal models themselves) because of the presence of operators with negative OPE coefficients in other sectors of the theory.

2.2.2 $d > 2$

In $d > 2$ we lose the power of Virasoro symmetry and thus obtaining exact results about non trivial CFTs becomes signifcantly harder. A notable exception are supersymmetric theories, where no-renormalization theorems and other properties give greater control over the scaling behaviour. The best example in this respect is $\mathcal{N} = 4$ Super Yang-Mills [32] where it can be shown that besides being classicaly scale-invariant, the gauge coupling's $\beta-$function vanishes at any perturbation order and the theory remains conformal at the quantum level. For a given gauge group the matter content of this theory is fixed by supersymmetry. However, there is a complex manifold of theories parametrized by the complex gauge coupling of the theory. (See [33] for a pedagogical exposition.)

Since Supersymmetric theories are beyond the scope of this work, we will focus in what follows on non-SUSY CFTs, where most examples are perturbative. We will first review a generic way of obtaining perturbative fixed points credited to [34] and [35] and a concrete realization in Gauge theories in $d = 4$. We will then review the critical Ising model and the critical $O(N)$ models of which the former can be considered a particular case.

Banks-Zaks Fixed Points

It often happens that theories that are classically scale invariant develop a dependence on the energy scale at the quantum level. This can be seen from a Renormalization Group (RG) approach by the introduction of a dimensionful parameter that describes how the couplings of the theory change with the scale. Thus, a CFT can only be found at the fixed points of the RG flow. We will here review a case of a Fixed Point that can be studied within perturbation theory of Non-Abelian Gauge theory, first noted by [34] and then explored for more phenomenologically relevant settins by Banks and Zaks in 1982[35].

Let us begin by considering a generic 2-loop $\beta-$function:

$$\beta(g) = -b_0 g^3 + b_1 g^5 + O(g^7).$$

It is clear that if $0 < b_0 << b_1$ then we will have a *Perturbative Fixed Point*, that is,

$$\beta(g_*) = 0, \quad g_* \approx \sqrt{\frac{b_0}{b_1}} << 1.$$

We note in passing that for this to work the higher order terms must be actually negligible, and this is not always guaranteed. Nonetheless, we will now see a small example where this is indeed the case and the existence of a fixed point has been confirmed otherwise.

Consider $SU(N)$ Gauge Theory with N_F Dirac Fermions in the fundamental. The Lagrangian for this theory can be written as

$$\mathcal{L} = -\frac{1}{4g} F_{\mu\nu} F^{\mu\nu} + i\bar{\psi}^j \gamma^\mu D_\mu \psi_j$$

where D_μ is the gauge-covriant derivative, γ^μ are the Dirac gamma-matrices and $j = 1, \ldots, N_F$. The first two coefficients for the beta function of g read

$$b_0 = \frac{1}{16\pi^2} \frac{1}{3} (11N - 2N_F)$$

$$b_1 = -\frac{1}{(16\pi^2)^2} \left(\frac{34}{3} N^2 - \frac{1}{2} N_F \left(2\frac{N^2 - 1}{N} + \frac{20}{3} N \right) \right).$$

We clearly see that for $N_F/N \lesssim 11/2$, $g_* << 1$. (For $N_F/N > 11/2$ the theory will be infrared free.) the theory will be infrared free.) On the other hand, towards smaller values of N_F/N, g_* becomes larger and perturbativity is expected to break down eventually, although lattice computations seem to show there is indeed a fixed point.

It is of great interest to determine whether CFTs exist that are compatible with those flavour and gauge symmetries. Although studying gauge theories with the conformal bootstrap involves several complications (see sec. 2.3.2 for a discussion), determining the lower end of the conformal window remains one of the dreams of the program.

Critical Ising

The Ising model is a cornerstone of statistical physics. We will keep our discussion of it succinct and closely bound to the critical point, where it can be described as a CFT.

This model can be described by a lattice of "spins" σ that can take the values ± 1 and the Hamiltonian

$$H(\sigma_i) = -J \sum_{\langle ij \rangle} -\sigma_i \sigma_j, \tag{2.2.32}$$

where the sum runs over all the first neighbor pairs $\langle ij \rangle$. This system has the partition function

$$Z = \sum_{\{\sigma_i\}} e^{H(\sigma_i)/T} \tag{2.2.33}$$

where we sum over all the configurations of spins in the lattice. From here we can see that the system presents two phases, a disordered one for small J/T and an ordered one for large values of this coupling (low temperature). The phase transition can be shown to be of second order and thus is describable as a CFT. This model has been shown to describe interesting physical systems such as uniaxial magnets and liquid-vapor transitions, among many others.

In $d = 2$ there is an analytic solution for the Ising model due to Onsager [36]. Moreover, the CFT that describes the universality class to which this model belong is the $\mathcal{M}(4,3)$. On the other hand, in $d = 3$ there is no known exact solution and only numerical or approximate methods are known.

One of the main representatives of the latter is the $\epsilon-$expansion, which uses that fact that the ϕ^4 scalar theory belongs to the same universality class and thus one can take the following action

$$S = \int \mathrm{d}^d x (\partial\phi)^2 + \frac{m}{2}\phi^2 + \frac{g}{4!}\phi^4 \tag{2.2.34}$$

and perform perturbation theory around the free theory. This is a sensible thing to due since the for $\epsilon = 0$ the ϕ^4 is marginally irrelevant and thus the theory flows towards $g = 0$ in the IR. Computing the beta function for g we have

$$\beta(g) = -\epsilon g + \frac{3}{16\pi^2} g^3 + O(g^5) \tag{2.2.35}$$

which has a zero for

$$g_* = \frac{16\pi^2}{\epsilon} + O(\epsilon^2) \tag{2.2.36}$$

which implies the existence of a fixed point for every ϵ (known as the Wilson-Fisher fixed point). This approach, when combined with more advanced machinery like resummation techniques can give surprisingly precise results (see, e.g. [37]).

It might seem that analytic continuation in d is just a tool to obtain results for $d = 3, 2$, but this is not necessarily the case. Since the fixed points exist at any value of $\epsilon > 0$ we have a continuum of CFTs instead. Although they have been proven not to be unitary (see e.g. [38]), they are of theoretical interest nonetheless.

Moreover, the existence of this continuum of CFTs implies that the spectrum of the Ising should be related to that of the free scalar field in $d = 4$. After all, the anomalous dimension of these operators for $\epsilon \neq 0$ is not expected to create discrete changes on the spectrum. From the Lagrangian (2.2.34) we also see that this theory will have a $\mathbb{Z}_2-$symmetry under which $\phi \to -\phi$. Thus, from analyzing the spectrum of the free theory in $d = 4$ we can see that the leading $\mathbb{Z}_2-$odd scalars will be ϕ, $\phi^3 \sim \Box\phi$ and so on, meanwhile for the even sector we should have ϕ^2, ϕ^4 and so forth.

Summarizing, the $d = 2, 3$ critical Ising models can be shown to belong to a one-parameter family of CFTs related to the free scalar field in $d = 4$. It is customary to denote the leading $\mathbb{Z}_2-$odd operator (related to ϕ) by σ and the lightest $\mathbb{Z}_2-$even scalar (equivalent to ϕ^2) by ϵ.

$O(N)$ models

A generalization of the action in (2.2.34) is to consider N fields ϕ_i transforming as a vector of $O(N)$ and with a quartic interaction $\sim (\phi_i\phi^i)^2$. Naturally, the lattice construction can also be generalized to an N dimensional spin in each point and for each N the universality class is the same.

For small N these models are also of experimental relevance. For example, in $d = 3$ the $O(2)$ model describes the superfluid ^{4}He transition whereas the $O(3)$ case models isotropic ferromagnets.

More concretely, we can consider the following action

$$S = \int \mathrm{d}^d x \frac{1}{2}(\partial\phi)^2 + \frac{1}{2}r(\partial\phi)^2 + \frac{1}{4!}\frac{u}{N}(\phi^2)^2 \tag{2.2.37}$$

and perform a similar analysis to that we described earlier for the Ising model (which can be considered the $N = 1$ case). Namely, in $d = 4 - \epsilon$ a WF fixed point exists and one can use renormalization group techniques to explore perturbatively the CFT that "lives" there. Moreover, the large N limit provides a useful check of the validity of the ϵ expansion for $\epsilon \sim 1$ (see [39] for an extensive review).

In this case, the spectrum of the theory is richer since the symmetry structure has to be taken into account. For example, in the OPE of two vectors $\phi_i \times \phi_j$ we will have operators transforming as singlets s, symmetric two-index tensors $t_{(ij)}$ and antisymmetric two index tensors $a_{[ij]}$. The anomalous dimensions of the leading

operators in each channel have been computed perturbatively both in the $1/N$ and ϵ expansions and through numerical methods such as Monte Carlo simulations. They are also the main subjects of interest of the numerical bootstrap, as will be reviewed in section 2.3.2.

Yang Lee edge singularity

Another family of WF fixed points are that of special interest are those obtained from the Lagrangian

$$S = \int \mathrm{d}^d x \frac{1}{2}(\partial\phi)^2 + \frac{1}{2} r(\partial\phi)^2 + \frac{g}{3!}\phi^3 \tag{2.2.38}$$

which flows in the IR to the free theory in $d = 6$ but has a non trivial fixed point in $d < 6$ for imaginary g. This CFT has been shown in [40, 41] to reproduce the critical exponents of the Yang-Lee edge singularity[42]. This statistical model describes the density of zeros of the partition function of the Ising model for imaginary magnetic field, which behave as $(h - h_c)^\sigma$ near the critical field h_c. Here $\sigma = \Delta_\phi/(d - \Delta_\phi)$ is the critical exponent related to the scaling dimension of the field ϕ. Moreover, other critical phenomena are related to the Yang-Lee singularity. For example, the number density of dilute branched polymers follows a critical exponent in d dimensions given by $\varphi(d) = \sigma(d - 2) + 2$ [43] and the pressure of fluids with a repulsive core has a singularity with universal exponent $\varphi(d) = \sigma(d) + 1$[44].

We finally note that this non-unitary CFT is present in $d = 2$ as the minimal model $\mathcal{M}(5, 2)$. This minimal model has only two Verma modules, that of the identity $[\mathbb{I}]$ and that of $[\phi]$ with $\Delta_\phi = -2/5$ and the fusion rule

$$\phi \times \phi = \mathbb{I} + \phi.$$

GFT

One can construct a one-parameter family of CFTs by considering the free scalar ϕ in d dimensions, whose scaling dimension is $\Delta_\phi = (d-2)/2$ and promoting Δ_ϕ to be a free parameter. In practice this means that all correlation functions constructed from this field will be computed through Wick contractions. For example, given that

$$\langle \phi(x_1)\phi(x_2)\rangle = \frac{1}{|x_1 - x_2|^{2\Delta_\phi}} \tag{2.2.39}$$

we will have that the next non trivial[5] correlation function will be

$$\langle \phi(x_1)\phi(x_2)\phi(x_3)\phi(x_4)\rangle = \frac{1}{|x_{12}|^{2\Delta_\phi}|x_{34}|^{2\Delta_\phi}} + \frac{1}{|x_{13}|^{2\Delta_\phi}|x_{24}|^{2\Delta_\phi}} + \frac{1}{|x_{32}|^{2\Delta_\phi}|x_{14}|^{2\Delta_\phi}} \tag{2.2.40}$$

[5]Naturally, the 3−pt function vanishes because there are no Wick contractions to be done and conformal invariance implies $\langle\phi\rangle = 0$.

It is important to note that this theory will be non local and thus the term "field" might not be appropriate. However, this theory is important as a benchmark and also plays an important role in the AdS/CFT correspondence.

2.3 Conformal Bootstrap

We now come to the main topic of this dissertation. Our discussion of this research program will be split in two subsections. First, in sec. 2.3.1 we will review the most important numerical methods developed to extract physical information from the crossing equations described at the end of section 2.1. The applications of these methods will be at first only superficially mentioned. A full review of the most important results of the bootstrap program will then be undertaken in 2.3.2.

2.3.1 Numerical Methods

One of the biggest field of development inside the bootstrap community has been the use of numerical techniques to get approximate or –in some outstanding cases– rigorous results on the characteristics of CFTs. In what follows we will discuss in a mostly chronological order the developments of the last 14 years.

Linear Programming Bounds

In 2008, [11] tried to answer a fairly simple question. Given a scalar field ϕ in $d = 4$ with scaling dimension Δ_ϕ, what is the smallest dimension of ϕ^2 (defined as the lightest scalar exchanged in the OPE $\phi \times \phi \sim 1 + \phi^2 + \dots$) consistent with conformal symmetry? Although the question was phenomenologically motivated, the method introduced for answering it would lead to the creation of a new technique for extracting non perturbative information from CFTs. We will now review their setup and the main results of this groundbreaking work.

Let us consider eq. (2.1.19) divided by $I(z)$. One can discretize this equation by taking derivatives with respect to the cross rations and evaluating them, say, at $z = \bar{z} = 1/2$. Thus, we can write schematically

$$\mathcal{F}_{\Delta,\ell}(z, \bar{z}) \to \mathbf{F}_{\Delta,\ell} \in \mathbb{R}^n$$

and transform the functional equation into a linear one that can be written as

$$\sum_{\Delta_\ell} \lambda^2_{\phi\phi\Delta_\ell} \mathbf{F}_{\Delta,\ell} = e_1, \tag{2.3.1}$$

where $e_1 = (1, 0, \dots)$ and the first component of the $\mathbf{F}_{\Delta_\ell}$ is $\mathcal{F}(1/2)_{\Delta_\ell}$, the rest being derivatives.

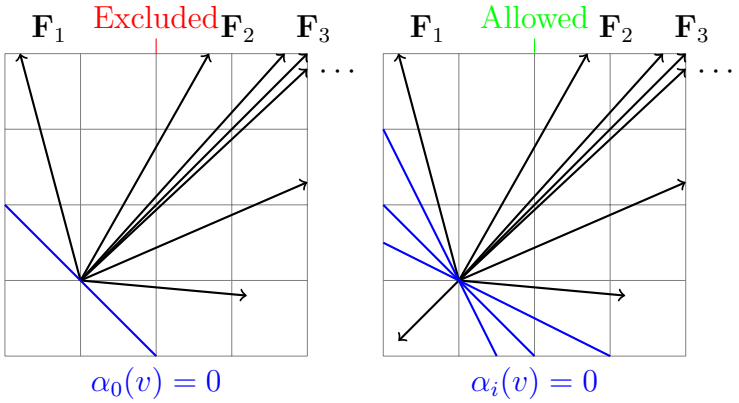

Figure 2.1: Schematic representation of the different vector inequalities that can be solved by Linear programming. In the disallowed case it is clear that the blue line defines a functional satisfying eq. (2.3.2), whereas no such functional can be constructed for the allowed case.

The crucial realization in Rattazzi et al.'s work is that if a linear functional exists such that

$$\alpha(\mathbf{F}_{\Delta_\ell}) \geq 0 \; \forall \; \Delta_\ell \in \mathcal{S}, \tag{2.3.2}$$

then the set $\mathcal{S}$ is rigorously ruled out. In practice $\mathcal{S}$ is a continuous set bounded only by unitarity and a finite number of assumptions that are being tested, e.g. bounds in some sectors. Then, if such a functional is found we know that those bounds are inconsistent. If such a functional does not exist then the method cannot say anything about the proposed bounds. We say informally that the set is "allowed" but that does not mean that using a different number of derivatives will not change this. For pedagogical clarity we show a schematic representation of allowed and disallowed cases in fig. 2.1.

Solving such a set of linear inequalities is a very well known problem in scientific programming and several efficient algorithms exist to deal with them. In [11], the authors used the Simplex Method [45] to determine whether α existed for a given set of values of Δ_ϕ and Δ_0^{min}, the minimum allowed dimension for Δ_{ϕ^2}. The result of this approach can be neatly visualized as a plot on the $\Delta_\phi - \Delta_0^{\text{min}}$ plane where the allowed and disallowed regions are indicated.

This approach was then generalized to theories with global symmetries in $d = 4$ by [46] (see also [47]). Where they studied the $4-$point function of fields transforming in the fundamental of $SU(N)$ or $SO(N)$ groups. The richer structure of these theories allowed for more channels (given by the different index structures that can be constructed with 4 fundamental or antifundamental indices) in which to impose bounds. With a similar logic to the one behind (2.3.2) they placed bounds on OPE coefficients, which in several interesting cases can be related to the different central

charges of the theory.

If we look closely at the method so far discussed, we see that one of the most important elements are the knowledge of the conformal blocks in a practical representation. The authors of [48] managed to exploit some properties of the conformal blocks in order to obtain expressions for their derivatives in arbitrary d. This allowed them to study the parameter space close to the Ising model (see sec. 2.2.2 for a detailed description of this theory) and found that the boundary of the allowed region was smooth except for a "kink" that coincided remarkably to the best estimates known so far. This approach was then generalized to CFTs with global $O(N)$ symmetry by [49] where they found analogous kinks for each value of N in agreement with the numerical and $\epsilon-$expansion results for small N and with the large $N-$expansion ones for larger values. These kinks would become a recurrent story in the study of the conformal bootstrap.

Semidefinite Programming Bootstrap (SDPB)

Although the results presented in the previous subsection are impressive in and of themselves, they are limited to the study of correlators of identical operators. This arises because in that case all the OPE coefficients λ appear squared, and this allows one to define a new variable $\rho \equiv \lambda^2$ with respect to which the crossing equations will be linear. However, we must bear in mind that CFTs are composed of more than one single scalar field –let us call it ϕ for the sake of the argument– and that selection rules usually limit which sectors can appear in the $\phi \times \phi$ OPE. Thus, in order to use the full power of conformal symmetry, another approach was needed.

We will set the stage for our discussion of this new method by considering two scalar primaries in a CFT, ϕ_1 and ϕ_2. Let us denote by $\lambda_{ij\mathcal{O}}$ the 3−pt function coefficient of $\langle\phi_i\phi_j\mathcal{O}\rangle$. If we consider the 4−point function defined by $\langle\phi_1\phi_2\phi_2\phi_1\rangle$ its expansion in the $s-$channel will be schematically of the following form:

$$\langle\overbrace{\phi_1\phi_2}\overbrace{\phi_2\phi_1}\rangle \sim \sum_{\mathcal{O}} \lambda^2_{12\mathcal{O}} g^{\Delta_{12},\Delta_{21}}_{\Delta_{\mathcal{O}},\ell_{\mathcal{O}}}, \tag{2.3.3}$$

where $g^{\Delta_{12},\Delta_{21}}_{\Delta_{\mathcal{O}},\ell_{\mathcal{O}}}$ is the conformal block for the $\mathcal{O}$ term in the OPE expansion of $\phi_1 \times \phi_2$, we omitted the dependance on the cross-ratios and $\Delta_{ij} = \Delta_i - \Delta_j$ are the differences between the external dimensions of the ϕ_i. The $t-$channel, on the other hand, will have the following expansion:

$$\langle\overbrace{\phi_1\overbrace{\phi_2\phi_2}\phi_1}\rangle \sim \sum_{\mathcal{O}} \lambda_{11\mathcal{O}}\lambda_{22\mathcal{O}} g^{0,0}_{\Delta_{\mathcal{O}},\ell_{\mathcal{O}}}. \tag{2.3.4}$$

From here we can clearly see that the crossing equations for non-identical scalars are an intrinsically quadratic problem.

However, one can still recover some sort of positivity from the system of crossing equations of non-identical scalars. For example, we can includeee the $4-$pt functions $\langle\phi_1\phi_1\phi_1\phi_1\rangle$ and $\langle\phi_2\phi_2\phi_2\phi_2\rangle$, with which we can build the following expression for the crossing equations

$$\sum_{\mathcal{O}} \left(\lambda_{11\mathcal{O}}\lambda_{11\mathcal{O}}\right) \begin{pmatrix} A_{\Delta_\mathcal{O},\ell_\mathcal{O}} & B_{\Delta_\mathcal{O},\ell_\mathcal{O}} \\ C_{\Delta_\mathcal{O},\ell_\mathcal{O}} & D_{\Delta_\mathcal{O},\ell_\mathcal{O}} \end{pmatrix} \begin{pmatrix} \lambda_{22\mathcal{O}} \\ \lambda_{22\mathcal{O}} \end{pmatrix} + \lambda^2_{12\mathcal{O}} E_{\Delta_\mathcal{O},\ell_\mathcal{O}} = 0, \tag{2.3.5}$$

where $A, B, C, D, E \in \mathcal{F}$ will be different linear combinations of the conformal blocks, $\mathcal{F}$ being the space of functions of the region where both channels converge.

In a problem of this case, one can look for functionals $\alpha : \mathcal{F} \to \mathbb{R}$ such that

$$\begin{pmatrix} \alpha(A_{\Delta_\mathcal{O},\ell_\mathcal{O}}) & \alpha(B_{\Delta_\mathcal{O},\ell_\mathcal{O}}) \\ \alpha(C_{\Delta_\mathcal{O},\ell_\mathcal{O}}) & \alpha(D_{\Delta_\mathcal{O},\ell_\mathcal{O}}) \end{pmatrix} \tag{2.3.6}$$

is a positive semidefinite matrix. If one demands moreover that $\alpha(E_{\Delta_\mathcal{O},\ell_\mathcal{O}}) \geq 0$ one can apply the familiar bootstrap logic and rule out certain conditions on the spectrum.

Although [49] and [50] had already used Semidefinite Programming as means to dealing with the infiniteness of the parameter space in Δ and ℓ, [27] were the first ones to apply it to a multicorrelator problem. In this seminal paper they bounded the scaling dimensions of the two relevant scalar operators of the $d = 3$ Ising model (known as Δ_σ and Δ_ϵ in the literature) and showed they were confined to a small "island" that roughly corresponded to the kink found in the single correlator studies (cf. previous subsection). Here we must clarify that the shape of these islands depended on the assumptions of the higher dimensional spectrum.

These first studies were performed with "out-of-the-box" semidefinite solvers. One of the first bootstrap revolutions took place when Simmons-Duffin developed a highly specific program for this sort of problems [16] and obtained the most precise estimates for Δ_σ and Δ_ϵ known at that time. This program was further optimized in [17], adding support for parallel computing.

One of the most important generalizations of this approach is the study of theories with global symmetries, where considering more ellaborate correlators opens up the study of other sectors of the theory. In this respect the results of e.g. [12] show that also in the $O(N)$ models –given certain assumptions on the scaling dimension of higher dimensional scalars) the scaling dimensions of the fundamental vector ϕ_i $(i = 1, \dots N)$ and the singlet s are confined in islands that overlap with the kinks found in single operator studies.

Spectrum extraction

So far we have explored very rigurous methods that given some assumptions on the spectrum could tell us whether that a CFT with those characteristics was consistent with crossing symmetry. This limits the information that can be extracted to a handful of scaling dimensions and OPE coefficients, usually one at a time. In this subsection we will review the approach pioneered by [18] known as the *extremal functional*, which allows obtaining extensive information about the higher-lying operators of a CFT, albeit less rigorously.

Let us consider a generic linear programming bootstrap setup. [6] Recall that inside the allowed region any linear functional α will have at least one vector $\mathcal{F}$ satisfying $\alpha(\mathcal{F}) < 0$. For concreteness let us suppose that we are minimizing the gap in a certain spin channel ℓ. Since in the excluded region any functional should be positive when acting in any vector, it is clear that at the boundary

$$\alpha_0(\mathbf{F}_{\Delta_{\min},\ell}) = 0, \tag{2.3.7}$$

for a specific linear functional. For this fixed α_0 only the operators that satisfy $\alpha(\mathbf{F}_{\Delta_\ell}) = 0$ can contribute to the OPE.

Then, for each spin ℓ we can define a function

$$f_\ell(\Delta) = \alpha_0(\mathbf{F}_{\Delta_\ell}) \tag{2.3.8}$$

whose zeros will give the approximate scaling dimensions of the spectrum at that point of the parameter space.

Although less rigorous than the information obtained from the conventional bootstrap, this method can efficiently show the approximate position of tenths of operators. The most concrete drawback, however, is that its regime of application is limited to the boundary of the allowed region.

Navigator function

In [19], Reehorst et al. built upon the SDPB framework an object they dubbed the "navigator function" which goes beyond the binary information given by the former methods (i.e. excluded vs allowed) and actually says how much a point in the parameter space is allowed or excluded. This then allows for a more efficient exploration of the parameter space, since this function is smooth and well-defined in most of the region of interest and can be minimized straightforwardly.

The general idea behind this function is quite simple. For a given set of assumptions on the spectrum of a putative CFT where the SDPB determines that the theory is

[6] A similar logic holds in SDPB applications, as can be easily shown.

excluded resp. allowed, the navigator function measures how many extra operators should be added in order for the theory to be allowed resp. disallowed. The challenge is the choice of this set of operators in a consistent way that guarantees differentiability for most of the parameter space.

Reehorst and collaborators showed that there are several options that achieve this in a systematic way. One of them consists in adding a term proportional to the first scalar of the Generalized Free Field CFT, that in the case of the $4-$point function of identical scalars with scaling dimension Δ_ϕ would correspond to (in the notation used above) $\mathbf{F}_{2\Delta_\phi,0}$. The constant of proportionality indicates how far away from satisfying the Crossing equations the initial solution was, and as such it is chosen as the navigator function. Moreover, they also develop numerical techniques in order to render more efficient the computation of this quantity.

Gliozzi's method (Determinants)

In his 2014 paper, Gliozzi [20] realized that approximate solutions to the truncated crossing equations could be obtained by analyzing the locii of vanishing maximal-range minors of the matrix $\mathcal{M}$ defined by derivatives of the conformal blocks for a given truncated spectrum. This method gave good results for the FT, the Ising and some non-unitary theories (such as the YL). The relevance of this approach to the work described in this thesis is twofold. First, we also make use of heavy truncations of the exchanged spectrum. Secondly, as will be shown later when discussing the different proposals for a functional to guide our exploration of the landscape of CFTs, we used one that was inspired in Gliozzi's method.

Gliozzi's motivation was to find an analogous set of equations to those found by Vafa [51] in his study of RCFTs in $d = 2$. Although conformal symmetry in $d > 2$ is less constraining, by considering a finite number of primary operators in the OPE of a scalar field with itself and demanding that a a solution to crossing exist one obtains a set of transcendental equations for the scaling dimensions of the proposed operators. This approach gives surprisingly good results in some cases, although it is not clear how to scale it or if every CFT can be studied in this way (a concrete example of a so-called untruncable theory will be exposed in detail later on). More concretely, let us consider a scalar operator ϕ with scaling dimension Δ_ϕ. As seen before, its crossing equations can be written as in (2.1.19),

$$\sum_{\Delta>0,\ell} \lambda^2_{\phi\phi\mathcal{O}_{\Delta_\ell}} \mathcal{F}_{\Delta,\ell}(z,\bar{z}) = I(z,\bar{z}), \tag{2.3.9}$$

with $I(z,\bar{z}) = |z|^{2\Delta_\phi} - |1-z|^{2\Delta_\phi}$, and

$$\mathcal{F}_{\Delta,\ell}(z) = |1-z|^{2\Delta_\phi} g_{\Delta,\ell}(z,\bar{z}) - |z|^{2\Delta_\phi} g_{\Delta,\ell}(1-z,1-\bar{z})\,, \tag{2.3.10}$$

In order to render the symmetries of these equations more manifest, one can perform the change of variables $z = (a + \sqrt{b})/2$, $\bar{z} = (a - \sqrt{b})/2$. Then, considering different derivatives of the crossing equations leads a single inhomogeneous linear equation for the vector of squared OPE coefficients $\rho_a := \lambda^2_{\phi\phi\mathcal{O}_a}$

$$\sum_{a=1}^{N_{\text{Ops}}} \frac{\mathcal{F}_{\Delta_a,\ell_a}(1/2,1/2)}{I(1/2,1/2)}\rho_a = 1 \tag{2.3.11}$$

and an infinite number of homogeneous ones:

$$\sum_{a=1}^{N_{\text{Ops}}} \partial_a^m \partial_b^n \frac{\mathcal{F}_{\Delta_a,\ell_a}(1/2,1/2)}{I(1/2,1/2)}\rho_a = 0, \tag{2.3.12}$$

where $m = 0, 2, 4, \ldots$, $n = 0, 1, 2, 3, \ldots$, $m+n > 0$, are the only non-zero derivatives. If we index the (m, n) pairs arbitrarily by i and take $i = 1, \ldots, M$ and choose an ansatz for the spectrum with $N_{\text{Ops}} < M$ it is easy to see that a vector of squared OPE coefficients ρ_a stasfying (2.3.12) exists if and only if the rank N_{Ops} minors of the $M \times N_{\text{Ops}}$ matrix $\mathcal{M}$ given by

$$\mathcal{M}_i^a = \partial_a^{m_i} \partial_b^{n_i} \frac{\mathcal{F}_{\Delta_a,\ell_a}(1/2,1/2)}{I(1/2,1/2)} \tag{2.3.13}$$

vanish. This implies in turn a set of transcendental equations for the scaling dimensions of the proposed spectrum.

It must be pointed out that not all of the $\binom{M}{N_{\text{Ops}}}$ minors will give independent constraints due to the Plücker relations, as noted in [52]. On the other hand, some of the scaling dimensions might be fixed due to the theoretical knowledge of the model, and thus, in most cases, taking $M \sim N_{\text{Ops}} + 2$ is usually enough to determine all the unknown Δs. In the overdetermined case, one could use different sets of minors to compute several approximate solutions to crossing. An empirical error could be then obtained from the spread between these different solutions.

The main applications of this approach have so far been mostly confined to non-unitary theories, where the methods so far reviewed are not applicable. For this same reason Gliozzi's method is useful in Boundary Conformal Field Theories where reflection positivity is not present (see, e.g. [53]). In [54] a very thorough exhibition of the applications of this method is presented. Namely, they use it to compute the scaling dimensions of the lowest-lying operators in the Ising model ($d = 2, 3$) and the Yang-Lee edge singularity in $d = 2, 3, 4, 5$ and $6 - \epsilon$.

Several reformulations of this method were proposed. Most importantly, [55] rephrased the existence of a vector of OPE coefficients satisfying crossing as demanding that the smallest singular value of $\mathcal{M}$ were approximately 0. Since minimization algorithms are usually more numerically stable than root-finding ones, this approach is significantly more robust.

Caveats This method, despite being one of the most promising avenues for studying non-unitary theories, suffers from several drawbacks that have hindered its adoption.

Most importantly, it is hard to assign sensible numerical (and most importantly) systematic error to the results. For the former one can use the spread of solutions obtained from different minors, but for the latter there is not a general expression.

Another caveat is the choice of derivatives of the crossing equations to include in the matrix $\mathcal{M}$. It has been pointed out that considering derivatives of too high an order leads to a matrix whose determinants do not vanish. This means in practice that for a given N_{Ops} there is a very restricted window of derivatives that lead to a well-posed problem. It is also possible that some theories might have too many operators at a given Δ^* in order to produce a matrix with vanishing minors at a fixed number of derivatives

There is also the conjecture that not every theory can be studied with this approach (such theories are said not to be "truncable"). A clear example can be found in the $4-$point function of the operator $\phi^2(x) := \phi^i(x)\phi_i(x)$ of a theory with N free scalar fields in $d = 4$. In this case

$$\begin{aligned} \langle \phi^2(x_1)\phi^2(x_2)\phi^2(x_3)\phi^2(x_4)\rangle &= \frac{g(z,\bar{z})}{|x_{12}|^4|x_{34}|^4}, \\ g(z,\bar{z}) = 1 + \frac{4}{N}\left(z\bar{z} + \frac{z\bar{z}}{|1-z|^2} + \frac{(z\bar{z})^2}{|1-z|^2}\right) &+ \frac{(z\bar{z})^2}{|1-z|^4} + (z\bar{z})^2 \end{aligned} \tag{2.3.14}$$

and thus one can easily see that the OPE coefficients for the different operators will depend on a free parameter N. This implies that the information captured by the matrix $\mathcal{M}$ is not enough to fix them, which in turn implies the determinant approach cannot work.

Reinforcement Learning

Recently, Kantor et al. [56, 57] have proposed a novel approach to finding approximate solutions to the crossing equations through reinforcement learning. Given the overlap between their approach and the main work upon which this thesis is based we will now review their method in order to better understand the similarities and differences between the two strategies.

Reinforcement Learning (RL) is a machine learning algorithm in which an *actor* explores an *environment* guided by a *reward* that measures how well a given task is performed by the actor. In this particular application the *actor* must choose a set of truncated conformal data (in their implementation they consider both the scaling dimensions and the OPE coefficients as unkowns) and then assess how well the crossing equations are satisfied by this choice. Thus, the crossing equations

constitute the *environment* of this RL implementation. The *reward* is computed as a weighted average of the error incurred in satisfying the crossing equations. This procedure is iterated and the actor updates a neural network that produces the guesses for the conformal data.

Besides specifying the hyperparameters of the Machine learning programs, this method requires the input of a spin partition (i.e. the number of operators in each spin channel) and a set of intervals for the Δ of each operator. Changing the size of these windows one can use the method in different regimes, ranging from wide, exploratory searches to high precision determination of the conformal data.

With this method the authors find the lowest lying operators of the $\sigma \times \sigma$ OPE in the $d = 2$ Ising CFT (σ being the spin operator, i.e. the lightest $\mathbb{Z}_2$-odd operator) and those of the $U(1)$-current $j \times j$ of an S^1-compactified boson $X(z)$ (here $j(z)\ \partial X(z)$ with very good precision (roughly below 1/100 relative error in most cases). The bootstrap equations of higher-dimensional scalars seem to give more erratic results, most likely due to the slower convergence of the OPE and the need to include more operators.

This method has the clear advantage of working "out-of-the-box" for many settings of interest. In simple cases it gives results with a very good accuracy and the authors point out that improvements in the numerical libraries will surely improve the efficiency of the computations. It remains to be seen whether the parameter space can be scaled indefinitely or whether a bottleneck arises in the learning procedure. It is also important to note that the fact that the method produces a probability distribution that can then be sampled for the different conformal data is on one hand interesting because it might give an idea of the spread of the data, but at the same time obscures the physical meaning of the object being trained with the method.

2.3.2 Applications

Since the seminal Paper [11] the numerical bootstrap has shed light on several mysteries of important relevant CFTs. We now present a by no means exhaustive list of the most important ones. We will focus mostly on non-supersymmetric theories in $d = 3, 4$ and only state briefly other results that we consider nonetheless important to showcase the potential of the bootstrap philosophy.

$d = 3$

This dimensionality is arguably the arena where the numerical bootstrap has performed best. We will center our discussion mostly on the critical Ising model and the $O(N)$ critical models, since they are some of the settings in which the bootstrap

has provided the best results, both in terms of precision and extensiveness.

The critical Ising model (see section 2.2.2 for more details) is one of the simplest non-trivial CFTs in $d = 3$, characterized by a $\mathbb{Z}_2$ symmetry and only one even, relevant scalar ϵ. In [48] it was pointed out that linear programming produced high-precision bounds on the scaling dimension of the relevant scalar ϵ by studying the constraints arising from the crossing equations for the correlator $\langle\sigma\sigma\sigma\sigma\rangle$. The most important feature of this study was the presence of a kink on the plot of the upper bound on Δ_ϵ as a function of Δ_σ in sharp agreement with the best estimates available so far (cf. black continuous line in fig. 2.2). It was also found that this point minimized the central charge c [58].

One of the biggest developments was the use of semidefinite programming for studying mixed correlators. In [27] the constraints of considering the set of correlators $\langle\sigma\sigma\sigma\sigma\rangle$, $\langle\sigma\sigma\epsilon\epsilon\rangle$, $\langle\epsilon\epsilon\epsilon\epsilon\rangle$, in addition to the assumption on gaps in the $\mathbb{Z}_2-$odd sector lead to the discovery of an "island" to which the critical Ising should be confined. Then, [59] used an innovative combination of analytical and numerical methods to yield what was at the time the most precise estimate for the 3d Ising critical exponents.

The wealth of results thus obtained has spurred the growth of a healthy ecosystem of computer programs for solving semidefinite programming problems such as SDPB (reviewed in section 2.3.1)[16] and its upgrade [17]. The latest development in this series is the navigator function [19] (see section 2.3.1) which allowed [60] to bound the scaling dimension of irrelevant operators in the $d = 3$ critical Ising model.

Theories with $O(N)$ symmetry are a natural generalization of the $\mathbb{Z}_2$ case. An interesting difference is that the $4-$point function of identical vectors $\langle\phi_i\phi_j\phi_k\phi_l\rangle$ decomposes into three channels: S for singlets, T for traceless-symmetric two index tensors and A for antisymmetric ones. Moreover, whereas only even spin operators appear in the first two, the antisymmetric channel has only odd spin operators[7]. This is particularly relevant when trying to derive bounds on the central charge with respect to the symmetry current C_J, as will be seen below.

By using linear programming, similar features to those of the Ising model were also found by Kos et al. [49]. In paritcular, a set of kinks were found at values consistent with previous numerical and/or analytical estimates (see fig. 2.2). Then, semidefinite programming was used to study the mixed correlator case ($\langle\phi_i\phi_j\phi_k\phi_l\rangle$, $\langle\phi_i\phi_j SS\rangle$ and $\langle SSSS\rangle$) in [13]. There, the authors found a set of islands (one for each value of N) consistent with the scaling dimensions of the critical models.

Multi-correlator studies admit a larger parameter space and thus render numerical

[7]Recall that in the identical scalar case only even spins contributed.

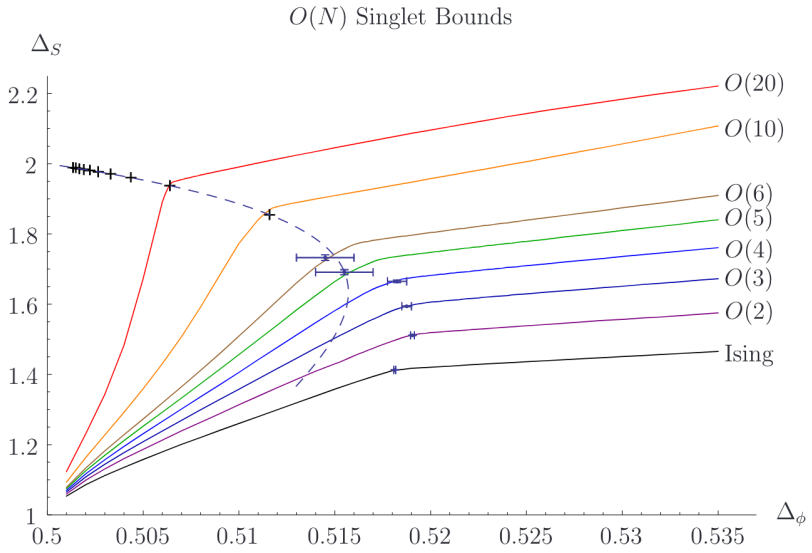

Figure 2.2: Figure taken from [27]. The colored lines show the upper bound for Δ_S, the scaling dimension of the leading singlet of the OPE $\phi_i \times \phi_j$. The error bars represent numerical estimates for the scaling dimensions, whereas the crosses and the dotted lines show the $1/N$ expansion estimate up to third order in Δ_ϕ and second in Δ_S

studies more resource-intensive. To improve the efficiency of these scans, several heuristic algorithms were developed in [61] which allowed the authors to determine the critical exponents of the $O(2)$ model with precision on par with that of MC. This model is particularly relevant for condensed matter since it describes experimental settings such as the superfluid ^{4}He phase transitions. Moreover, there are experimental determinations of the critical exponent related to Δ_S that are in significant tension with the most accurate numerical results, which renders this problem more pressing.

Another case of interest is the $O(3)$ model, where [62] determined the scaling dimensions of several operators and by considering crossing equations of symmetric-traceless operators obtained an upper bound on the scaling dimension of the leading rank-4 traceless operator Φ, namely $\Delta_\Phi < 2.99056$. This is particularly important because it implies that two related fixed points (known as cubic and biconical) are stable. Similarly, systems of correlators including traceless symmetric tensors were analyzed for general N by [63].

To close our discussion of $O(N)$ theories we note that the navigator function was applied to the $O(N)$ archipielago in [64]. and that CFTs with other global symmetries have been studied, e.g. $O(M) \times O(N)$ in [65].

Another class of CFTs of special interest are those with fermionic operators. First, in [66] the 4−point function $\langle\psi\psi\psi\psi\rangle$ (where ψ is a Majorana fermion) was considered and the bounds on the scaling dimensions of the first parity odd and even scalars (denoted by σ and ϵ, respectively) were computed. The exclusion plots produced by this bootstrap analysis show kinks at the same value of Δ_ψ both for Δ_σ and Δ_ϵ. There is no known candidate in this region and besides, the position of the kink would set $\Delta_\sigma, \Delta_\epsilon > 3$ both scalars to be irrelevant, which mean that this CFT would have no relevant scalars at all. To this date, it is still an open question whether this kink corresponds to a physical theory or is instead an artefact.

Studying gauge theories with the conformal bootstrap is less straightforward than it seems because the requirement of studying gauge-invariant operators effectively hides the particulars of the gauge group and thus makes the 4−point function morally equivalent to that of another CFT with the same global symmetry. The most fruitful approach so far is that of considering monopole operators (charged under the topological $U(1)$ symmetry) undertaken by Chester et al.[67]. If one considers the 4−point function of minimal charge monopoles ($|q| = 1/2$) then one can obtain bounds on the scaling dimensions of those with $|q| = 1$.

Besides scalars and fermions, the bootstrap of conserved currents (see, e.g. [68]) and that of the stress energy tensor [69] is another interesting area of inquiry. Naturally, these studies required the development of the conformal block machinery to deal with spinning external operators. These 4−point functions constrain other parity sectors and put more stringent bounds on the central charge and the particle charge under continuous symmetries.

$d = 4$

Although the first works in the numerical bootstrap worked in this dimensionality it must be pointed out that convergence is significantly slower because the unitarity bound restricts the scaling dimension of external operators to be $\Delta_\phi > 1$. Nonetheless, some interesting results have been achieved, mostly in the realm of gauge theories and other phenomenologically relevant models.

The first use of the conformal bootstrap was phenomenologically motivated. In particular, the authors of [11] used linear programming to explore the feasibility of certain models proposed in order to alleviate the hierarchy problem, where the Higgs scalar H is proposed to be a field with $\Delta_H \sim 1$ in the fundamental of the custodial $SO(4)$ but the first singlet S in the OPE $H \times H^\dagger$ has a scaling dimension close to 4, thus requiring a smaller tuning in order to be natural. The seminal work and then [47] imposed very stringent bounds on this kind of models effectively ruling out the settings with the least tuning required.

Regarding theories with global symmetries we highlight the early work of [70], where the technology for analyzing the bootstrap equations of scalars in fundamental representations of $SO(N)$ and $SU(N)$ groups was explored. The work of Caracciolo et al. is also relevant. There, the authors of [71] used semidefinite programming to obtain bounds on the OPE coefficients for conserved currents in theories with $SU(N)$, $SO(N)$ and $SO(N) \times SO(M)$.

Gauge theory in $d = 4$ is arguably the cornerstone of our microscopic understanding of nature. Although the standard model itself is not a CFT, it is expected some of its less understood components (e.g. QCD at low energies) could be elucidated by understanding the limits in which they are indeed a CFT. In that respect, Nakayama [72] used the $4-$pt function of a meson (a gauge invariant product of fermions that transforms in the bifundamental of the flavour symmetry) to determine its minimum scaling dimension while demanding that the IR fixed point be self-critical, i.e. that no flavour-neutral scalar with $\Delta < d = 4$ be present.

Another interesting application of the bootstrap program is to study the $4-$point function of Majorana fermions and determine whether conformal symmetry is more or less constraining than Pauli's exclusion principle [73]. In the realm of fermionic correlators we must also highlight the work of Karateev et al.[15] where the $4-$point function of Weyl fermions was analyzed. This correlator has a richer Lorentz structure and thus explores representations that do not appear in scalar correlators, thus allowing them to place bounds on their scaling dimensions and OPE coefficeints. In this work they also analyze the analytical structure of the conformal blocks and realize that some discontinuities previously discovered in other fermionic studies were due to the so-called "fake primary effect".

Non-integer dimension

Although non-unitary, CFTs in general d are of theoretical interest and might help uncover the inner workings of some models. For example, in [74] the critical Ising model for $2 < d < 4$ was studied with SDPB and the scaling dimensions of the leading operators were extracted from the extremal functional. This works shows how the spectrum of these CFTs interpolates from that of the free scalar field in $d = 4$ to that of the $\mathcal{M}(4, 3)$ minimal model in $d = 2$.

Similarly we have [75] [76] [77] [78] that studied different aspects of the CFTs defined by the UV fixed points of $O(N)$ models in $d > 4$. These CFTs are in a somewhat looser footing than the WF fixed points present for $d < 4$ but under reasonable assumptions can be detected by the conformal bootstrap. Analogously, [79] explored ϕ^3 theories for $d > 6$.

Non-unitary Theories

In this respect the most outstanding results are due to Gliozzi's method [20]. Most specifically, this approach has managed to determine some of the critical exponents in the Yang-Lee model [54]. In $d = 2$ this theory is exactly known since it corresponds to the $\mathcal{M}(5, 2)$ non-unitary minimal model, but for $d > 2$ there are only approximate or numerical results. In the $d = 2$ the *determinant method* gave results in good agreement with the exact values, which lends trust to the results obtained in greater d, some of which were not computed before. This method was also applied to boundary theories, where positivity is not present. For example, in [53] the authors obtained the lowlying spectrum of boundary CFTs related to the Ising model.

There have also been evidences that other methods like the extremal functional might be able to find the spectrum of non-unitary theories, but this approach has not yielded consistent results yet.

Other applications

We finally summarize in this subsection some interesting results that were not fit for the previous ones.

For example, the bootstrap has helped gain insight into the spectrum of $(2, 2)$[80] and $(4, 4)$[81] superconformal theories in $d = 2$, while $\mathcal{N} = 2$, $d = 4$ SUSY theories were studied in [82].[8] It is also important to highlight the exploration of the supersymmetric version of the YL model in [83].

We finally note that the bootstrap philosophy can also be applied to other physical systems that do not exhibit conformal symmetry but where some kind of crossing symmetry allows for the writing of certain equations in a semidefinite programming language. For example amplitudes in Mellin space[84], S-Matrix[85], and certain mass-gapped theories in $d = 2$[86] and $d = 4$[87].

Another application that deserves mentioning is that proposed in [88], where a fast algorithm for determining hundreds of operators in the spinless modular bootstrap was devised. This was applied to the spherepacking problem in [89]. And then improved in [90] to deal with spin. Although it must be pointed out that in this case the results are less striking.

[8] This is naturally only a small sample of the great amount of work done in SCFTs, which also includes all the technology regarding superconformal blocks. Unfortunately we cannot review it in depth since it deviates from the main subject of this work.

Chapter 3

Numerical Methods

In this chapter we will describe some of the numerical methods used in our work. Although many of them predate the invention of the modern computer (some of them by several centuries) most of them saw a renewed interest with the technological developments of the last century, leading to improvements which we will briefly describe.

In the first section we will describe deterministic methods for minimizing functions. Most emphasis will be on the Levenberg-Marquardt algorithm, an improvement of the Newton-Rhapson method that makes it more efficient in finding minima. The second section will deal with stochastic methods, specifically with the Metropolis Monte Carlo algorithm. This algorithm is the core tool of the scientific enterprise reported in this thesis.

This discussion will try to be as general as possible, refraining from mentioning the bootstrap equations whenever possible. The methods described in this chapter will then be crucial for the protocol presented in sec. 5.2.

3.1 Deterministic methods

We will now review shortly some important deterministic methods for minimizing functions. These methods will in general be straightforward to implement but have certain caveats regarding the convergence rate and the sensitivity to the initial conditions.

3.1.1 Gradient Descent

This method is possibly one of the most straightforward ones for minimizing differentiable functions. Given a $\mathcal{C}^1$ function $f(x) : \mathbb{R}^n \to \mathbb{R}$ and a point x_i the steepest

descent method finds x_{i+1} by computing the gradient $\nabla f(x_i)$ and moving in the direction opposite to it, either by a small step or by performing a line search and finding the minimum along the segment parametrized by $x_i - a\nabla f(x_i)$ with $a > 0$.

Although this method is very efficient for a certain kind of functions, for very anisotropic ones the landscape hinders the advancement of the method up to rendering it nearly useless. For example, moving along narrow, curved valleys is notoriously difficult with this method. (See e.g. discussion in chapter 10 of [45]).

3.1.2 Newton Rhapson

The Newton-Rhapson algorithm is a way of finding the local minima of $\mathcal{C}^2$-functions with a positive definite Hessian H. It must be noted that most sources report it as a root-finding algorithm, but the roots of the gradient are indeed the location of critical points; whether they are minima, maxima or saddle points depends on the properties of the Hessian. We will now discuss the basic idea behind this method and the implementation used in this work.

In short, the method uses the Hessian matrix to approximate the function to be minimized up to quadratic order and solves iteratively for the minimum of this hyper paraboloid. In this work a modified version of this method is used (known as the Levenberg–Marquardt algorithm [91, 92]), in which a damping factor β interpolates between gradient descent and the bare Newton-Rhapson method, avoiding the overshooting of the minimum when very close to it. This is necessary because, due to numerical noise, some eigenvalues of the hessian might not be positive, which violates the conditions for the convergence Newton-Rhapson method. We must point out that this dampening is not ad-hoc, but instead arises from adding a quadratic term to the action penalizing large movements in the parameter space, as can be seen in [91].

We now describe concretely the implementation that will be used in the main body of this text. This should also help make the above discussion clearer. Let $f(x) : \mathbb{R}^n \supset U \to \mathbb{R}$ be a twice-differentiable function. Given an initial guess x_0 we find the next point by using the following formula:

$$x_1 = x_0 - \left(H(x_0) + \beta\mathbb{I}\right)^{-1} \cdot \nabla f(x_0)\,. \tag{3.1.1}$$

At each step, if $f(x_1) < f(x_0)$ then β is decreased by a factor of 3. Otherwise it is increased by a factor of 2. This is known in the literature as "Delayed gratification" [93] and gives stable results in the minimization problems explored in this work.

The rule for updating β deserves some further clarification. Since one can imagine that at a local minimum the algorithm will start rejecting any step, β will then grow

exponentially. This gives then a natural termination condition for the algorithm: when $\beta > 10^6$ it is clear that a stationary point has been reached.

3.2 Stochastic optimization

Deterministic methods as the ones exemplified above are the most natural solution for convex functions with one single basin of attraction. For more general functions, and specifically for higher dimensional parameter spaces where several minima are expected to be present, these methods suffer from poor convergence rates and high sensibility to the initial conditions. Since we are interested in characterizing a representative subset of the minima of a function defined in a high dimensional parameter space, it is clear that more sophisticated tools are needed.

In this thesis we will make heavy use of stochastic optimization algorithms, which can overcome some of the ailments common to most deterministic methods. We will concentrate mostly on the Metropolis-Hastings algorithm, which is one of the most powerful methods for Markov Chain Monte Carlo and is the one used in chapters 4 and 5. To this end we introduce the concept of Markov Chains in section 3.2.1 and then describe how this algorithm generates configurations with the desired properties in section 3.2.2.

3.2.1 Markov Chains

Markov Chains are a cornerstone of many statistical methods and a subject of wide research themselves. We will briefly summarize in this subsection the key definitions and properties that will be necessary for proving that Markov Chains generated with a Monte Carlo method follow a distribution that will be useful in stochastic optimization. We will follow loosely the presentation in [94].

A Markov Chain (MC) is a set of states X_t, $t \in \mathbb{N}$ related by a *transition kernel* $K(x, y)$ such that

$$p(X_{t+1} = x | X_t = y) = K(y, x). \tag{3.2.1}$$

This means that the distribution of X_{t+1} can be computed as

$$X_{t+1} \sim p_{t+1}(x) = \int \mathrm{d}y \, K(y, x) p_t(y) \tag{3.2.2}$$

We say the chain is time homogeneous because K does not depend explicitly on t. The ordered set of states $\{X_t\}$ is a Markov Chain because p_{t+1} depends only on the value taken by X_t and not all the previous elements in the chain.[1]

[1] Although continuous-time Markov Chains exist, we will limit this discussion to discrete time ones, since they are the most relevant for numerical simulations.

In some cases (and in particular, in those relevant to the Monte Carlo methods) there will be a stationary distribution π such that if $X_n \sim \pi$ then $X_{n+1} \sim \pi$. Moreover, this distribution might be limiting in the sense that for large enough n $X_n \sim \pi$ regardless of x_0. For this to happen, K must satisfy the property of detailed balance. Namely,

$$K(x, y)\pi(x) = K(y, x)\pi(y). \tag{3.2.3}$$

This is actually related to a requirement about the reversibility of the chain generated by K, but for the applications in this work it suffices to know that indeed, if we set $p_t = \pi$ in eq. (3.2.2) then (3.2.3) guarantees that π will be the invariant distribution of K.

3.2.2 Metropolis-Hastings

The Metropolis-Hastings algorithm is one of the most widespread approaches for generating Markov Chains that reproduce a given probability distribution. We will first sketch the algorithm steps and then show why they define a transition kernel that satisfies the detailed balance condition stated in the previous subsection.

Given a function $f(x) : U \to \mathbb{R}$, where $U \subset \mathbb{R}^n$, this algorithm generates a Markov chain with initial point $x^{(0)} \in U$ and thence moving randomly by proposing an update

$$x^{(1)} = x^{(0)} + \delta x\,, \tag{3.2.4}$$

which is accepted with a probability given by

$$P(x^{(0)} \to x^{(1)}) = \min\left(1, \exp\left(-\frac{f(x^{(1)}) - f(x^{(0)})}{T}\right)\right)\,. \tag{3.2.5}$$

Here T is a positive constant whose role will become clear shortly.

In order to make contact with the previous discussion on Markov Chains, we must see how the transition kernel of this algorithm looks like. To obtain this we need, besides the probability shown in (3.2.5), the distribution from which δx is sampled. More concretely, if the proposed step is sampled as $x_{t+1} = x_t + \delta x$ with $\delta_x \sim g(x_t, x_{t+1}) - x_t$ we will have

$$K_{MH}(x, y) = g(x, y)P(x \to y). \tag{3.2.6}$$

It is straightforward to prove that as long as $g(x, y) = g(y, x)$, the kernel K_{MH} defined above satisfies eq. (3.2.3) with invariant density $\pi(x) = \exp(-f(x)/T)/Z$. We note in passing that it is possible to define a more general $P(x \to y)$ probability such that the symmetry requirement on g can be relaxed, but this is not needed for the applications explored in this work.

We see here immediately one of the great advantages of this method: there is no need to compute the normalization factor Z when generating a sample with Markov

Chain Monte Carlo (MCMC). This might not seem so striking at first, but for high dimensional spaces computing the integral for normalizing π might be too costly to be practical. On the other hand, we also see that in order to get any meaningful information about f, T must be chosen carefully, and in order for the empirical distribution obtained from the Markov Chain to converge to π, the number of steps must be long enough and the function $g(x, y)$ must be carefully chosen.

Let us now further discuss the role of T. Suppose that the at some point t of the chain x_t is close to a local minimum of f. If this is the case, then there must be a lowest barrier height Δf required to "escape" the minimum. Analyzing K we can see that the number of steps needed to escape this minimum will grow at least exponentially wrt to Δf. This makes it clear that in order to efficiently sample the whole domain we must use higher temperatures. On the other hand, the limit $T \to \infty$ trivially erases all the information about f, so T cannot be taken arbitrarily large. In practice one explores the behaviour of the chains for different values of T and chooses the one that seems to explore local minima for an appropriate amount of time without remaining frozen in any of them. We show more specific examples of these different kind of behaviours in section 5.2.1.

We also mention two more systematic approach to dealing with the choice of T. The first one of them is *simulated annealing* (see [45] for a thorough description). As the name indicates in this method the simulation starts at a high value of T and gradually relaxes to lower values. On the other hand *replica exchange* (also known as *parallel tempering*) is a method first proposed by [95] where M copies of the system are evolved in parallel with different temperatures T_i. At certain points an exchange of two copies is proposed, say $x_i \leftrightarrow x_j$. This exchange is accepted with a probability given by

$$\min\left(1, \exp\left[\frac{f(x_i)}{T_i} + \frac{f(x_j)}{T_j} - \frac{f(x_j)}{T_i} - \frac{f(x_i)}{T_j}\right]\right). \tag{3.2.7}$$

In short, if exchanging the two replicas results in a smaller overall value of the ensemble average of f then the move is accepted. This allows for sampling both the high and low regions of f without suffering from "freezing".

In what respects the choice of $g(x, y)$ it is widely believed that achieving an acceptance-rejection rate of 1 is the most efficient way to obtain a Monte Carlo that converges to the stationary distribution. To achieve this one can use different functional forms for g. For example, having $g(x, y) \propto \exp((x-y)^2/\sigma^2)$ with an appropriately chosen σ is a common choice. In this work we will use a uniform distribution on the interval $[x - a, x + a]$ and implement the following update rule for the width a:

$$a \to a' = \begin{cases} a * \kappa & \text{if the move was accepted} \\ a/\kappa & \text{otherwise.} \end{cases} \tag{3.2.8}$$

Here $\kappa > 1$ is a constant that must be chosen beforehand. In practice any value around 1.1 is good enough. As long as f does not have any pathological features (and κ is not chosen too large) this update rule guarantees that in the stationary state roughly 50% of the steps will be accepted.

Performing the optimization So far we have been very general about the role of f. We will now specialize to an action $S : \mathrm{R}^n \supset U \to \mathrm{R}$ whose minima we want to determine. It is clear that the maxima of $P(x) = \exp(-S(x)/T)/Z$ correspond to minima of $S(x)$. However, the result of the algorithm describes so far is not $P(x)$ itself but a sample drawn from a probability distribution that resembles it in the large N limit. In order to recover the possible minima of S we take inspiration from the work of [96] and analyze the points that have a great number of nearest neighbors with a higher action. These are quite likely to be local minima of S.

For concreteness, suppose we have a sample $\{x_t\}$ with $t = 1, \ldots N$. For each x_t we can define

$$d_m(x_t) = \min_{x_i \neq x_t,\, S(x_i) < S(x_t)} |x_i - x_t|$$

as the distance to the nearest point with lowest action. We can then define the ranking of each point x_t as follows:

$$\rho(x_t) = \frac{1}{N} \sum_{x_j \neq x_t} \theta \left(d_m(x_t) - |x_j - x_t| \right)$$

effectively counting the number of points in the sample with higher action but closer to x_t than the closest point with lower action.

The validity of this approach is justified by the following reasoning. From the above discussion about escaping local minima, it is clear that if the trajectory passes through a point contained in the attraction basin of a minimum x_m, then the algorithm will sample several steps in the neighborhood before escaping this basin of attraction. A list of approximate values for the different local minima x_m can be then recovered from the trajectory by sorting all the points by decreasing value of ρ and considering those points with $\rho > \rho_c$.

The determination of ρ_c is not straightforward, but it is usually feasible to be conservative by choosing relatively small value and then checking a posteriori the validity of the different putative minima. The stability of these points can be assessed by a secondary minimization which could be either one of the deterministic ones described in sec. 3.1 or an MC with very small T. If starting from a putative minimum leads to a stable configuration we can declare it a true minimum within the numerical precision used. If our initial list of x_m includes too many points (i.e. ρ_c was chosen too low) then the points with smaller ρ will either converge to other minima or belong to runaway directions. If reducing ρ_c further does not change the final set

of stable minima we can then be certain that no relevant features of the landscape are being neglected.

Chapter 4

Minimizing Determinants

4.1 Motivation

Drawing inspiration from Gliozzi's work, our first approach was to make the action to be minimized proportional to a sum of the different minors of the matrix constructed with the truncated crossing equations. Since one of the bottlenecks of the original implementations was solving for the zeros of highly nonlinear functions, we explored the hypothesis that stochastic optimization techniques could be more efficient than the standard algorithms provided in `Mathematica`'s `FindRoot`.

In the following sections we will describe two attempts to use stochastic optimization in order to find approximate solutions to the crossing equations. First, in section 4.2 we implement a method that mimicks Gliozzi's approach, in that the matrix elements are obtained through different derivatives of the crossing equations. Then, in section 4.3 we will briefly sketch the alternative approach of sampling the space of conformally invariant ratios and how this leads to an action with minima roughly around the Free Theory point but that suffers from many numerical instabilities. Finally, in section 4.4 we will present some remarks on these explorations.

4.2 Determinants on derivatives

4.2.1 Set Up

Our construction is analogous to that of Gliozzi (see sec. 2.3.1) except for the role of the identity column, which we keep as part of the over-constrained linear system instead of dividing the crossing equations by $I(z,\bar{z})$. More concretely, we compute the matrix $\mathcal{M}$ (cf. eq (2.3.13)) as

$$\mathcal{M}_i^a = \partial_z^{m_i}\partial_{\bar{z}}^{n_i}\left(\mathcal{F}_{\Delta_a,\ell_a}(z,\bar{z})\right)\big|_{z=\bar{z}=1/2} \tag{4.2.1}$$

where the identity column is

$$\mathcal{M}_i^0 = \partial_z^{m_i}\partial_{\bar{z}}^{n_i}\left(\mathcal{F}_{0,0}(z,\bar{z})\right)\big|_{z=\bar{z}=1/2}\,. \tag{4.2.2}$$

We must choose a set of derivative orders (m_i, n_i) that satisfy $m+n \equiv 0 \mod 2$ and $m \neq n$. Every other derivative will be zero due to the symmetries of the crossing equations in this form, i.e.$f(x,\bar{x}) - f(-x,-\bar{x})$.

The choice to keep the identity contribution as a column deserves some extra comments. First, we point out that both Gliozzi's (cf eqs. (2.3.11) and (2.3.12)) and our formulation are equivalent. In our case, we demand that the minors vanish because this happens iff a $1-$dimensional system of solutions exists. This degeneracy is then fixed by choosing the coefficient of the identity contribution to be 1.

$$S(\Delta_a) = \log\left(\sum_{m\in\text{minors}(\mathcal{M})} |m|\right). \tag{4.2.3}$$

The role of the log is to ensure the action has a deep minimum when one of the minors gets close to 0. It is important to note that one could also take the logarithm of each minor before summing them, namely

$$\tilde{S}(\Delta_a) = \sum_{m\in\text{minors}(\mathcal{M})} \log|m| = \log\left(\prod_{m\in\text{minors}(\mathcal{M})} |m|\right). \tag{4.2.4}$$

The main issue with an action of this form is that not all the minors need vanish for the $\tilde{S}$ to become greatly negative: as soon as one of them gets close to zero $\tilde{S} \to -\infty$. In our experiments we realized that this is undesirable because it leads to a proliferation of local minima where the Metropolis Algorithm can easily freeze. It must be also noted that all the minors must vanish in order for a solution to the truncated crossing equations to exist.

Our protocol for this approach is to find the minima of eq.(4.3.3) using Metropolis Monte Carlo. Since this has been our first attempt to use stochastic optimization, we start with a very simple protocol:

1. An ansatz for the spectrum, a value of Δ^* and a list of derivatives are taken as input.

2. The temperature for the algorithm is determined by choosing the smallest temperature that guarantees no freezing. This happens when the MC reaches a configuration it cannot escape at a given T. (See 3.2.2 for a more detailed description of this phenomenon.)

3. An integer between 1 and N_{Ops} is sampled randomly and the corresponding Δ_a is changed by a random value sampled from a normal distribution $\Delta_a \to \Delta_a + \delta\Delta_a$, $\delta\Delta_a \sim \mathcal{N}(0, \sigma_a)$. The initial variance for each operator is given by

$$\sigma_a = s\frac{T}{\partial_a S(\Delta_a)},$$

where the overall factor s has to be determined empirically. In our case, we decreased this value until the acceptance rate became small but finite.

4. The action with the modified Δ_a is computed and the move is accepted with a probability given by $\min(1, \exp((S' - S)/T))$. For an accepted move we update $\sigma_a \to \sigma_a(101/100)$. Otherwise, $\sigma_a \to \sigma_a(100/101)$ (cf. eq. (3.2.8)). This guarantees that the average size of the steps will be representative of the profile of S in each coordinate direction.

5. The previous two steps are then repeated.

4.2.2 Results

To exemplify the use of this method we took the CFT of a free scalar field in $d = 4$. After tuning[1] T we obtained a method that converges to the exact values of the CFT with less than 1/1000 error. In this case Δ_σ (the scaling dimension of the external operator) is kept fixed to its exact value. The precise setting that we used was a spectrum of one operator per spin with different ℓ_{max}.

For $\ell_{\text{max}} = 6$ and 6 different derivatives we can start from arbitrary values in a window given by $[\Delta_{\text{FT}}, (1.5)\Delta_{\text{FT}}]$ for each operator and the method will find a consistent minimum in under 5 minutes. We show an example of this convergence in the left panel of fig. 4.1, where in less than 2000 steps all 4 operators have already converged to very good approximations of the exact values (shown by dashed lines). In the right panel we show the evolution of S for all of the 8000 steps. One can appreciate several horizontal segments where the MC "freezes" and for several steps does not find an acceptable new configuration. In general we found that despite using the logarithm of the sum of the minors as an action the curvature of the action close to the minimum was very steep. This was determined by numerical inspection of the action close to the exact values, but can also be appreciated from the sharp decrease of S even after sensible values of Δ have been attained.

By taking the minimum of the run depicted in fig. 4.1 as a starting point we can successively add higher spin operators, using the MC to minimize only the new operator at each step. We show in table 4.1 the scaling dimensions for the operators

[1] In practice, we started several test runs with an array of T values and chose the one that showed the less freezing while still leading to regions of smaller S.

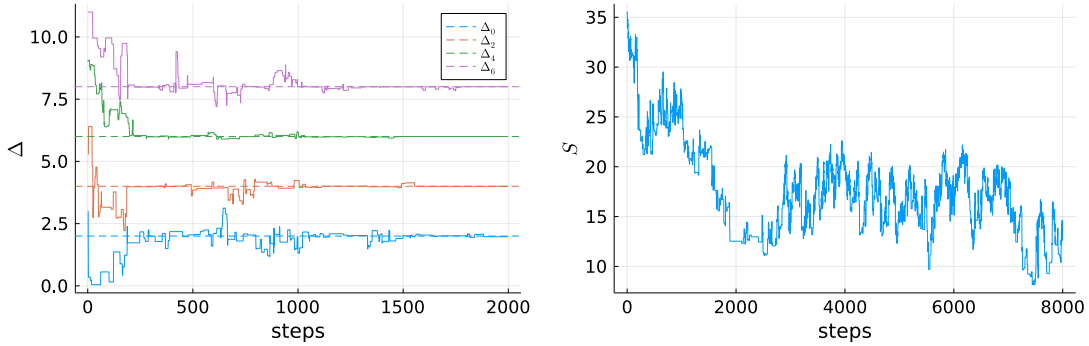

Figure 4.1: Evolution of a Metropolis Monte Carlo search with action (4.2.3). The ansatz consists of one operator per spin (i.e. 1_1_1_1) with the external operator fixed at the exact value ($\Delta_\phi = 1$). 6 derivatives were considered: $((2,0), (3,1), (4,0), (4,2), (5,1), (6,0))$. The Metropolis temperature was $T = 2/3$ and it ran for 8000 steps, taking approximately 8 minutes on a laptop computer. *Left*: Values of Δ for the first 2000 steps. *Right*: Evolution of S. Unlike in the left panel, we display the full extent of the 8000 step run in order to show that S continues to decrease even though the change in Δ is no longer perceivable.

Table 4.1: Scaling dimensions of the first operators appearing in the OPE of σ in the Free Scalar Theory. This configuration corresponds to the lowest action obtained in an 8000 step run.

Δ_0	Δ_2	Δ_4	Δ_6	Δ_8	Δ_{10}	Δ_{12}	Δ_{14}
2.00048	4.00009	5.99999	7.99999	9.999988	11.99998	13.99998	15.99998

up to $\ell_{\text{max}} = 14$ obtained in this manner. This approach can work for higher ℓ_{max} in principle, but the need of using higher order derivatives makes it more time consuming.

4.2.3 Caveats

Using S defined as in eq. (4.2.3) poses a crucial problem for numerical optimization. Namely, we look for configurations where all the minors vanish, but at this point the derivative of the action will behave like m^{-1} and thus the numerical exploration of this region will be highly unstable. While it is true that in a general setting not all minors will vanish at the same point this issue remains a fundamental limitation to the efficient use of this method.

Related to this issue is the fact that even the local minima of S have very sharp features that make escaping them very time-consuming. We tried to alleviate this fact by regularizing the action in different ways. For example, we could "smear" the

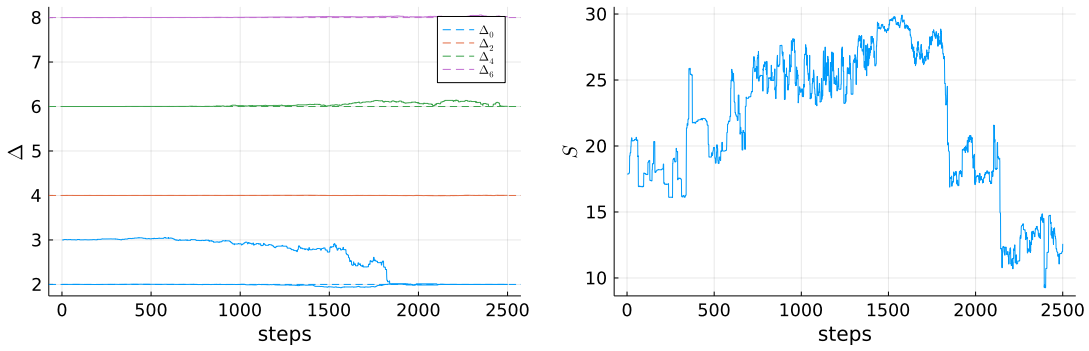

Figure 4.2: Evolution of a Metropolis Monte Carlo search with action (4.2.3). The spectrum is of the form 2_1_1_1 with the external operator fixed at the exact value ($\Delta_\phi = 1$). 7 derivatives were considered: $((2,0), (3,1), (4,0), (4,2), (5,1), (6,0), (5,3))$. The Metropolis temperature was $T = 1$ and the first 2500 steps are shown. *Left*: Values of Δ. One can see clearly how the two scalars (shown in blue) collide around the 2000 step mark. *Right*: Evolution of S. Notice the big drop in the action when the two scalars attain the same Δ.

action along some coordinates, which would look schematically like this:

$$S_{\text{reg}}(\Delta_i) = S(\Delta_i) + S(\Delta_i + \epsilon_i) + S(\Delta_i - \epsilon_i). \tag{4.2.5}$$

This alleviated the problem slightly, but freezing was still an issue. In retrospect, this is hardly surprising, since a logarithmic singularity cannot be resolved by adding a function that behaves locally like a finite constant.

We also found generalizing this approach to more complicated settings quite cumbersome. For example, we tried to determine whether the Yang-Lee non-unitary CFT was amenable to our approach but our results were inconclusive. The biggest problem that we found when trying to analyze theories with more general spectra was that as soon as the ansatz has two or more operators with the same spin, all the minors develop a zero in the region where $\Delta_\ell = \Delta'_\ell$. This makes wide explorations of the landscape more complicated, since one must not only specify the spin partition but have a clear idea of the range in which each operator is expected to lie.

As an example of this problem we can consider a Metropolis Monte Carlo minimization starting from the best solution found for $\ell_{\text{max}} = 6$ in the previous section (i.e. the first four scaling dimensions shown in table 4.1) with the addition of an extra scalar (also shown in blue) at $\Delta'_0 = 3$. We show the evolution of this scenery at $T = 1$ for 2500 steps in figure 4.2. Given that the solution without the extra scalar was a very stable minimum, it is natural that in the beginning the action doesn't change greatly and all the operators except the extra scalar do not vary much. However, around the 1000 step mark the solution becomes unstable and the MC slowly converges to a setting where both scalars have roughly the same dimension. The

action decreases further and some of the previously stable operators destabilize. It is then clear that a blind search with this ansatz will certainly finish a similar scenario.

It must also be said that our method inherits from Gliozzi's approach the problem of choosing the derivatives in a sensible way. One must have $N_{\text{derivatives}} > N_{\text{Ops}}$ in order for our approach to work, but introducing derivatives of higher order spoils the truncability of the crossing equations. This has been studied in more detail by El Showk et al. in [97].

Summarizing, minimizing an action based on derivatives of the crossing equations gave very stable results in the most simple case of a sparse spectrum with one operator per spin but does not have clear handles for generalization.

4.3 Determinants on the space of cross-ratios

4.3.1 Set-up

Our next idea was to construct the matrix from the truncated crossing equations evaluated at different $z-$points and demand that its minors vanished. This worked acceptably well for sparse spectra but if more operators at a given spin were included, it suffered from numerical noise due to the correlations between the elements of the matrix. It was hoped that using a random selection of $z-$points would regularize the $\log -$singularity but the numerical noise overpowers this effect.

More concretely, we consider a matrix $\mathcal{M}$ (the anlogous of eq.(2.3.13))

$$\mathcal{M}_i^a = \mathcal{F}_{\Delta_a,\ell_a}(z_i, \bar{z}_i) \tag{4.3.1}$$

with the identity column as

$$\mathcal{M}_i^0 = \mathcal{F}_{0,0}(z_i, \bar{z}_i) = I(z_i, \bar{z}_i). \tag{4.3.2}$$

Here, the z_i are either taken from a fixed grid or sampled from a normal distribution. The choice of the $z-$ is highly relevant to the shape of the landscape, as we will further discuss in the next chapter.

We must now use the condition $\det \mathcal{M}^a_{i_j} = 0$ (with $i_j \in 1, 2 \dots N_z$ and $j = 1, \dots N_{\text{Ops}}$) to create an action that as a function of Δ_a has a minimum where the crossing equations are best satisfied. As in the previous section, this will look schematically like

$$S(\Delta_a) = \log \left(\sum_{m \in \text{minors}(\mathcal{M})} |m| \right). \tag{4.3.3}$$

To avoid repetition, we will describe only the differences with respect to the approach explored in the previous section (4.2). The rest of the protocol is totally analogous to the one outlined there.

For the MC searches with this action we realized that for $N_{\text{Ops}} \sim 5\ N_z$ had to be of $O(20)$. For smaller values (and most importantly, for points too close to $z = 1/2$) the determinants were often not restrictive enough. This value for N_z makes a straightforward implementation of eq.(4.3.3) highly inefficient since it the number of minors grows factorially with N_z. Moreover, not all of these minors are independent, so considering all of them would not improve the predictive power of our method. In practice we found that considering a fixed number of non-overlapping minors (with $N_{\text{minors}} > N_{\text{Ops}}$) was a good compromise.

Summarizing, instead of choosing a list of derivatives, the $z-$point approach requires fixing N_z and N_{minors}, besides choosing a prescription for sampling the space of conformal ratios N_z times.

4.3.2 Results and caveats

We decided to test this proposal for S with the Free Scalar Theory in $d = 4$, as done in the previous section. Using a similar set-up we could reproduce the Free Theory with similar accuracy although the need to compute such a large matrix $\mathcal{M}$ made it less efficient. When trying to adapt this method to more general spectra we were not able to choose the $z-$points in order to have a well-defined S with noticeable minima in the region of interest. It is clear that the biggest obstruction in the implementation of this approach is the choice of $z-$points. One could wonder how come such a large N_z was necessary in the first place. After careful inspection we can posit the following heuristic explanation. In the $z-$plane, we know that the crossing equations converge the fastest at $z = \bar{z} = 1/2$ (see, e.g. [98]). On the other hand, the crossing equations vanish trivially in this point, and as such in order to obtain sensible matrix elements we must demand that $z, \bar{z} \neq 1/2$, thus going into the regime in which the contribution of higher Δ operators becomes relevant.

Moreover, the crossed conformal blocks $\mathcal{F}$ are continuous functions, and as such the matrix elements of nearby $z-$points will be very similar between them. This calls for a very sensible choice of the z_i. Empirically we found that grids performed better than sampling the points with a normal distribution centered around $1/2$, but even this was still suboptimal when compared to the derivative-based results.

As an illustration of these issues we show the best results in fig. 4.3 with a setting analogous to that of 4.1. The minimum number of $z-$points found to work was $N_z = 8$ but even in this case this approach was a factor of 4 slower than the derivative-based S studied in the previous section, mostly due to the high computational cost of the determinant when the rows are so similar. Concretely, we used 100 digits of precision in the computation of the determinant because otherwise the differences between the rows could not be resolved accurately.

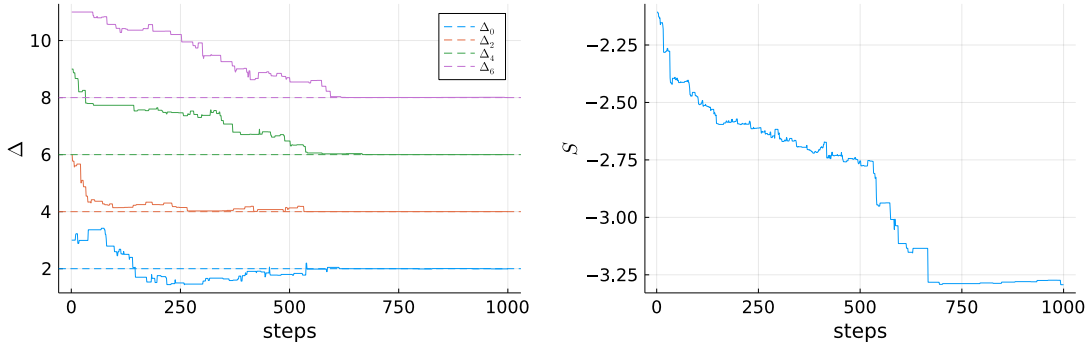

Figure 4.3: Evolution of a Metropolis Monte Carlo search with action (4.3.3). The ansatz consists of one operator per spin (i.e. 1_1_1_1) with the external operator fixed at the exact value ($\Delta_\phi = 1$). The following 8 points in the z plane were used to compute the crossing equations, $0.501 + 0.021i, 0.521 + 0.081i, 0.581 + 0.061i, 0.511 + 0.161i, 0.531 + 0.181i, 0.631 + 0.101i, 0.661 + 0.021i, 0.671 + 0.061i$. The Metropolis temperature was $T = 1/100$ and it ran for 3200 steps, taking approximately 30 minutes on a laptop computer. *Left*: Values of Δ for the first 1000 steps. *Right*: Evolution of S for the same steps.

4.4 Determinant-based actions: the verdict

The aim of this chapter was to illustrate the several non-trivial problems that our project found in the early stages. Since our approach required the truncation of the spectrum, using Gliozzi's method as an inspiration was clearly the most natural starting point. This allowed for a clear comparison with his results.

Our implementation used different combinations of minors computed from derivatives of the crossing equations and alternatively from the crossing equations themselves evaluated in different points around $z = \bar{z} = 1/2$. The action thence computed was minimized through a metropolis montecarlo algorithm. This approach gave very good results when confined to simple spectra, but there were not any clear roads for its generalization. We discovered that making the relevant deep enough to be easily found with our algorithms induced many spurious minima. In short, the main challenge was to concoct an action S that was both numerically stable and representative of the crossing equations. In the next chapter we will show our proposed solution.

Chapter 5

Minimizing Residuals

In this chapter we present the main scientific work on which the thesis is based. We will introduce it by fleshing out the concept of *residuals*, which are nothing but the error when computing the truncated crossing equations. We will begin by motivating in section 5.1 why this is a more robust measure of the quality of a truncated spectrum. This section contains some technical descriptions that might be omitted in a first reading, as they are later summarized in section 5.2, where we focus mostly on the protocol used to produce the results of section 5.3. We close the chapter with some concrete outlooks in section 5.4.

5.1 Introducing residuals

In this section we will review in depth all the ideas and observations that led us to using residuals as the building block for our action. In 5.1.1 we outline the general rationale behind them. Then, in section 5.1.2 we discuss the different options available for normalizing the residuals. In section 5.1.3 we take a small detour to point out the complications of implementing an analogous method but on the derivative space (as opposed to the configuration space). We then present a proof of concept of our method in `Mathematica` in section 5.1.4 and explain why a more efficient way to compute the action is needed, which is then explained in great detail in 5.1.5.

5.1.1 Definition and motivation

Let us consider the crossing equations for 4 identical scalar fields σ with scaling dimension Δ_σ

$$\sum_{\Delta>0,\ell} \lambda^2_{\sigma\sigma\mathcal{O}_{\Delta_\ell}} \mathcal{F}_{\Delta,\ell}(z) = I(z)\,. \tag{5.1.1}$$

Here $\lambda_{\sigma\sigma\mathcal{O}_{\Delta_\ell}}$ are OPE coefficients, Δ and ℓ are the scaling dimensions and spin of the exchanged primary operator $\mathcal{O}_{\Delta_\ell}$ (even spin traceless symmetric tensors), z and $\bar{z}$ are the usual Dolan-Osborn conformal invariant cross ratios [23, 24], $I(z,\bar{z}) = |z|^{2\Delta_\sigma} - |1-z|^{2\Delta_\sigma}$ is the identity contribution to the OPE expansion, and finally

$$\mathcal{F}_{\Delta,\ell}(z) = |1-z|^{2\Delta_\sigma} g_{\Delta,\ell}(z,\bar{z}) - |z|^{2\Delta_\sigma} g_{\Delta,\ell}(1-z,1-\bar{z})\,, \tag{5.1.2}$$

with $g_{\Delta,\ell}(z,\bar{z})$ the conformal blocks, normalized as in [11] with an extra 2^ℓ factor (cf. eq. (2.1.23) for the explicit expression in even dimension).

If we truncate the spectrum and consider only operators up to a given scaling dimension we must account for an error in the crossing equations and eq. (5.1.1) now becomes

$$\sum_{\Delta<\Delta^*,\ell} \lambda^2_{\sigma\sigma\mathcal{O}_{\Delta_\ell}} \mathcal{F}_{\Delta,\ell}(z) = I(z) + \mathcal{E}(z)\,. \tag{5.1.3}$$

This gives a very clear candidate for the action, one just needs to fix a finite sample of N_z $z-$points [1]and sum the residuals ($\mathcal{E}$) squared. Schematically, we have

$$S(\Delta_a,\rho_a) = \log\left(\sum_{i=1}^{N_z} \mathcal{E}^2(z_i)\right), \quad \rho_a = \lambda^2_{\sigma\sigma\mathcal{O}_{\Delta_\ell}}. \tag{5.1.4}$$

It would seem at first that this approach doubles the number of parameters that our stochastic search would have to sample, but this can be avoided by noting that since the ρ_a enter at most quadratically in the action we can minimize them analytically. Moreover, the OPE coefficients are important physical quantities themselves, and thus our method computes them at each step for free.

We need to note here that since the residuals will have very different values on the $z-$plane a straightforward least square minimization will be numerically unstable. This is clearly seen from the fact that $\mathcal{E}(1/2) \equiv 0$ regardless of the spectrum and thus the region closest to $z = 1/2$ will contribute very little to the sum. Thus we need to introduce a weight $\sigma^2(z_i)$ that can account for this. Otherwise, the points further away from $z = 1/2$ will dominate the residuals and our algorithm will concentrate on solutions that minimize those without actually solving the crossing equations close to 1/2. In practice we found that these solutions were usually spurious minima.

The precise form of this error estimator will be discussed shortly, but for now we can discuss the general features of this approach. Let us define the $N_z \times N_{\text{Ops}}$ matrix $\mathcal{M}$ and the N_z vector I_i

$$\mathcal{M}_{i,a} \equiv \mathcal{F}_{\Delta_a,\ell}(z_i), \quad I_i \equiv I(z_i), \quad i = 1,\ldots,N_z\,,\ a = 1,\ldots,N_{\text{Ops}}\,. \tag{5.1.5}$$

[1]In what follows we will use the quantity $\lambda(z) = |\rho(z)| + |\rho(1-z)|$ with $\rho = z/(1-\sqrt{1-z})^2$ to quantify how far from the best convergence for each channel (i.e. $\rho = 0$ the $z-$points are. This idea follows from the work of [99].

The weighted action will have the following form

$$\exp(S(\Delta_a, \rho_a)) \equiv \frac{1}{N_z} \sum_{i=1}^{N_z} \sigma_i^{-2} \left| \sum_{a=1}^{N_{\text{Ops}}} \rho_a \mathcal{M}_{i,a} - I_i \right|^2 . \tag{5.1.6}$$

Minimizing with respect to ρ_a gives

$$\rho_a^{(0)} = \sum_b A_{ab}^{-1} \sum_i \text{Re}(\mathcal{M}_{b,i}) \sigma_i^{-2} I_i, \quad A_{ab} \equiv \sum_i (\mathcal{M}_{ai}^* \mathcal{M}_{bi} + \mathcal{M}_{ai} \mathcal{M}_{bi}^*) \sigma_i^{-2} , \tag{5.1.7}$$

and thus we arrive at an action that depends only on the Δ of our ansatz.

Here we already see two advantages with respect to the previous proposals for S. First, since the residuals will only vanish for $\Delta^* \to \infty$, $S(\Delta_a) > -\infty$ for all Δ_a. Thus, S should remain differentiable around the minimum. Secondly, this action is better suited for studying general spectra (with more than one operator per spin, that is) because having coincident operators in the same spin channel induces only a small ambiguity in the determination of the relevant OPE coefficients instead of a logarithmic singularity as in the determinant action.

5.1.2 Determining the best error estimator

Now it only remains to find a suitable error estimator. Let us recall which are the desirable properties: i) it should capture the fact that the crossing equations are better satisfied around the neighborhood $z = 1/2$, ii) it should scale appropriately with Δ^*.

In [98], Rychkov et al. used tauberian theorems to estimate the tail of the OPE expansion of a 4-pt function. This was naturally our first candidate for an error estimator. More concretely, they show that the contribution to the 4-pt function of the operators with $\Delta > \Delta^*$ is bounded by

$$g_{\Delta > \Delta^*}(z, \bar{z}) = \frac{1}{\Gamma(2\Delta_\sigma + 1)} (\Delta^*)^{2\Delta_\sigma} r^{\Delta^*}, \quad r = |z|, \tag{5.1.8}$$

subjected to the condition $\Delta^* >> \Delta_\sigma/(1-r)$. This implies, among other things, that if Δ^* is big enough, the convergence of the OPE is exponential.

Applying this to the crossing equations, we get that

$$\sigma(z) \sim \frac{(\Delta^*)^{2\Delta_\sigma}}{\Gamma(2\Delta_\sigma + 1)} \left(|1-z|^{2\Delta_\sigma} |z|^{\Delta^*} + |z|^{2\Delta_\sigma} |1-z|^{\Delta^*} \right),$$

and here it is clear that although $\sigma(z)$ has a minimum at $z = 1/2$, it grossly overestimates the error there, where we know that the crossing equations are identically satisfied.

Our next candidate stems from a much simpler observation. Given the convergence properties of the OPE, one can assume that the last term of the series should be a good estimator of the error. Thus, if Δ^* is chosen appropriately for a given sample of $z-$points it is easy to see that the contribution of an hypothetical scalar operator with $\Delta = \Delta^*$, (i.e. $\mathcal{F}_{\Delta^*,\ell}(z)$) should be of the order of magnitude of the rest of the tail. Moreover, this satisfies the crucial condition that $\sigma(1/2) \equiv 0$. Our numerical explorations show that this poor-man's approach is actually quite effective in reducing the hierarchy between residuals at different points in the $z-$plane.

The only drawback of this estimator is rooted in one of the most complex issues with this approach to discretizing the crossing equations, namely, the choice of the $z-$points. If the sum in (5.1.6) includes points that are too far away from $z = 1/2$ then Δ^* must be big enough in order for the crossing equations to be possibly satisfied. Otherwise, the error estimate will not capture properly the order of magnitude of the neglected terms. This underlines the need to choose the $z-$points carefully. The choice used in the paper will be described in detail in section 5.1.5.

5.1.3 Residuals in derivative space

Before diving into the actual protocol used to explore the landscape of approximate CFTs, we would like to do a parenthesis to describe our preeliminary explorations with residuals in the space of derivatives and why we deemed it harder road than the $z-$residuals.

We may consider a situation analogous to eq.(5.1.3) but with derivatives instead of $z-$points. In this case, one could apply the same logic and use a weighted least-squares minimization to obtain the OPE coefficients and the residuals. The biggest difference is that whereas the error for larger values of z is expected to grow in a power-like fashion, [97] showed that in the derivative case it grows exponentially in $m + n$ and thus choosing an error estimator is numerically more complicated.

5.1.4 Implementation in `Mathematica`

One could try to use the codebase already developed for the approaches described in the previous chapter and implement the residual-based action directly in `Mathematica`. This has the advantage of allowing for arbitrary precision calculations and consequentlconsequentlyhigh degree of confidence in the action. The biggest draw back is that the computational cost makes anything except a very local analysis practically impossible.

As an example, we can take the spectrum 2_1_1_1 and run a MC with $T = 1$ for 10^4 steps. This takes takes over a day (34 hours) on a desktop computer and produces a trajectory like the one shown in the left panel of fig.5.1. Exploring such a small

parameter space is already a complicated task that can barely be accomplished with long running times. Using the approximated action discussed in the next section (see 5.1.5) we can run for 1000 times more steps in less than a 10th of the time, as can be seen in the right panel of 5.1. Although the difference between the two trajectories might not be so striking, it is important to recall that in order to characterize properly the different minima it is important to have enough statistical information about the nearby points around the putative minimum. In our experiments we realized that in many cases having less than 10^4 points in the neighborhood of a minimum was in some cases not enough for distinguishing it properly from a numerical artifact. It is in this context that we realized that a wide search using `Mathematica` was untractable.

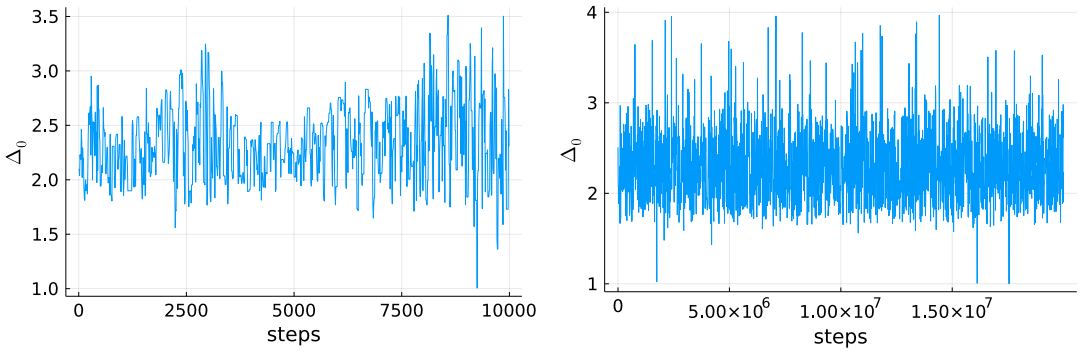

Figure 5.1: Evolution of the scaling dimension of the lightest scalar during a Metropolis Monte Carlo search with action (5.1.6). The spin partition is (i.e. 2_1_1_1) with the external operator fixed at $\Delta_\phi = 1.1$. 200 points satisfying $\lambda(z) < 0.42$ were used. *Left*: 10^4 steps done with `Mathematica`. This run took over 30 hours. *Right*: Analogous search but using the optimized approximation implemented in `FORTRAN` (cf. 5.1.5). This search ran for 2×10^7 steps and took less than an hour.

5.1.5 Numerical evaluation of S

Since our approach to finding the minima of S requires extensive sampling, one must render the evaluation of this function as efficient as possible. We start by discussing the approximation and numerical evaluation of (5.1.6). We describe each of the approximations used in order to render computationally feasible sampling $O(10^8)$ points in ~ 10 hours on a single CPU.

i) Discretization in z The grid from which the points will be sampled is parametrized as $z = x_0 + an + y_0 + ibm$ with $m, n \in \mathbb{N}$ and $x_0 = 1/2 + 1/1000$, $y_0 = 1/1000$. In this work we used $a = 1/100$ and $b = 1/50$ but in the computation of S only a randomly chosen sample of `nZ` points was considered. This was done by ordering them with respect to their value of λ and then sampling the subset with $\lambda < \lambda_0$ of this list.

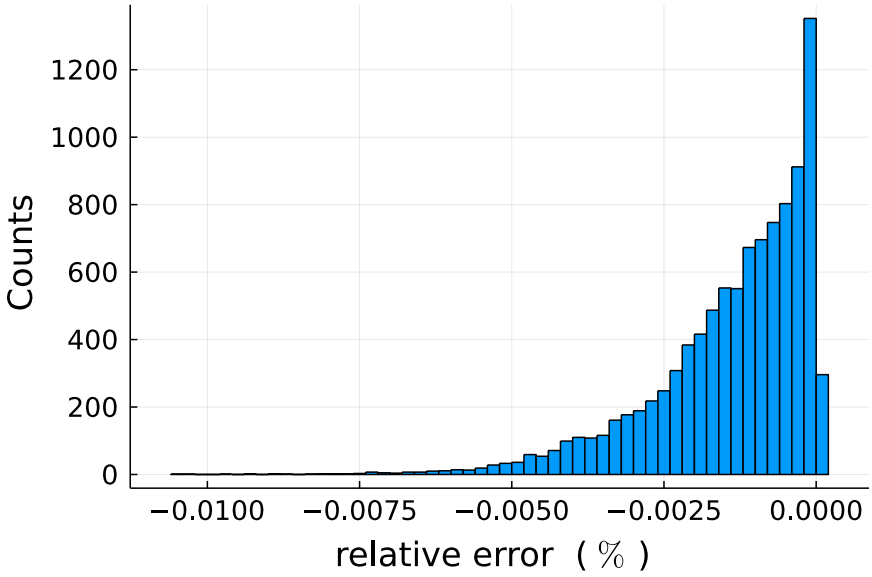

Figure 5.2: Distribution of the relative error defined as $S_{\texttt{Mathematica}} - S_{\texttt{FORTRAN}}$. The action was evaluated at 10^4 points normally distributed around an apparent local minimum in $d = 3$ with spin sector 2_2_1_1_1, $\lambda_0 = 0.42$ and `nZ` $= 200$. Note the long tail for negative values.

ii) Truncation of the spectrum This step consists in passing to the `FORTRAN` routine the list of the spins of each operator in the truncation under study. It is in this step that we input important parameters such as the spin partition, Δ^* and $\ell_{\max}$.

iii) Evaluation of the conformal blocks The conformal blocks were tabulated using 160 digits of internal precision in `Mathematica` and stored as plain text files for each ℓ. In $d = 2, 4$ we used the closed expressions in terms of hypergeometric functions [23]. For $d = 3$ the recursion relations implemented as in [49] were used. For each point in z we computed the CBs at 5000 points evenly spaced in $[\Delta_{unit}(\ell) - 99/100, \Delta^*]$ with $\Delta^* = d + 15$. We note in passing that this gives a lower bound on the error in our determination of the scaling dimensions (Δ) of the exchanged operators. In the `FORTRAN` code, the interpolation is done with cubic splines.

iv) Determination of the OPE coefficients Once the matrix of the conformal blocks for each z and operator (Δ, ℓ) has been computed, the determination of the OPE coefficients is then a weighted least squares problem which we solve using `LAPACK` (see 5.2.5).

If `positiveOPEs` is true, this is not the end of the story because the OPE coefficients that solve the quadratic problem might as well be negative. To enforce unitarity, we

iteratively decouple the offending operators until every OPE coefficient is positive. It is important to underline that this is done at each point evaluated in our algorithm, and thus operators do not decouple for the whole test but only for those particular configurations.

v) Computation of S As described above, we obtain S by taking the logarithm of the sum of the squared residuals. If any operator has a Δ outside its allowed boundaries we impose a quadratic penalty that is then added to the action. This guarantees the analyticity of our potential and thus avoids noxious boundary effects.

More concretely, suppose an operator bound to be in the interval $[\Delta_0, \Delta_1]$ has $\Delta < \Delta_0$. In that case, the effective action will be

$$S_{eff} = S + \texttt{wall}(\Delta - \Delta_0)^2,$$

where the constant `wall` is set to 10^4.

Numerical error

After all the approximations discussed above, reasonable doubt could remain about the accuracy of S computed with our method. Thus, we consider it necessary to quantify the magnitude of the numerical errors in our implementation. We accomplish this by computing S at representative points with our framework and by comparing them to the values of S obtained in `Mathematica` with arbitrary precision.

From this analysis we find that the action computed with `Mathematica` is systematically lower than the approximated one using our `FORTRAN` implementation. However, the discrepancy is such that at the values of Δ^* studied in this paper we can still trust the results. Naturally, the errors become larger for bigger N_{Ops} and Δ^*, but even in the cases with the worst agreement the relative errors are smaller than 10^{-3}. Moreover, the largest discrepancy sets a natural lower bound for T, since we must allow for fluctuations of this height in order not to wrongly identify artifacts as minima. For example, in $d = 3$ the minimum temperature for $\ell_{\text{max}} = 6$ is $T \sim 10^{-4}$, whereas for $\ell_{\text{max}} = 8$ is $T \sim 10^{-3}$. We note that this resolution is likely enough for any physical minimum, given that in the $\Delta^* \to \infty$ limit any physical theory should have $S \to \infty$.

As an example, we show in figure 5.2 the relative error computed for 10^4 gaussian perturbations of a local minimum in sector 2_2_1_1_1 for $d = 3$, $\lambda_0 = 0.42$ and `nZ` $= 200$. The fact that the error is mostly negative can be easily understood from the delicate numerics of the bootstrap equations. It is known that in order to solve (2.1.19) to a high degree of precision, very fine-tuned cancellations between the terms must occur. When using our double-precision interpolation of the blocks,

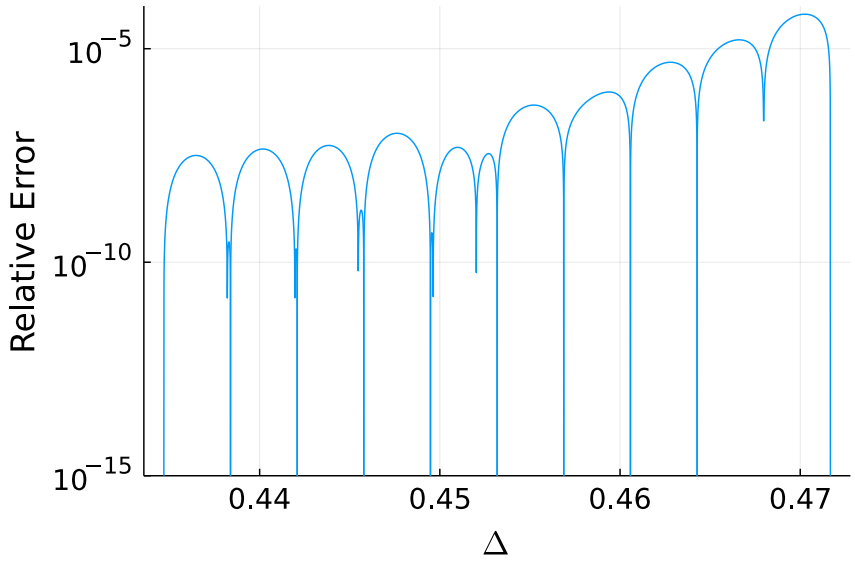

Figure 5.3: Scalar conformal block evaluated at the point $z = 0.521 + i0.021$. The line shows the relative error of the interpolated value wrt the analytical one. The logarithmic singularities represent the points where Δ Δ_i, Δ_i being one of the tabulated values.

there will be points where these errors will spoil the cancellations and thus the value of S can only be bigger than the "exact" one.

We can identify two main contributions to this error in computing S: the cubic interpolation of the conformal blocks and the cancellation errors when computing the residuals. For the latter there is not much we can characterize, but analyzing the former is important to understand better the possible improvements we could implement on this method. To this end, we compute the block $g_{\Delta,0}(0.521 + i0.021)$ both exactly and with our `FORTRAN` interpolation. The relative error of our interpolated results is shown in fig. 5.3.

Another point that deserves discussion is the determination of the OPE coefficients (ρ in eq. (5.1.6)). Solving for ρ amounts to finding the minimum of a quadratic form. We find that the curvature of this form is very anisotropic, with hierarchies of as much as 10 orders of magnitude. This is in fact one of the main bottlenecks to adding too many operators: the curvature of the subleading operators at some points becomes too small to be resolved with double precision and the OPE coefficient of these operators cannot be reliably determined. This might in turn be another contribution to the error of S, given that an operator with a suboptimal OPE might not lower S as much as it would with the correct one.

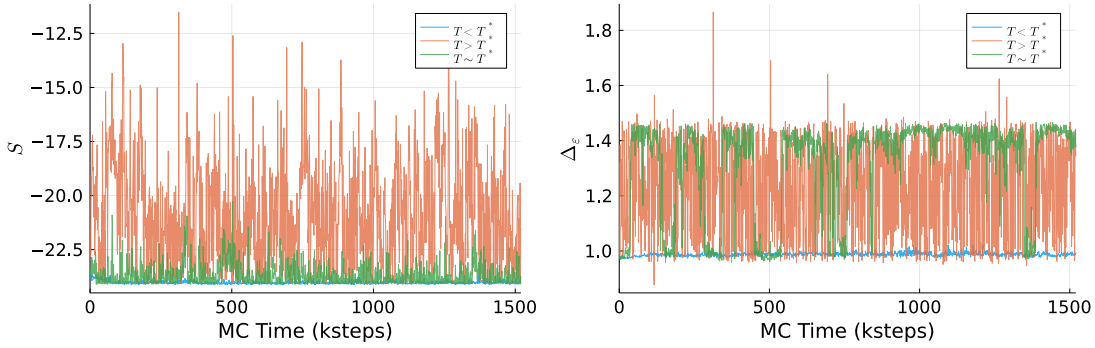

Figure 5.4: Sample trajectories for MC runs at different temperatures. *Left:* Value of the action S of the points visited. *Right:* Scaling dimension of the lightest exchanged scalar operator. This particular test was done in $d = 3$ by taking $\Delta_\sigma = 0.519$ fixed, with a spin partition 3_2_2_1 and $\Delta^* = 10$. The trajectories are shown for $T = 0.05, 0.3, 0.9$. In this case, $T^* = 0.3$.

5.2 The search protocol in detail

We present in this section the numerical method we used to find approximate solutions of the bootstrap equations for a 4-point function of identical scalar primary operators in a generic CFT in d dimensions.

As discussed in the introduction, we do not look for rigorous disallowed regions in the space of CFT data, but rather for approximate solutions of the above equations, namely for approximate possibly allowed CFT data. To this aim, we severely truncate (2.1.19) to the finite set of primary operators with scaling dimension up to a given Δ^* (chosen to be integer), and assign a given number of operators n_ℓ to each spin channel ℓ up to some value ℓ_{max}. If unitarity is imposed, Δ^* and ℓ_{max} are related. We take

$$\ell_{\text{max}} = \Delta^* - d - 1\,, \tag{5.2.1}$$

so that the scaling dimension of the operators with spin ℓ_{max} have a large enough range where they can be varied, compatibly with unitarity: $\Delta^* - 3 \leq \Delta_{\ell_{\text{max}}} \leq \Delta^*$. The total number of exchanged operators $\mathcal{O}_a$ that we consider is

$$\sum_{\ell=0,2,\ldots,\ell_{\text{max}}} n_\ell = N_{\text{Ops}}. \tag{5.2.2}$$

As explained in 5.1.1, to perform the minimization we choose a finite sample of N_z points in the complex z-plane in the neighborhood of $z = \bar{z} = 1/2$ and define the $N_z \times N_{\text{Ops}}$ matrix $\mathcal{M}$ and the N_z vector I_i

$$\mathcal{M}_{i,a} \equiv \mathcal{F}_{\Delta_a,\ell}(z_i), \quad I_i \equiv I(z_i), \quad i = 1, \ldots, N_z\,,\ a = 1, \ldots, N_{\text{Ops}}\,. \tag{5.2.3}$$

We define an "action" as (spin dependence omitted for simplicity)

$$\exp(S(\Delta_a, \rho_a)) \equiv \frac{1}{N_z} \sum_{i=1}^{N_z} \sigma_i^{-2} \left| \sum_{a=1}^{N_{\text{Ops}}} \rho_a \mathcal{M}_{i,a} - I_i \right|^2 , \tag{5.2.4}$$

where $\rho_a \equiv \lambda^2_{\sigma\sigma\mathcal{O}_a}$, by taking a weighted sum of the absolute square of the truncated crossing equations (2.1.19) at the N_z points, with

$$\sigma_i = |\mathcal{F}_{\Delta^*,0}(z_i)|. \tag{5.2.5}$$

The factor (5.2.5) is introduced to take into account that the points with the best convergent conformal block expansion are around $z = 1/2$, point where on the other hand the function $\mathcal{F}$ vanishes. For any finite truncation, our aim would be then to minimize S in the space of CFT data.

We choose to sample the N_z points in the z-plane from a uniform grid with the constraint

$$\lambda(z) < \lambda_0 \,, \tag{5.2.6}$$

with $\lambda(z)$ defined as in (3.11) of [99]. This condition defines a compact and convex region around $z = \bar{z} = 1/2$, the point of best convergence of the bootstrap equations. The parameter λ_0 is, together with Δ^* and T, the most relevant "hyperparameter" of our computational pipeline, and has to be chosen carefully in order for the method to work.

We then perform a stochastic minimization using a Metropolis Hastings algorithm (cf. section 3.2.2). This Markov Chain Monte Carlo method produces a sample of points from a distribution that resembles $\exp(-f(x)/T)/Z$ in the large sample size limit. The number of Monte Carlo iterations N_{steps} needed to get sensible results can be quite large ($\sim 10^8$). In order to be able to perform exhaustive searches in parameter space we developed a numerical approach which allows estimating *efficiently* the action S defined in (5.2.4). Indeed, conformal blocks are computationally-expensive functions of Δ, ℓ and z, which would make an extensive sampling impossible with moderate computational resources without an appropriate numerical optimization. We tabulate the blocks for a fixed $z-$point sample and each ℓ, and then use cubic splines [45] to interpolate their values. In this way we get a speedup of $O(10^4)$. The interpolation grid is chosen in such a way that the numerical error induced by this procedure is negligible compared to the truncation error (see figure 5.2 and the discussion in section 5.1.5).

It is important here to note that this speed up comes with the tradeoff of limiting our working precision to that of double type in Fortran (i.e. 64−bit). This might come as a surprise to our more technical bootstrap readers, but an important result of this paper is indeed that approximate solutions to the bootstrap equations can be

found without resorting to 200 digits of precision. Nevertheless, limited precision is a bottleneck to go to larger values of Δ^* and to improve the quality of our approximate solutions.

We now describe each step of the protocol more thoroughly.

1. Determining the hyper parameters Once a physical system of interest (understood as a global symmetry structure and the relevant bounds on the operators' scaling dimensions) has been chosen, some exploratory work must be done in order to make our search protocol as efficient as possible. In appendix 5.2.1 we list the choices for each search discussed in section 5.3. We will here concentrate on motivating our choice for T, since we have found empirically that the other hyperparameters are not as determinant to the success of the search.

Since we will explore different truncations, the order of magnitude of δS, see eq.(3.2.5), can be very different from spectrum to spectrum[2] and thus the temperature T must be adjusted accordingly. Although we will use an adaptive step that guarantees that in the stationary state roughly half of the moves will be rejected, choosing a temperature that is too high will make $\delta\Delta$ too coarse and the MC will "miss" narrow features of the landscape. On the other hand, if T is too small our method will move too slowly around the landscape or might even "freeze" in the basin of a local minimum.

In the following we will empirically choose T in such a way that the projection of the trajectory to each coordinate axis (which in our case correspond to the operators' scaling dimensions) covers the whole allowed range at least 10 times, but still low enough so that the dynamics does not become diffusive, namely the local minima can still be detected as metastable states.

For further detail, we show in figure 5.4 an example of archetypal trajectories. This figure and further considerations about the choice of T are presented and analyzed in 5.2.1.

2. Finite temperature MCs For each ansatz $\Delta_a^{(0)}$[3] we sample the CFT parameter space at the temperature T chosen according to the criteria discussed in the previous step. This is the most important and computationally expensive step, but one must bear in mind that it gives all the necessary information to understand the landscape of possible CFTs at several different truncations.

The variation of the scaling dimensions $\delta\Delta_a$ is taken randomly with uniform distri-

[2]We have found empirically that the most important parameter in this case is $\ell_{\max}$, not necesarily Δ^* on its own.

[3]For simplicity of notation, we do not explicitly report $\Delta_\sigma^{(0)}$ as input data.

bution over an hyperparallelepiped centered around the origin. This was observed to be more efficient than moving one operator at a time since the landscape shows highly correlated features and thus attempting moves in which all the operators change simultaneously improves the sampling efficiency. The user can choose the length of each side but the overall scale is adaptive and changes at each Monte Carlo step. This is done in order to guarantee a 50% acceptance rate in the stationary state. In practice, when a move is rejected (resp. accepted) this overall scale is decreased (resp. increased) by a fixed factor. Each operator scaling dimension is confined within a finite region within two boundary values, decided by the user. The MC then explores the landscape for $\sim 10^8$ steps. Our choice of the temperature guarantees that after this number of iterations the initial conditions are irrelevant. For each of these spin partitions we store each 1000th configuration visited. We will refer to these as frames.

3. Separation by sectors In a given MC run not all the operators in the ansatz will have sizable OPE coefficients at each iteration step. In this work we assume that if the OPE coefficient associated to a primary operator is smaller than a given tolerance (we found 10^{-8} to be a sensible choice for the ℓ_{max} used in this paper) this operator is decoupled and can be neglected. If unitarity is imposed, OPE coefficients that turn out to be negative from (5.1.7) are set to zero in that iteration. These two effects lead to a classification of the different points visited by the MC in terms of the effective spectrum contributing to the crossing equations. In order to describe these different sectors we introduce the following shorthand notation to indicate each one of them: $(m_0)\_(m_2)\_\cdots\_(m_{\ell_{\text{max}}})$. For example, a point with 3 scalars, 2 spin-2 operators, 2 spin 4 and one spin-6 would belong to spin sector 3_2_2_1. Crucially,

$$\sum_{\ell} m_\ell \leq N_{\text{Ops}}\,. \tag{5.2.7}$$

This implies that there is no need to consider different partitions of operators in each spin channel. All partitions with $m_\ell \leq n_\ell$ will be automatically searched for by MC. Moreover, the same sector can be visited in two different MC runs with different n_ℓ. Thus, this step effectively recombines all the information from the different spin partitions studied in the previous step.

4. Identification of putative local minima Now that we have sampled the landscape we must identify the points that are more likely to be close to a local minimum of the action. For a low-dimensional parameter space we could visualize the action as a contour plot and identify the points by inspection. It is clear, though, that for more than 3 scaling dimensions, this approach cannot be followed.

Our proposal is thus the following. For each set of frames obtained in the previous step (namely, those corresponding to spin sectors with more than 120k frames and

those describing the trajectory of every search)[4] we sort their elements according to the number of nearest neighbors with higher action, in the philosophy of Density Peak clustering[96]. We consider as putative local minimum the 20 configurations with highest rank. We have observed empirically that in each sector the number of actual minima is always much smaller than this number, and that many of the smaller rank frames actually converge to other minima, so this is a conservative estimate. To clarify, the point with the highest rank will be the global minimum of that set of frames because every other point will have higher action.

5. Local minimization For each putative local minimum we launch Newton - Rhapson (NR) minimizations. This deterministic algorithm is justified because the points found in the previous step are likely contained in the basin of attraction of a local minimum. More details about the implementation of this algorithm can be found in section 3.1.2.

All the endpoints from the NR minimizations are collected and those that violate the bounds imposed on the spectrum are discarded.[5] We then assign to the corresponding sector the minima where one or more operators decouple (in the sense described above). In the case of two or more minimizations converging to the same point (i.e. the relative difference for any scaling dimension is smaller than 20%) we keep only the point with the lowest action. At the end of this step we have a list of approximate solutions to crossing that are local minima of S.

6. Convergence and boundary check Since we usually impose boundaries on the subleading operators in order to better control the type of CFTs that we might find, it is important to rule out the possibility of some of the local minima found in the previous step actually being induced by the presence of this boundary.

To this end, a final NR minimization is performed from all the minima found in the previous step, relaxing all the boundaries except strict unitarity (if imposed). We consider as true minima the ones that reach convergence according to our NR implementation and are contained within the region of interest: this means a minimum can be at the boundary of unitarity, but not at one of the boundaries introduced in step 1.

7. Identifying akin minima at different truncations Minima belonging to diferent spin sectors but with similar CFT data in their common operators should

[4]It might seem redundant to analyze sector by sector frames that are already contained in the trajectories that result from the MC search described in point 2. Since exhaustivity is paramount and the definition of local minimum depends on the neighboring points, it makes sense to consider the same frame in two different settings in order not to miss any interesting features.

[5]Spectra where a whole spin sector is missing, such as 2_1_0_1_1, have been ignored for simplicity.

be identified. In this case the minimum with more primaries should have a value of S lower than the minimum with less primaries. This is a necessary (but by no means sufficient) condition to associate such akin minima to approximate solutions of the crossing equations of one and the same CFT. In order to find akin minima and quantify their similarity we organize all the minima in a directed graph where the minima are the nodes and $A \to B$ if: (i) the sector to which A belongs is contained in the one of B, namely if B has at most `maxMismatch` more operators than A and (ii) the operators which are in common between the two sectors differ in their scaling dimensions by at most `relTol` in relative error. The final result of our protocol are the leaves of this directed graph, namely the nodes with no outgoing links. One can also study the branches (i.e. subsets of this directed graph) in order to understand the asymptotic behaviour of certain values, such as the action S or the Δ of some leading operators.

Issues with alternative approaches Since the protocol might seem convoluted, we now discuss some alternatives and the problems that arise in their implementation, in hope of further justifying our choices. For example, instead of searching for minima in different truncations and then grouping them in branches, one could find stable minima (at fixed Δ_σ) for small ℓ_{max} and then recursively improve this solution by adding operators to the ansatz and looking for minima in the neighborhood of the initial minimum. This approach has two drawbacks. First, it is not straightforward to choose the spin of the new operator. We have empirically found that a naive choice usually leads to a new S that is convex wrt the new operator. Although this would imply that the proposed operator does not exist in the spectrum of the CFT we have seen that in many cases adding the same operator after the addition of another one did lead to a stable minimum. In short, the addition of operators is not commutative and does not always lead to a local minimum. Second, it cannot be known beforehand which is the right ℓ_{max} to start this procedure. To circumvent this problem we would have to perform several searches (morally equivalent to those of step 2 above) thus arriving at a protocol quite similar to ours.

5.2.1 Technical implementation of the protocol

The above described protocol was implemented in a series of automatized bash scripts that used `Julia` for the data processing and `FORTRAN90` (compiled with `ifort v2021.2`) for the numeric evaluation of the action and the different minimization algorithms. `LAPACK` was used for the linear algebra manipulations. They were run on `Intel Xeon`$^{\text{TM}}$ processors in an institutional cluster. The CPU time to run 10^8 steps was of roughly 12 hours for representative spin partitions. The parameters used in the searches are shown in table 5.1.

Table 5.1: Summary of the relevant parameters for the wide searches (first step of the protocol).

Parameter	Value(s)	Description
`nZ`	200	Number of points taken in the $z-$plane.
`lambda0`	0.42	Size of the region in which the points are sampled.
`NT`	2×10^8	Number of steps (MC time).
`positiveOPEs`	`true`	Enforcement of real OPE coefficients.
`externalInOPE`	`false`	Fixing the first exchanged scalar to be equal to the external operator.
`Temp`	$0.3 - 0.9$	Temperature (T) of the Metropolis Monte Carlo algorithm.
`MCstep`	0.001	Overall scale factor for the MC-step.
`wall`	10^4	Constant for the quadratic penalty that enforces the bounds on Δ_i.
`frameRate`	1000	The MC saves one out of `frameRate` steps as a frame.
`nops`	$3 - 20$	Number of operators (besides the identity).
`boundaries`	$[\Delta_{unit.}, \Delta^*]$	Range to which each operator is constrained.

Ideal Temperature As mentioned earlier in section 5.2, the key step of our protocol is the wide search performed using the Metropolis Monte Carlo algorithm. In order for this step to be efficient the temperature must be chosen wisely. To this end we performed test searches for different values of d, N_{Ops} and Δ^*, where several different temperatures were used. Then, we determined by inspection the ideal one in each setting, according to the criterion described in section 5.2.

In figure 5.4 we show a concrete example of how to identify the ideal temperature. We show "cold", "hot" and just right temperatures in blue, red and green (respectively). We can see clearly that the blue line "freezes" into the first local minimum found by the MC and then stays there for the whole test, whereas the red trajectory travels back and forth randomly. We consider the green trajectory to be representative of an efficient search because it oscillates around local minima for some time before making a transition into another one. While this could mislead the reader into thinking that the time spent oscillating around a local minimum is in some sense "wasted" one must bear in mind that during those steps, the MC effectively samples the rest of the scaling dimensions, thus refining the solution to crossing in that neighborhood.

5.3 Results

We report in this section the results obtained with our method. We have considered a single 4-point function with four identical scalar operators in $d = 2, 3, 4$ dimensions. Except for a short discussion of the Yang Lee CFT (see section 5.3.5), we have considered CFTs where the fusion rules are compatible with a $\mathbf{Z}_2$ discrete symmetry under which the external operator is odd.[6] We will use a Ising-like notation and denote the external operator by σ and the lowest dimensional exchanged scalar (besides the identity) by ϵ. As will be later explained, demanding that ϵ be the only $\mathbf{Z}_2$-even relevant (in the renormalization group sense) primary operator that can appear in the $\sigma \times \sigma$ OPE is necessary to avoid the proliferation of minima. We consider both local and non-local theories, demanding or not the existence of a spin-two energy-momentum tensor operator at the unitarity bound $\Delta_T = d$. Given its relevance in our analysis, we have also considered the space of non-local theories where the scaling dimension of the first spin 2 operator is fixed and equals that of Generalized Free Theories (GFT), $\Delta_T = 2\Delta_\sigma + 2$. We then get further insights by allowing Δ_T to vary. We focus mostly on unitary theories, though our method does not rely on it. As a proof of concept, we study the non-unitary landscape around the 2d Yang-Lee model.

As already anticipated in the introduction, when Δ_σ is allowed to vary, the landscape of S becomes very simple: the global minimum is at the lower edge of the unitarity region, which in $d = 3, 4$ coincides with the Free Theory (FT) of a scalar field. Moreover, for generic spectra we find that it is in fact the only reachable minimum. For this reason in most of our analysis we will study "slices" of the landscape by keeping fixed Δ_σ in each MC run.

The section is structured as follows. We start in section 5.3.1 by showing that the FT is the global (and in many cases the only) minimum of S. From section 5.3.2 we look for local minima by keeping the external operator fixed. We first consider the simplest possible scenario, namely very sparse CFTs where just one operator per spin appears below Δ^*. We then discuss in section 5.3.3 more general CFTs with multiple operators per spin. In section 5.3.4 we discuss non-local theories with a special focus on the GFT. Finally, we briefly discuss the 2d Yang-Lee model as a proof of concept of the validity of the method for non-unitary theories in section 5.3.5.

[6] Note that in general such a $\mathbf{Z}_2$ symmetry is not required to be a genuine faithful symmetry of the whole CFT. We will encounter an instance of this phenomenon when discussing $2d$ minimal models in section 5.3.3.

5.3.1 The Free Theory is the global minimum of S

Although we have already specified that there are no other minima than the free theory in the full parameter space, it is illustrative to see how they could have appeared in a search with our method. We will thus spend some lines describing our first approach to the problem, hoping it will show even more convincingly how the landscape in each case has a single minimum.

In order to efficiently sample the whole landscape, the MC has to be performed at a relatively high temperature ($O(1)$). This makes the probability density as a function of the Δs relatively smooth. Local minima, if present, cannot be easily distinguished from statistical fluctuations of the density. To mitigate this problem, we reweight the probability density, estimating it at a lower temperature $T = 0.1$. This is done as follows. We estimate the probability density as a function of Δ_σ and Δ_ϵ. From a sample of N configurations $y_t = (\Delta_\sigma, \Delta_\epsilon)_t$, where $t = 1 \dots N$, visited at a temperature T', we estimate the probability density at T by the following formula:

$$\rho_T(x) = \frac{1}{Z} \sum_{t=1}^{N} \exp\left(S(y_t) \left(\frac{1}{T'} - \frac{1}{T} \right) \right) K(y_t - x) \tag{5.3.1}$$

where Z is an irrelevant normalization constant and K is a two-dimensional Gaussian kernel of width $(0.0018, 0.018)$. The reference temperature T was chosen so that the region close to the FT appeared as a probability maximum. This should be always the case for $T \to 0$, but at higher T we find that due to entropic reasons this region is seldom visited. On the other hand, T cannot be chosen arbitrarily low due to the numerical errors induced by the reweighting factor in (5.3.1).

One can then identify the local maxima of ρ_T and select from the original sample the points with lowest action near this local maximum. When applied to the $d = 3$ landscape the results of this algorithm showed 2 cluster of minima, one around the FT point and one roughly compatible with the Ising model. However, a closer stability analysis showed that these configurations were not actual minima but points along a "valley".

The results that we sketched above would in principle be quite conclusive to the statement presented in this subsection, but a more thorough search is both a necessary check and, as will be shown shortly, produces a compelling visual representation of the landscape.

Numerically, we can rule out the existence of other minima by choosing a big enough sample of initial conditions and determining whether all of them converge to the same point or not. This analysis can be made by launching MC runs with a given temperature and spin partition of operators, and simply looking for the values of the Δ's corresponding to the lowest value of S explored during the run. For small

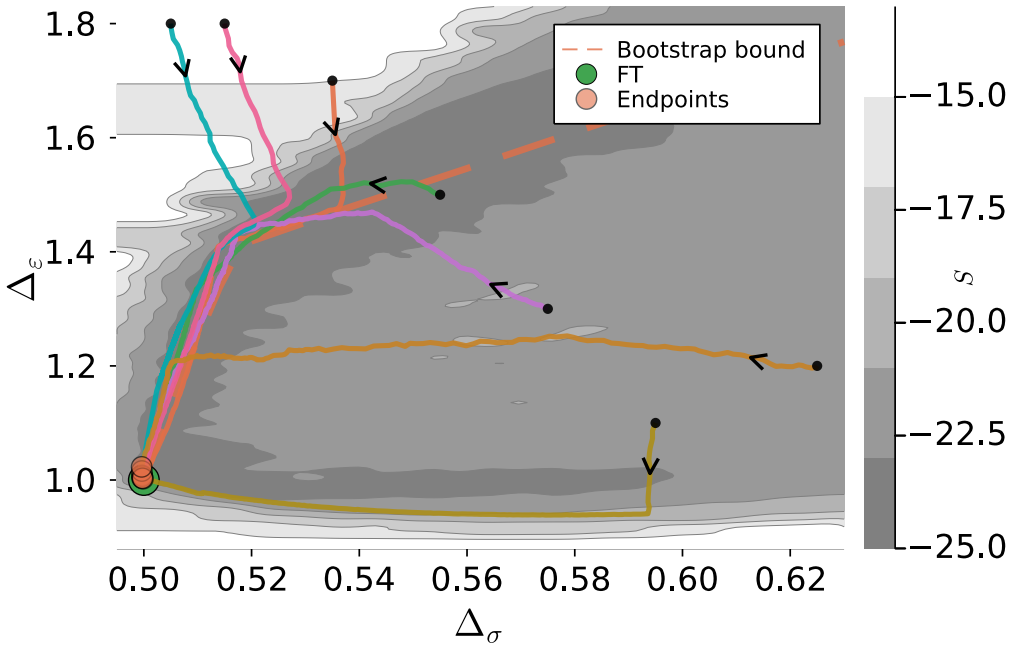

Figure 5.5: Convergence of different trajectories to the $d = 3$ free scalar CFT. The contour lines represent the minimum value of the action in each bin for a spectrum of the kind 3_2_2_1. The dashed line is the upper bound for Δ_ϵ from [48]. The black arrows on the colored lines indicate the direction of the MC evolution.

T this will usually be attained around the end of the run.

The most important property that comes out from this analysis, common to every scenario studied in this paper, is that the *global* minimum of S corresponds to the FT (or the point $\Delta_\sigma = \Delta_\epsilon = 0$ for $d = 2$). This has been observed in all our searches, and in particular for all the spin partition of operators which we considered. Of course, this does not imply the non-sensical result that the FT is the only consistent CFT. Rather, it implies that among all the physical CFTs allowed within the given assumptions at fixed truncation, within our numerical accuracy and in absence of further constraints, only the FT shows up as an isolated minimum of S.

In order to test the (non-)existence of other minima, we performed a very large number of MC minimizations at $T = 10^{-4}$. This temperature, being of the order of the numerical error of the action,[7] guarantees that the MC can only diffuse towards configurations of lower action, since the temperature is too low to cross any relevant barrier. Independently of the choice of n_ℓ and of the operator scaling dimensions $(\Delta_\sigma^{(0)}, \Delta_a^{(0)})$, all the low temperature MC runs we performed converge to the FT point within 10^8 steps, although longer times might be needed for higher N_{Ops}.[8]

[7] See appendix 5.1.5.

[8] There is an important exception described in detail in section 5.3.2. In $d = 3$ for spectra of

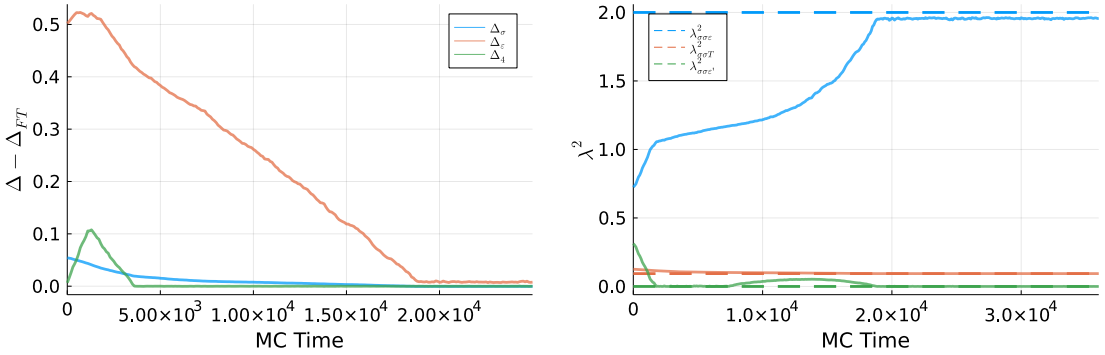

Figure 5.6: Convergence in t_{MC} for representative scaling dimensions (left) and squared OPE coefficients (right).

We report as an example in figure 5.5 the low$-T$ evolution for a $3d$ CFT spectrum with $\ell_{\text{max}} = 6$, $N_{\text{Ops}} = 8$ and an initial spin partition 3_2_2_1. Here the first spin two operator is fixed at $\Delta_T = 3$ and no gap on the number of relevant scalars has been imposed.[9] The starting point of each colored line (indicated with a black bullet) corresponds to a MC with initial values of $(\Delta_\sigma^{(0)}, \Delta_\epsilon^{(0)})$ at that point. The black arrows on the colored lines indicate the direction of the MC evolution. As can be seen, the final point of all the MC runs (highlighted by red circles) have $\Delta_\sigma \approx 1/2, \Delta_\epsilon \approx 1$. The contour plot shown in the background is indicative of the value of S for the same spin partition but sampled at a much higher temperature (roughly 100 times larger). A two-dimensional representation of S is then obtained by binning the points visited on the $(\Delta_\sigma, \Delta_\epsilon)$-plane and plotting the minimum value of S in each bin.[10] They are reported as a visual aid. As can be seen from the figure, the initial values of $(\Delta_\sigma^{(0)}, \Delta_\epsilon^{(0)})$ can be taken in the excluded region, in which case they quickly approach the extremality line. The discrepancy between the rigorous bootstrap extremal line and the trajectories of our MC solutions is due to the severity of our truncation. During the MC evolution the OPE coefficients of the extra scalars and higher spin operators decrease in such a way that at the final point we effectively have the FT spectrum with one operator per spin. We illustrate this phenomenon by plotting in figure 5.6 the scaling dimensions of σ, ϵ and the spin-4 current as well as the squared OPE coefficients of ϵ, T and ϵ' (the second exchanged scalar) associated to the green line starting at $(0.55, 1.5)$ in figure 5.5. A similar situation occurs for other choices of initial partitions and by keeping Δ_T unconstrained. The same also holds in $d = 2$ and $d = 4$ dimensions. This is the first important result

the kind 1_1_1 and 1_1_1_1 there are actually two local minima, though the FT still is the global one.

[9] Note that in $d = 3$ (the case shown in figure 5.5), if a scalar gap is imposed (for example, demanding that there can only be one exchanged relevant scalar), depending on the initial CFT data it can happen that the FT cannot be reached and a local minimum is induced.

[10] Understood as a cell of fixed width in Δ_σ and Δ_ϵ.

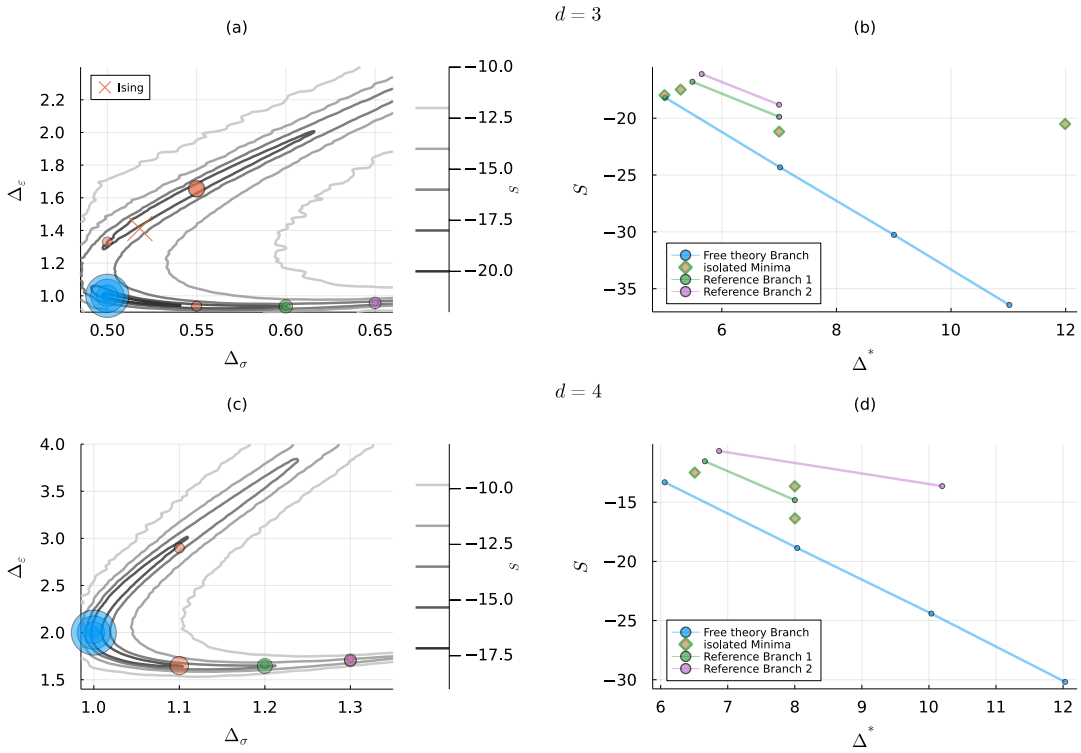

Figure 5.7: Overview of the different minima found in $d = 3$ (top) and $d = 4$ (bottom) with spectra containing one operator per spin. The color code is the same across the panels. *Left:* Minima at fixed Δ_σ. The radii indicate the value of the action S. The larger the radius the smaller S. The contour lines are taken from an high$-T$ search with $\ell_{max} = 6$. *Right:* Value of S for each point along the colored branches in the left panel, identified by its Δ^*.

of our analysis: for most of the spin partitions studied in this work, the landscape of S has a single minimum, which can be reached by trivial gradient descent from (generically) any initial configuration. Note that most trajectories in figure 5.5 reach the FT point following two broad paths in the $(\Delta_\sigma, \Delta_\epsilon)$-plane: i) the extremality line from above, ii) a curve, almost constant in ϵ, from below. The presence of regions in the $(\Delta_\sigma, \Delta_\epsilon)$-plane where the bootstrap equations are more easily satisfied is going to be a common theme in our results.

As we are going to show next, if one fixes at least another Δ one can find local minima along these slices. In the following subsections we will apply the protocol described in section 5.2 for fixed values of Δ_σ and we will show that some of the local minima that are present correspond to known theories (for example the Ising model). However, it is important to remark that none of the minima that we will describe are stable if Δ_σ is allowed to vary, not even the minimum corresponding to the Ising models in $d = 2$ and $d = 3$, in agreement with the results presented in this subsection.

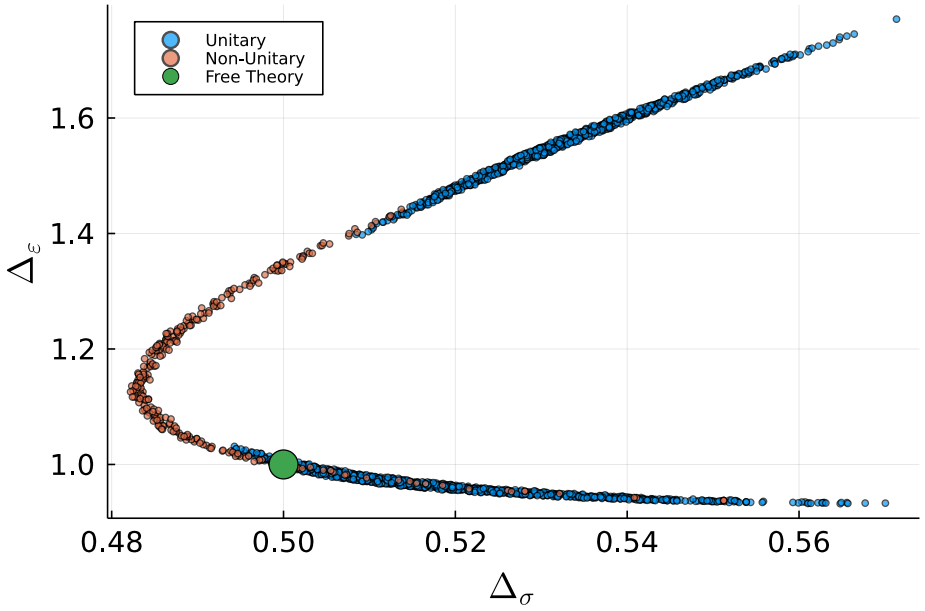

Figure 5.8: Locus of the lowest-action points visited by a wide-search MC in $d = 3$ with spectrum 1_1_1_1. When unitarity is imposed we find two disjoint basins. Allowing for non-unitary configurations gives rise to a single connected basin.

5.3.2 One operator per spin: $d = 3, 4$

We now describe the results of a systematic search of local minima at fixed Δ_σ by the protocol described in subsection 5.2. It is instructive to begin by exploring the simplest possible scenario where

$$n_\ell = 1, \quad \ell = 0, 2, \cdots, \ell_{\text{max}} \,. \tag{5.3.2}$$

Although this assumption looks very restrictive, some basic features of the shape of the landscape of CFTs is already visible in this set-up. Step 3 of the protocol is clearly unnecessary when $n_\ell = 1$, since all the configurations in each run will belong to just one spin sector. We focus on $d = 3$ and $d = 4$ CFTs and ask the following question: aside from the FT, are there other viable approximate solutions to the crossing equations in which (5.3.2) is satisfied? This question might seem academic, given that interacting CFTs have an infinite number of Regge trajectories [100]. However, we are severely truncating the spectrum, so the question we address here is if we can have CFTs where there is a substantial gap between the first Regge trajectory and the others.

An extensive high-T search in $d = 3$ with $\ell_{\text{max}} = 6$ and free Δ_σ – the contour lines in the background of figure 5.7 (a) – shows that there are two (very elliptic) disjoint basins of attraction. The one at the bottom of the panel contains the FT. The upper one, elongated along the extremality bootstrap line, approximately contains

the Ising point in the $(\Delta_\sigma, \Delta_\epsilon)$-plane. Note that the latter basin of attraction has a higher action with respect to the former one.

We searched local minima of S at different fixed values of $\Delta_\sigma = 1/2 + n/20$, $n = 0, 1, 2, 3$, with input spin sectors 1_1_1, 1_1_1_1, 1_1_1_1_1 and 1_1_1_1_1_1. The minima that we found are represented in figure 5.7 (a). In order to better appreciate the value of S at the minima i, the latter are indicated with a circle whose radius r_i is given by

$$r_i \propto S_{\max} - S_i + \alpha \,, \tag{5.3.3}$$

where $S_{\max}$ is the value of S in the minimum with larger action, and α is an offset so that this minimum can still be visible in the figure.

For $n = 0, 1$ two classes of minima are found, one for each of the two basins of attraction. For $n = 2, 3$, instead, we find only minima along the lower basin, with $\Delta_\epsilon < 1$. It should be clear that there is nothing special to the above chosen values of Δ_σ. For each fixed value of Δ_σ we expect to find two local minima if $\Delta_\sigma \lesssim 0.6$ and one for higher values.

We then use the protocol described in section 5.2 with `relTol`= 0.1 and `maxMismatch`= 2 to identify the different branches, which correspond to sets of minima with different input sectors that can however be considered to represent the same "theory" at different truncations. In this way we find that, among these minima, some are isolated and do not from any branch (orange diamonds in panel (b) of figure 5.7), while others form branches (green, pink and blue bullets). The only branch in which the action decreases as a function of Δ^* is the one associated to the free theory, the blue branch in panel (b) of figure 5.7.

In $d = 4$ a similar high-T search with $\ell_{\max} = 6$ and free Δ_σ gives rise to the contour lines in the background of panel (c) of figure 5.7. A search of the minima at different fixed values of $\Delta_\sigma = 1 + n/10$, $n = 0, 1, 2, 3$, with input sectors 1_1_1, 1_1_1_1, 1_1_1_1_1 and 1_1_1_1_1_1 with `relTol`= 0.1 and `maxMismatch`= 2 allows us to identify, also in this case, some local minima at fixed Δ_σ. Like in the $d = 3$ case, some minima are isolated and do not from any branch (orange circles in panel (d) of figure 5.7), while others form branches (green, pink and blue circles). The only branch in which S consistently decreases with Δ^* is the one associated to the FT, the blue branch in figure 5.7 (d).

As we will show in the following, the main structure of the S landscape with two elongated basins of attractions (valleys) will appear repeatedly in the analysis of more complex situations. Note the striking difference between the $d = 3$ and $d = 4$ cases: in the former the basins are two, in the latter the basin is only one. One could argue that this difference is due to the presence of another actual theory in $d = 3$ close to the FT point, the Ising theory, and none in $4d$ within the above

Table 5.2: Scaling dimensions of the first operators appearing in the OPE of σ in the Free Scalar Theory. In these settings $\Delta_\sigma = (d-2)/2$ and $\Delta_T = d$.

	Δ_0 (Δ_ϵ)	Δ_4	Δ_6	Δ_8	Δ_{10}
$d=3$	1.0000	5.0000	6.9999	8.9999	11.0178
$d=4$	1.9999	6.0000	7.9999	9.9993	12.0308

Table 5.3: Scaling dimensions of σ and of the first operators appearing in the OPE of σ in the Free Scalar Theory. Besides unitarity the only constraint imposed is $\Delta_T = d$.

	Δ_σ	Δ_0 (Δ_ϵ)	Δ_4	Δ_6	Δ_8	Δ_{10}
$d=3$	0.50009	0.9997	5.0009	6.9974	8.9973	11.1505
$d=4$	1.00000	2.0035	6.0000	7.9995	9.9997	12.0368

Table 5.4: Comparison between the exact and the numerically determined values of the OPE coefficients squared for the first operators in the Free Scalar Theory. Besides unitarity the only constraint imposed is $\Delta_T = d$.

	λ^2_ϵ	λ^2_T	λ^2_4	λ^2_6	λ^2_8	λ^2_{10}
$d=3$	2.0022	0.093796	0.0042723	0.00022128	1.1604×10^{-5}	8.3384×10^{-7}
Exact	2.0	0.09375	0.0042725	0.0002203	1.1986×10^{-5}	6.7214×10^{-7}
$d=4$	1.9927	0.33343	0.02853	0.0021857	0.00014554	1.4538×10^{-5}
Exact	2.0	0.33333	0.028571	0.0021645	0.0001554	1.0825×10^{-5}

assumptions. Indeed, our results in sections 5.3.2 and 5.3.3 further point to this explanation.

We also find that if the unitarity bounds are relaxed (both on Δ and on the OPE coefficients squared), the aforementioned disjoint valleys in $d = 3$ join in a non-unitary point of the parameter space. This is shown in figure 5.8, where we compare the lowest-lying points in an unitary MC search to those of a non-unitary setting.

The main take-away of this test is that the evolution with respect to Δ^* of the action in branches formed by akin minima seems to be a discriminant factor between spurious minima and physically meaningful ones (the FT in this case); namely, the spurious minima do not create long branches that go down into small values of the action S, while the FT is present for every truncation with very high consistency. We find that in the FT minimum high spin operators are determined quite accurately ($\sim 1\%$ error) except for the highest$-\Delta$ at each truncation, as can be seen in table 5.2.

Although it is clear that the minima at $\Delta_\sigma = (d-2)/2$ are deeper than those away from it, we performed a MC search at $\ell_{\max} = 10$ without any constraint on Δ_σ

besides unitarity. This allows us to understand the precise shape of the landscape around the FT point. After 2×10^8 steps of an extensive search ($T \sim 1$), we chose the global minimum and performed a $T = 10^{-4}$ minimization in order to refine the precise location of this minimum. In table 5.3 we report these values. For completeness we also show in table 5.4 the OPE coefficients determined in this case.

We finally note that for higher Δ^*, namely higher N_{Ops}, the FT minimum is much deeper than the other minima. This means that the latter are very poor solutions to the crossing equations. In other words, we did not find other consistent approximate solutions to the crossing equations, besides the FT, where (5.3.2) is satisfied up to $\ell_{\text{max}} = 10$.

5.3.3 More operators per spin

We now use our protocol to study CFTs with more than one operator per spin with the assumptions discussed at the beginning of the section (presence of an effective $\mathbf{Z}_2$ symmetry and only one relevant $\mathbf{Z}_2-$even scalar).

We here consider viable solutions to the crossing equations the end-point of branches[11] that arrive up to a given ℓ_{max} and include at least 2 different minima with strictly decreasing S. For brevity, we will refer to these end points simply as "end-minima". For example, in the case of only one operator per spin, the "end-minima" are the blue, pink and green circles at the end of the branches in the right panels of figure 5.7. The rationale behind concentrating on end-minima is that they summarize the information from minima at higher ℓ_{max} and thus allow for a cleaner visualization. Since this approach might exclude possible branches that start only at the largest Δ^* here considered, we will also include in our discussion isolated minima at the largest ℓ_{max} considered. They will be also called end-minima in a slight abuse of notation.

Our whole search space includes spectra with $\ell_{\text{max}} = 4, 6, 8, 10$. For $d = 2$ we limit the analysis to $\ell_{\text{max}} = 8$, since at $\ell_{\text{max}} = 10$ the end-minima that we find are so many that they obscure the visualization. Here we only observe that, qualitatively, all the minima that we find at $\ell_{\text{max}} = 10$ differ only by the least relevant operators.

The role of the stress-energy tensor deserves some consideration. For the study of local theories it is necessary to impose the presence of a spin-2 operator with $\Delta_T = d$. In practice, we have also found necessary to impose a gap on the scaling dimension $\Delta_{T'}$ of the second spin-2 operator so that it does not come too close to d and create the effect of a non-local theory by "supplanting" the stress energy tensor. In section 5.3.4 we will study the effect of allowing for non-local theories but

[11] Our parameters for determining the connection between minima are `relTol`= 0.2 and `maxMismatch`= 2.

hereafter it should be understood that unless specified otherwise we fix $\Delta_T = d$ and impose the gap $\Delta_{T'} \geq d + 1$.

We report the end-minima found in the $(\Delta_\sigma, \Delta_\epsilon)$-plane in figures 5.9, 5.13 and 5.16 for the $d = 2, 3, 4$ cases, respectively. We discuss these results separately in the sections below, but a few considerations apply to all cases. The contour lines of the lowest-lying configuration sampled by an high$-T$ MC is shown in the background as a visual aid. The orange dashed line corresponds to rigorous bootstrap bounds, while the green continuous line is the line of GFTs. We use the radius of the points to represent the action as before (see (5.3.3)) and use transparent markers so that coincident minima appear darker. To understand the fact that several minima are superimposed in this representation it is important to keep in mind that there can be up to 10 other dimensions not shown in the plot. Indeed, in many cases there are end-minima which have almost identical values of Δ_σ and Δ_ϵ but differ in the scaling dimensions of the other operators.

$d = 2$

One can wonder if our method can work in $2d$ given that the landscape of CFTs is notoriously very rich. On the other hand, $2d$ is the ideal playground to test the method, since entire classes of CFTs are exactly soluble.

We have considered various MCs for 8 different fixed values of Δ_σ:

$$\Delta_\sigma = \frac{1}{8}, \frac{3}{20}, \frac{7}{40}, \frac{1}{5}, \frac{1}{4}, \frac{2}{7}, \frac{3}{10}, \frac{\sqrt{5}}{10}\,. \tag{5.3.4}$$

When Δ_σ is too small the numerical analysis becomes quite noisy. For this reason, we did not explore values of $\Delta_\sigma < 1/8$. 7 of the values in (5.3.4) have been chosen to be "small" rational numbers, while one was chosen irrational, e.g. numerically equivalent to a "large" rational number. Rational scaling dimensions can be associated to exactly known rational conformal field theories (RCFT). As we will see, in order to limit the number of allowed theories and make the analysis feasible, the assumption of having only one relevant $\mathbf{Z}_2$-even scalar turns out to be particularly important in $2d$. Before presenting our results, it is useful to report some (by no means exhaustive) instances of known CFTs admitting scalars with the above scaling dimensions.

A glimpse at the $2d$ CFT Landscape The landscape of the known CFTs in $2d$ is amazingly rich (cf. section 2.2 for a discussion of some of these theories in more general terms). In contrast to the situation for $d > 2$, in particular, $2d$ CFTs can have a continuum spectrum (e.g. Liouville field theory). It is clear that we

cannot detect such theories.[12] Exactly marginal deformations are ubiquitous in $2d$. These theories will not give rise to minima of S, but to a valley of minima, each corresponding to a CFT as we vary the marginal couplings. Since we look for isolated minima in our search, such theories will also be difficult to detect. The CFTs we can hope to find should have a discrete, relatively sparse, spectrum and should be isolated. Their central charge c is expected to be of order one. Prototypical theories of this kind are RCFTs. Even if we focus on these theories only, we need to further restrict our search space to avoid a proliferation of theories. We will do so by assuming, as mentioned, that only one relevant scalar ϵ can appear in the $\sigma \times \sigma$ OPE. The importance of this assumption can be appreciated by focusing on specific exactly soluble CFTs. We will briefly consider in what follows the space of diagonal unitary minimal models ($c < 1$), the $S^1/\mathbf{Z}_2$ orbifold ($c = 1$) and $SU(2)_k$ Wess-Zumino-Witten (WZW) models ($c > 1$).

Recall that the scaling dimensions of the (Virasoro) primary fields $\phi_{r,s}$ in diagonal unitary minimal models $\mathcal{M}(m+1,m)$ is (conventions as in [21], see also 2.2.1):[13]

$$\Delta_{r,s} = h_{r,s} + \bar{h}_{r,s}\,, \tag{5.3.5}$$

where

$$h_{r,s} = \bar{h}_{r,s} = \frac{((m+1)r - ms)^2 - 1}{4m(m+1)}\,, \quad 1 \leq r \leq m-1\,, 1 \leq s \leq m\,,\ m \in \mathbf{Z}_{\geq 3}. \tag{5.3.6}$$

The range in s in (5.3.6) can be restricted to $1 \leq s \leq r$ using the field equivalence

$$\phi_{r,s} = \phi_{m-r,m+1-s}\,. \tag{5.3.7}$$

Minimal models feature a faithful discrete $\mathbf{Z}_2$ symmetry for any m (see e.g. [101] for a pedagogical exposition).[14] Using the equivalence class (5.3.7), for any r and s we can choose the representative field $\phi_{r,s}$ with $r+s$ an even integer. On these representatives, $\mathbf{Z}_2$-even fields are those with r and s odd, while $\mathbf{Z}_2$-odd fields have r and s even (the identity operator is $\phi_{1,1}$). It is a straightforward exercise to show that there are one or more unitary minimal models which contain a $\mathbf{Z}_2$-odd field σ with scaling dimension equal to each of the first 7 values of Δ_σ reported in

[12] Unless the continuum starts beyond Δ^* in all spin channels, in which case the CFT will simply appear discrete.

[13] In the $2d$ CFT literature, Virasoro and $SL(2,\mathbb{C})$ primaries are usually denoted primaries and quasi-primaries (respectively). In numerical bootstrap analysis we usually care about $SL(2,\mathbb{C})$ primaries, which are the analogues of the primary fields in $d > 2$ CFTs. Most of the considerations that follow can be made at the level of Virasoro primaries with no need to decompose them in $SL(2,\mathbb{C})$ primaries.

[14] The presence of such a $\mathbf{Z}_2$ symmetry is clear from the equivalence of minimal models with Wess-Zumino-Witten cosets of the form $[SU(2)_{m-2} \times SU(2)_1]/SU(2)_{m-1}$, where $\mathbf{Z}_2$ is the combination of the two $\mathbf{Z}_2$ center symmetries of $SU(2)_{m-2}$ and $SU(2)_1$ which is not gauged by the center of $SU(2)_{m-1}$.

(5.3.4).[15] For instance, for $\Delta_\sigma = 3/20$ within minimal models with $m \leq 100$ we find two which contain a Virasoro primary with that dimension: $\phi_{8,8} \subset \mathcal{M}(15,14)$ and $\phi_{14,14} \subset \mathcal{M}(26,25)$. The fusion rules $\sigma \times \sigma$ contain respectively 42 and 132 Virasoro primaries. Aside from the identity operator, 11 and 21 of these $\mathbf{Z}_2$-even fields have $\Delta < 2$, respectively. The smallest Virasono primaries in the two cases are $\phi_{5,5}$ and $\phi_{3,3}$, with scaling dimensions $\Delta_\epsilon = 2/105, 2/325$, respectively. Models in such kind of field correlators cannot be detected by our method, because i) their OPE contain too many light operators and ii) operators with a too small scaling dimension makes the numerical analysis unfeasible. Imposing that we have only one relevant $\mathbf{Z}_2$-even scalar removes most of these field identifications. The only identification left, for any $m \geq 3$, is the one where $\sigma = \phi_{m-1,m-1} (\sim \phi_{1,2})$ and $\epsilon = \phi_{1,3}$, already considered in [102], which have

$$\Delta_\sigma = \frac{1}{2} - \frac{3}{2(m+1)}\,, \qquad \Delta_\epsilon = 2 - \frac{4}{m+1}\,, \tag{5.3.8}$$

and the simple fusion rules

$$\sigma \times \sigma = 1 + \epsilon\,. \tag{5.3.9}$$

Only 4 among the 7 rational values of Δ_σ in (5.3.4) equal the scaling dimensions of $\phi_{m-1,m-1}$: ordinary ($m = 3, \Delta_\sigma = 1/8$), tricritical ($m = 4, \Delta_\sigma = 1/5$), tetracritical ($m = 5, \Delta_\sigma = 1/4$) and pentacritical ($m = 6, \Delta_\sigma = 2/7$) Ising theories. Note that for even m we have $\mathbf{Z}_2(\sigma) = +\sigma$. However, as far as we consider the four-point function of σ only, given the fusion rules (5.3.9), we can effectively assign an unfaithful $\mathbf{Z}_2'$ charge to σ such that $\mathbf{Z}_2'(\sigma) = -\sigma$ and identify such $\mathbf{Z}_2'$ as the global discrete symmetry of the four-point correlator.

Another notable example which shows the importance of restricting to one relevant scalar is given by the theory of a free compact scalar on a $S^1/\mathbf{Z}_2$ orbifold. This CFT has two Virasoro primaries with $\Delta_\sigma = 1/8$, which are the twisted ground states of the orbifold. They are odd under the quantum $\mathbf{Z}_2$ global symmetry that emerges after the gauging and hence we can consider any of them as our field σ. As well-known, the $S^1/\mathbf{Z}_2$ orbifold is a $c = 1$ theory admitting an exactly marginal deformation, given by the radius R of S^1. At $R^2 = 1$ the theory is equivalent to a decoupled pair of Ising theories.[16] Deforming the radius gives rise to a family of theories related to the Ashkin-Teller model, namely the theory obtained by coupling two Ising models [103]. The OPE of two twist fields give rise to an infinite number of Kaluza-Klein and winding vertex operators (Virasoro primaries) with scaling dimensions [104]

$$\Delta_{m,n} = \frac{m^2}{R^2} + \frac{n^2 R^2}{4}\,, \qquad m \in \mathbf{Z}\,, n \in 2\mathbf{Z}\,. \tag{5.3.10}$$

[15] Of course, minimal models associated to the irrational value of Δ_σ reported in (5.3.4) can also be found provided we take m large enough and approximate $\sqrt{5}/10$ with an appropriately chosen rational number.

[16] In our normalizations, like those of [21], the self-dual radius is $R^2 = 2$.

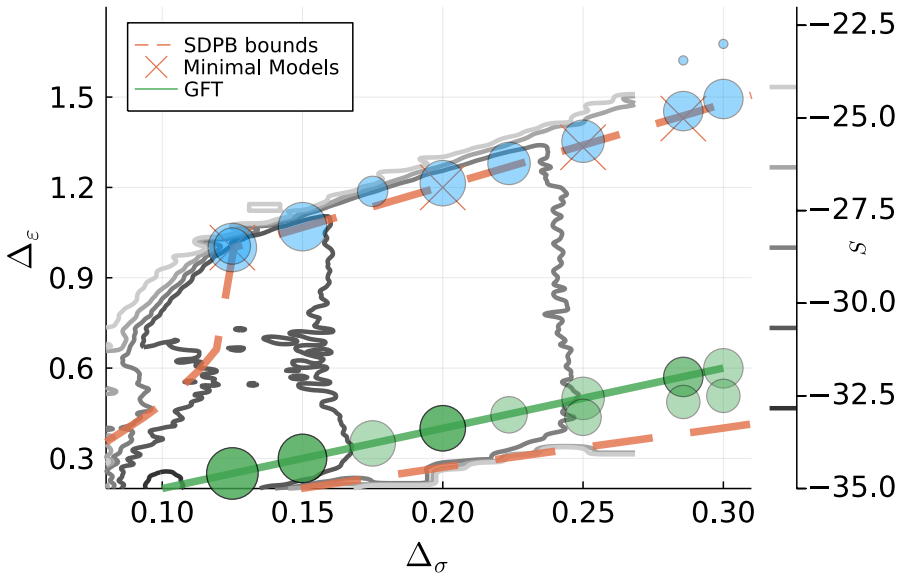

Figure 5.9: $d = 2$. Location of the end-minima with $\ell_{\max} \leq 8$ in the $(\Delta_\sigma, \Delta_\epsilon)$-plane. The end-minima belong to different sectors all of them contained in 4_4_3_2_1. The dashed orange line corresponds to the bounds obtained in [31] assuming only one $\mathbf{Z}_2$-even relevant scalar. All the end minima correspond to local theories $\Delta_T = 2$, $\Delta'_T \geq 3$.

At $R^2 = 1$, the two Ising theories are decoupled and this theory is indistinguishable from a single Ising copy. When $R \neq 1$ the two couples to each other and we get a continuum of $c = 1$ CFTs parametrized by R. For any R such theories contain more than 1 relevant $\mathbf{Z}_2$-even scalar, as we see from (5.3.10) by setting either m or n to zero. In this case, restricting to only one relevant $\mathbf{Z}_2$-even scalar is crucial to avoid a continuum of theories, which would be a challenge for our numerical methods.

The external operator σ could also be part of a CFT with a continuous global symmetry G. CFTs with continuous global symmetries should of course be analyzed in a covariant way exploiting the symmetry, see e.g. [70]. However, if $G \supset \mathbf{Z}_2$ the field σ could be considered some (real) component of a multiplet in a representation of G for which $\mathbf{Z}_2(\sigma) = -\sigma$. For example, σ could be the real component of a spin j multiplet, with half-integer j, of a $SU(2)_k$ WZW model. More specifically, we could have

$$\sigma \sim \phi_{j,m}(z)\bar{\phi}_{j,-m}(\bar{z}) + \phi_{j,-m}(z)\bar{\phi}_{j,m}(\bar{z})\,, \tag{5.3.11}$$

where $\phi_{j,m}(z)$ and $\bar{\phi}_{j,\bar{m}}(\bar{z})$ are the holomorphic and anti-holomorphic highest-weight state components of the spin j field. The symmetry $\mathbf{Z}_2$ could be identified with the center of either the holomorphic or of the anti-holomorphic $SU(2)$ gauge group.

With the identification (5.3.11), we have

$$\Delta_\sigma = \frac{2j(j+1)}{k+2}\,, \qquad j \in \frac{\mathbf{Z}}{2}\,. \tag{5.3.12}$$

At $\Delta_\sigma = 1/5, 2/7$ there are no solutions with integer k and half-integer j of (5.3.12). For the remaining rational values in (5.3.4) we have an infinite number of solutions with increasing values of j and k. Solutions with $j > 1/2$ have more than one relevant $\mathbf{Z}_2$-even scalar exchanged in the $\sigma \times \sigma$ OPE. On the other hand, for $j = 1/2$ we get only one relevant $\mathbf{Z}_2$-even scalar with[17]

$$\Delta_\epsilon = \frac{4}{k+2}\,. \tag{5.3.13}$$

This occurs for 4 of the values reported in (5.3.12):

$$\Big(k=3, \Delta_\sigma = \frac{3}{10}\Big), \quad \Big(k=4, \Delta_\sigma = \frac{1}{4}\Big), \quad \Big(k=8, \Delta_\sigma = \frac{3}{20}\Big), \quad \Big(k=10, \Delta_\sigma = \frac{1}{8}\Big). \tag{5.3.14}$$

This quick detour on some well-known $2d$ CFTs shows the importance of reducing the space of viable theories by demanding only one relevant scalar. Needless to say, the space of CFTs is vastly larger than the three classes we discussed, so it is likely that other CFTs with σ operators with scaling dimensions as in (5.3.4) and only one relevant $\mathbf{Z}_2$-even scalar exist.

Results in $d = 2$ We report in figures 5.9 and 5.10 the location of the end-minima found with $\ell_{\max} \leq 8$ in the $(\Delta_\sigma, \Delta_\epsilon)$ and (Δ_σ, c)-planes, respectively. The end-minima belong to different sectors, all of them contained in 4_4_3_2_1.

Most of the end-minima are aligned along two approximately straight trajectories in the $(\Delta_\sigma, \Delta_\epsilon)$-plane. The blue end-minima are along the upper extremal bootstrap bounds, while the green ones are aligned along the GFT line, despite the constraint $\Delta_T = 2$.

Let us first discuss the blue end-minima. Two less significant blue end-minima appear above the extremal line in the disallowed region, indication of being fake end-minima not associated to CFTs. The rest are in good agreement with the bootstrap bounds.

It is reassuring that, among such end-minima, we reproduce the first 4 minimal models (red crosses in figure 5.9), with the field identification as in (5.3.8) discussed before. The remaining four points along the line correspond instead to the so called

[17] We also have marginal scalars with $\Delta = 2$ associated to the $J\bar{J}$ operators arising from the identity character.

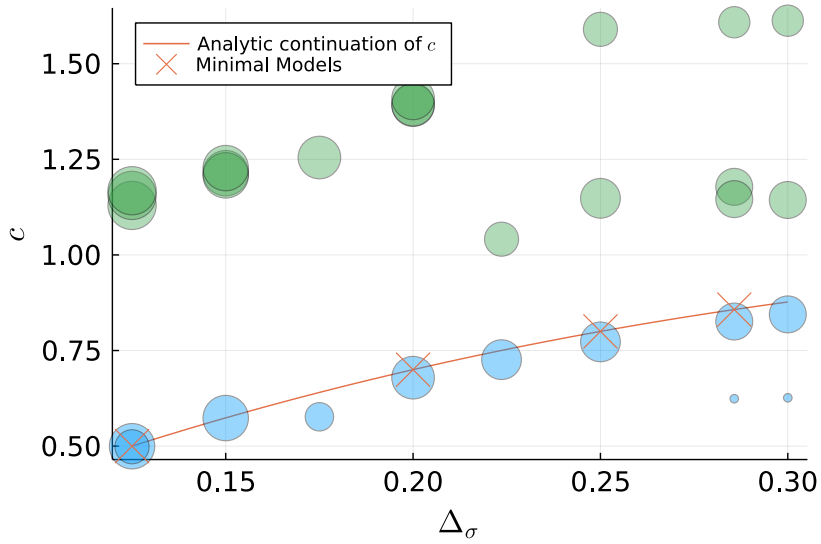

Figure 5.10: Central charge c as a function of Δ_σ for end-minima with $\ell_{\text{max}} \leq 8$ in $d = 2$. The end-minima belong to different sectors all of them contained in 4_4_3_2_1. Comparison of our results to the analytic expectation (5.3.16) (red line) for the generalized minimal models. All the end minima correspond to local theories $\Delta_T = 2$, $\Delta'_T \geq 3$.

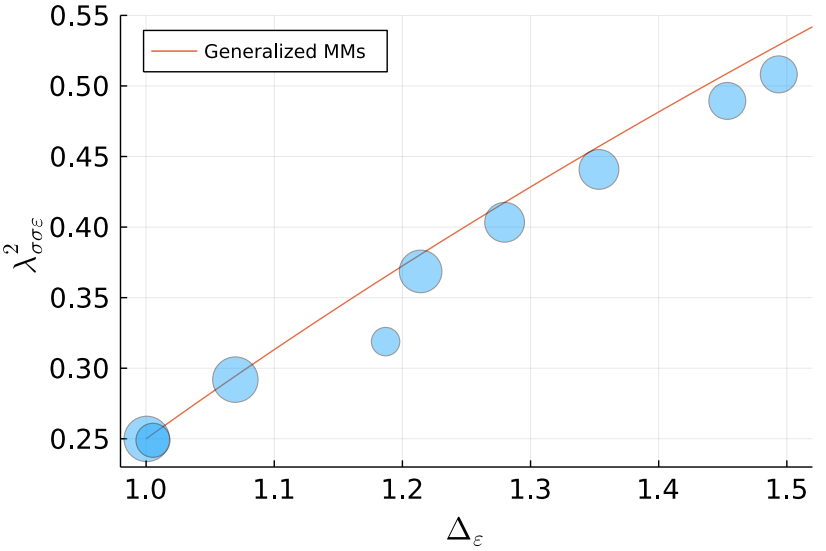

Figure 5.11: $d = 2$. Comparison between the OPE squared coefficient $\lambda^2_{\sigma\sigma\epsilon}$ numerically determined from the blue end-minima in figure 5.9 and its analytic expression for generalized minimal models (red line) [30], as a function of Δ_ϵ.

generalized minimal models [30], i.e. non-unitary minimal models obtained by analytically continuing the CFT data appearing in the 4-point correlation function from integer values of m (minimal models) to real values of m (generalized minimal mod-

els). Such theories are visible in the conformal bootstrap, despite the enforcement of unitarity, because the OPE coefficients squared of the exchanged quasi-primaries have been conjectured in [30] (see also [58]) and then proved in [31], to be positive for any m.

Given (5.3.8), the blue end-minima should be aligned along the line

$$\Delta_\epsilon = \frac{2}{3} + \frac{8}{3}\Delta_\sigma \,. \tag{5.3.15}$$

In terms of the central charge, we have

$$c = \frac{9\Delta_\sigma}{\Delta_\sigma + 1} - 4\Delta_\sigma \,. \tag{5.3.16}$$

We compare in figure 5.10 the central charge (5.3.16) with the one extracted from the OPE coefficient $\lambda_{\sigma\sigma T}$ by means of the relation

$$c = \frac{d}{d-1}\frac{\Delta_\sigma^2}{4\lambda_{\sigma\sigma T}^2} \,, \tag{5.3.17}$$

valid for general d dimensions. We see that the agreement is very good, despite the severity of our truncation, and confirm also the identification of such end-minima with generalized minimal models.

As a further check we compare in figure 5.11 the OPE coefficient squared $\lambda^2_{\sigma\sigma\epsilon}$ with the one analytically found for such models in appendix B of [30]. The good agreement found is yet another indication of the accuracy of our determination and of the nature of the blue end-minima. The only exception is the minimum at $\Delta_\sigma = 7/40$, which falls slightly above the SDPB bounds in figure 5.9 and its values of c and $\lambda^2_{\sigma\sigma\epsilon}$ in figures 5.10 and 5.11 are slightly misaligned with those of the generalized Minimal Models. We expect this to be due to some numerical artifact and that a more thorough study will find a lower action minimum that better agrees with the theoretical values.

Let us now discuss the green end-minima of figure 5.9. In contrast to the blue ones, we do not have a convincing explanation for the nature of these end-minima as local CFTs, assuming they are not numerical artifacts. Most of them lie on the GFT line $\Delta_\epsilon = 2\Delta_\sigma$. A notable class of local CFTs that have in their spectrum operators with scaling dimensions related in this way are $\mathcal{N} = 2$ CFTs. It would be interesting to understand if the green points along the GFT line (or some of them) can be identified as $\mathcal{N} = 2$ Supersymmetric Minimal Models, provided an appropriate identification of σ is made. This analysis would probably require also to understand whether generalized $\mathcal{N} = 2$ minimal models, in the spirit of [30], exist and can be constructed.

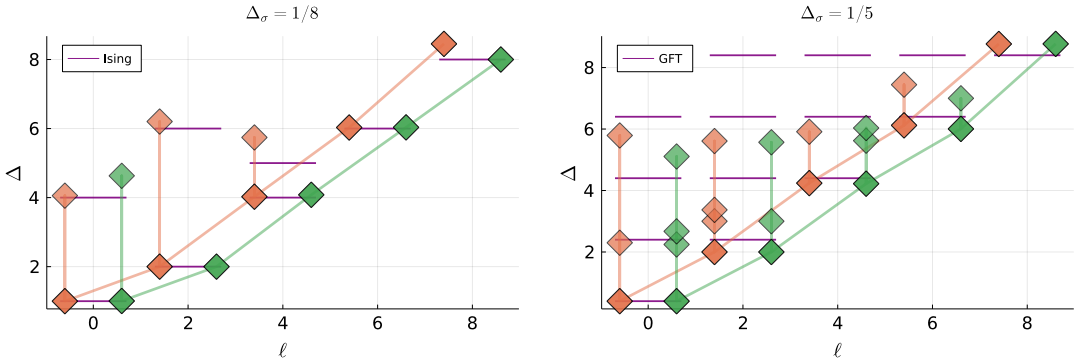

Figure 5.12: Full spectrum of selected end-minima in $d = 2$ with $\Delta_T = 2$ and $\Delta_{T'} \geq 3$. *Left:* Ising-like end-minima. *Right:* GFT-like end-minima. The colors and the lines connect operators within the same end-minimum. For comparison we also report the exact scaling dimension of the 2d Ising and GFT with purple lines.

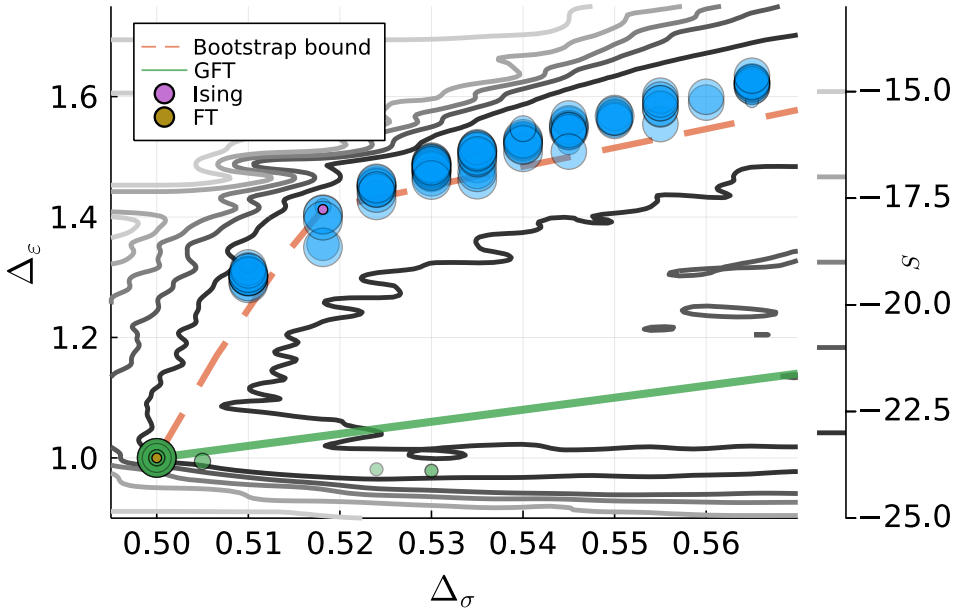

Figure 5.13: $d = 3$. Location of the end-minima with $\ell_{\max} \leq 10$ in the $(\Delta_\sigma, \Delta_\epsilon)$-plane. The end-minima belong to different sectors all of them contained in 4_4_4_3_2_1. The dashed line is the upper bound for Δ_ϵ from [48].

Despite we enforced the presence of an energy momentum tensor, the green end-minima along the GFT line could simply be an approximation of GFTs themselves. This observation is supported by the fact that if we remove the gap assumption $\Delta_{T'} \geq 3$ most of the green minima are unstable. In particular, $\lambda^2_{\sigma\sigma T} \sim 0$ and $\Delta_{T'} \approx 2\Delta_\sigma + 2$ effectively replaces T as the first spin-2 operator. Similarly, if we do not assume the existence of an energy momentum tensor, most minima turn out to be GFTs. As we will see in the next subsections, the analogue of the green

points in figure 5.9 will not occur in $d > 2$ when we enforce the presence of an energy-momentum tensor.

It is useful to also report the spectrum of $SL(2,\mathbb{C})$-primary operators which appear at the end-minimum at a given truncation. We report as an example in figure 5.12 the full spectrum of some end-minima found at $\Delta_\sigma = 1/8, 1/5$ (two in each case). The operators associated to the same end-minimum are connected with lines. In the Ising case, where the identification of the end-minima with the Ising model is quite convincing, we see how the agreement of the whole low-lying spectrum is quite accurate, with small deviations occurring for higher-spin operators in the first Regge trajectory (the spin-8 orange diamond) or for operators in the second Regge trajectory (the second spin-0 green diamond, the second spin-4 orange diamond).

In the GFT-like case, as already mentioned, we do not have a convincing explanation for the nature of such theories. Despite having enforced the presence of a spin 2 operator at $\Delta = 2$, we can see from the right panel of figure 5.12 that the spectrum resembles roughly the one of GFTs. The presence of more operators with respect to the Ising case makes the accuracy of the numerics less accurate. In particular, it is not possible to disentangle if the significant deviations from the GFT spectrum at higher Regge trajectories are, in addition to numerical noise, due trivially to the fact that we have imposed the presence of a non-existent operator (the stress-tensor), or because the theory under question is in fact distinct from a GFT. See appendix 5.3.3 for some further details, in particular for examples of selected branches, the endpoints of which correspond to the blue and green end-minima discussed above.

It is well possible that other theories with a relatively sparse spectrum satisfying our assumptions (or effectively doing it, like the generalized minimal models) might have not been found by our search protocol, given also the limitations imposed by machine precision computations and the small values of Δ^* and N_{Ops} we sampled. Possible theories of this kind are for instance the $SU(2)_k$ WZW models (5.3.14) with the field identification (5.3.11).

$d = 3, 4$

In $d = 3$ we run our protocol for the following values of Δ_σ:

$$\Delta_\sigma = 0.5,\ 0.505,\ 0.51,\ 0.5181489,\ 0.524,\ 0.53,\ 0.535,\ 0.54,\ 0.545,\ 0.55,\ 0.555,\ 0.56,\ 0.565. \tag{5.3.18}$$

We plot in figure 5.13 the end-minima found in the $(\Delta_\sigma, \Delta_\epsilon)$-plane, with $\Delta_T = 3$, $\Delta_{T'} \geq 4$, $\Delta_{\epsilon'} \geq 3$. All the end-minima lie at the extremality bound, like in the $d = 2$ case. In contrast to the latter, no end-minima along the GFT line appear, while we

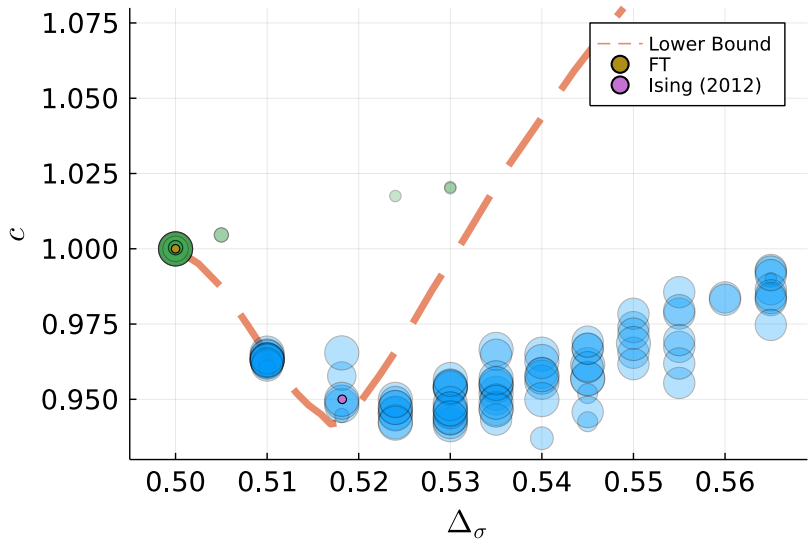

Figure 5.14: Central charge c as a function of Δ_σ for end-minima with $\ell_{\text{max}} \leq 10$. The end-minima belong to different sectors all of them contained in 4_4_4_3_2_1. The rigorous lower bounds are taken from [58]. The color code of the end-minima is the same as in figure 5.13.

find a couple of faint end-minima with $\Delta_\epsilon < 1$, below the GFT line.[18]

Reassuringly, we get end-minima in correspondence of the 3d Ising model, which sits at the kink of the dashed orange lines. End-minima are found for all the Δ_σ in (5.3.18) with the exception of $\Delta_\sigma = 0.505$. The lack of an end-minimum at such value is due to the imposed gap $\Delta_{\epsilon'} \geq 3$. Indeed, by repeating the MC analysis of section 5.3.1 with Δ_σ unconstrained assuming $\Delta_{\epsilon'} \geq 3$, the "flow" towards the FT passing through the valley connecting the Ising point with the FT in figure 5.5 gets interrupted around $\Delta_\sigma = 0.510$. This is an indication that possible extremal CFTs with $0.5 \leq \Delta_\sigma \leq 0.510$ do have more than one $\mathbf{Z}_2$-even scalar.[19]

We plot in figure 5.14 the central charge of the end-minima, computed using (5.3.17), as a function of Δ_σ. The dashed orange lines delineate the rigorous lower bound of [58]. Most of the end-minima in figures 5.13 and 5.14 lie in the forbidden region, slightly in the former case and more evidently in the latter. This difference should not come as a surprise, since it is known that the bounds on the central charge are more sensitive than those on Δ_ϵ to higher dimensional operators. Compare e.g. figures 3 and 4 of [99] to appreciate the different convergent properties of the two bounds as the degree of truncation is varied.

[18] At low ℓ_{max} we get an entire line of minima, but these do not create consistent branches. As we will see later when discussing non-local theories, end-minima along the GFT line are reassuringly found when we fix $\Delta_T = 2\Delta_\sigma + 2$ (the GFT value), as expected.

[19] Note that this region is devoid of not only end-minima, but of minima at all.

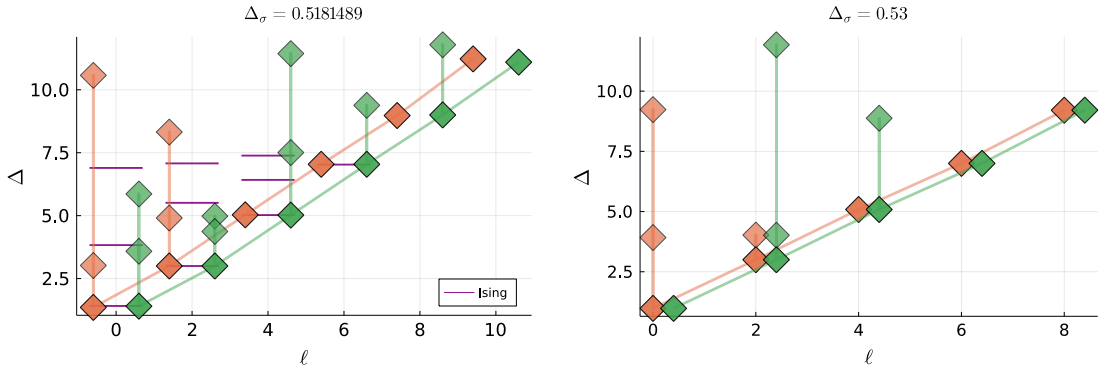

Figure 5.15: *Left:* Full spectrum of the minima found at $\Delta_\sigma = 0.5181489$, $\Delta_T = 3$ that resemble the critical Ising model in $d = 3$. Ising reference values taken from [105]. *Right:* Full spectrum of the minima found at $\Delta_\sigma = 0.53$, $\Delta_T = 3$ that have Δ_ϵ below the GFT line. The colors and the lines connect operators within the same end-minimum.

The spectra associated to the branches with $\Delta_\sigma = 0.5181489, 0.53$ is reported in figure 5.15. In the left panel we also report as reference values the Ising spectrum found in [105] using the Extremal Functional Method (purple lines). The operators associated to the same end-minimum are connected with lines. In the Ising case we see how the accuracy is significantly worse with respect to the $2d$ case. We have a reasonably good agreement of the low-lying spectrum in the first Regge trajectory, but the remaining operators have a significant indeterminacy. Similarly, in the right panel of figure 5.15 the operators in the first Regge trajectory agree among the two orange and green branches, but significantly differ at higher levels.

In $d = 4$ we run our protocol for the following values of Δ_σ:

$$\Delta_\sigma = 1,\ 1.05,\ 1.1,\ 1.15,\ 1.2,\ 1.3. \tag{5.3.19}$$

Due to the limited numerical accuracy of our protocol in $d = 4$ we just report in figure 5.16 the end-minima found in the $(\Delta_\sigma, \Delta_\epsilon)$-plane with $\Delta_T = 4$, $\Delta_{T'} \geq 5$, $\Delta_{\epsilon'} \geq 4$, with $\ell_{\text{max}} \leq 10$. Once again we have end-minima along the extremality bound but it is interesting to see how our minima satisfy the older bounds (with less derivatives) of [11] but are slightly excluded by the bounds in [47]. Interestingly enough, for each value of Δ_σ sampled we also find end-minima below the GFT line.

Minima and End-Minima

We now take a small detour to better illustrate the relation between minima and end-minima. As discussed in the main text, end-minima are defined as those special minima which are the end-points of branches. The latter are a set of akin minima, which can arguably be associated to the same CFT in the $\Delta^* \to \infty$ limit.

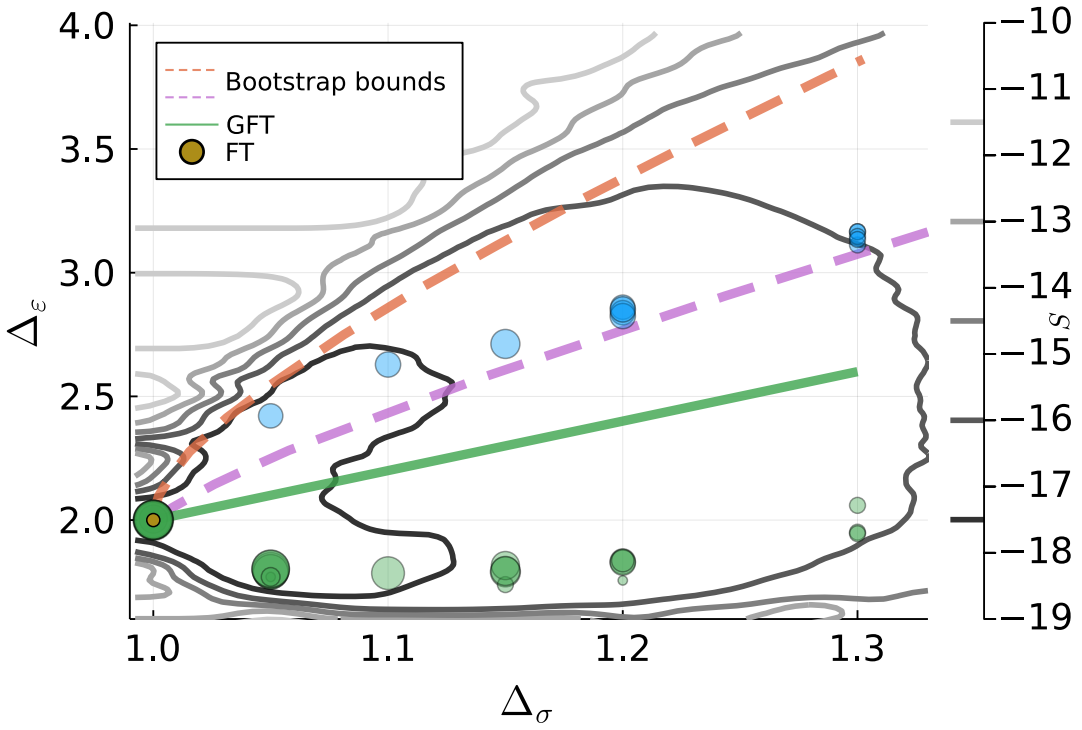

Figure 5.16: $d = 4$. Location of the end-minima with $\ell_{\max} \leq 10$ in the $(\Delta_\sigma, \Delta_\epsilon)$-plane. The end-minima belong to different sectors all of them contained in 4_4_4_3_2_1. The dashed orange and purple lines correspond to the bounds obtained in [11] and [47], respectively.

We report in the left panel of figure 5.17 the individual minima found in $d = 2$ for some selected branches at $\Delta_\sigma = 1/8$ (Ising) and at $\Delta_\sigma = 1/5$ (GFT-like). Note the difference with respect to figure 5.9 where we reported only the end-minima associated to the end-points of *all* the branches. Here, we pick up a given branch and show all the minima contained in it. Since most of these minima overlap in figure 5.17 and similarly several branches overlap in figure 5.9 (detectable from the darker color of the circles), the difference between the two figures can be overlooked at first glance. In the right panel of figure 5.17 we report the value of the action S for each of these minima making the branches manifest. We also note in passing that the spectrum at the end-minimum for each value of Δ_σ is shown in figure 5.12 in orange (the green spectrum corresponds to a similar spectrum not belonging to the same branch).

In order to have an estimate of how the action is supposed to decrease with Δ^*, we also report the branch obtained by starting low T-MCs from several truncations of the exact Ising scaling dimensions (purple squares in the right panel of figure 5.17). This implies that there are several minima in the vicinity of the exact Ising values and that our protocol is able to find at least a subset of them. It is also reassuring

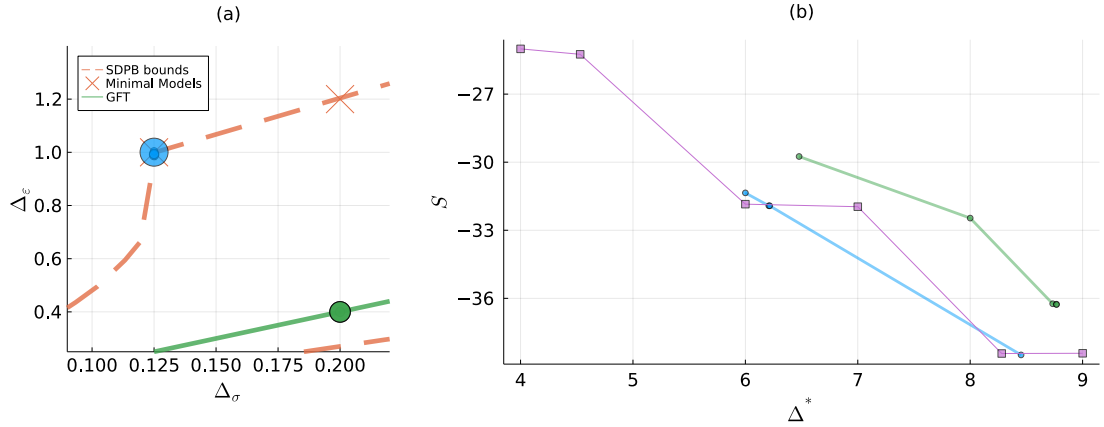

Figure 5.17: Representative branches in $d = 2$ local CFTs. (a): Location of individual minima (colored circles) with $\ell_{\text{max}} \leq 8$ in the $(\Delta_\sigma, \Delta_\epsilon)$-plane. The minima belong to different sectors all of them contained in 4_4_3_2_1. The dashed orange line corresponds to the bounds obtained in [31] assuming only one $\mathbf{Z}_2$-even relevant scalar. (b) Value of the action as a function of Δ^* for each branch. Color codes are the same in the two panels. Namely, each minimum in (a) corresponds to a related small circle in (b) of the same color. The purple Ising ref. branch is the one obtained by our protocol when starting from the exact scaling dimensions for the 2d Ising model.

to see that the decrease in S of the branches found and of the Ising benchmark branch are fully compatible. The good behaviour of the GFT-like branches is the main reason why we believe such theories are not numerical artifacts.

As further example we show in the left panel of figure 5.18 the individual minima for three selected end-minima in $d = 3$. The blue one corresponds to the Ising model, the green one to the end-minimum below the GFT green line and the olive one to one of the end-minima at $\Delta_\sigma = 0.55$. In the right panel we show the value of the action S for each of these minima (the color code indicates the different branches).

We point out in passing that a consistent branch should not necessarily be monotonically decreasing as Δ^* increases, because it can happen that minima with less operators have a slightly higher Δ^* than a related minima with a denser spectrum. For instance, the green branch in figure 5.18 (b) would seem to "turn around" at the beginning, but the important fact is that we make sure that minima with more operators have strictly smaller S.

5.3.4 Non-local theories

In this subsection we analyze the structure of the minima found when relaxing the condition $\Delta_T = d$. The most notable and exactly calculable non-local theory is

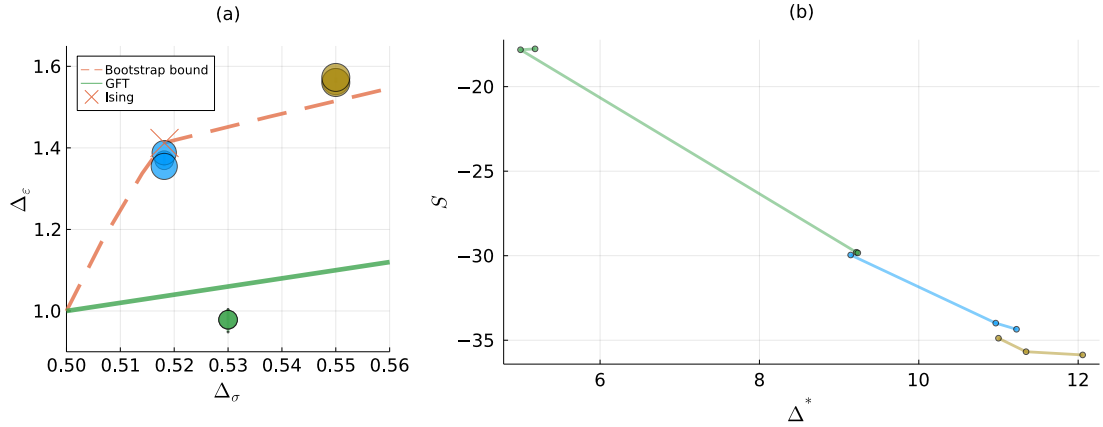

Figure 5.18: Representative branches in $d = 3$, $\Delta_T = 3$. (a): Location of individual minima (colored circles) with $\ell_{\max} \leq 10$ in the $(\Delta_\sigma, \Delta_\epsilon)$-plane. The minima belong to different sectors all of them contained in 4_4_4_3_2_1. Several minima overlap and appear as a single one. The dashed orange line is the bound reported in [58]. (b) Value of the action as a function of Δ^* for each branch. Color codes are the same in the two panels. Each minimum in (a) corresponds to a related small circle in (b) of the same color.

the GFT. At a given Δ^* the number of operators in the GFT spectrum is larger than the maximal truncation we considered in this paper. Although in principle this rules out the possibility of finding exactly the GFT as end-minima in our approach, the limitation is only theoretical, considering that our numerical accuracy does not anyhow allow to precisely determine operators beyond the first Regge trajectories, as we have seen. In fact, we will find end-minima which seem quite compatible with the leading operators of the GFT at different values of Δ_σ.

The landscape of end-minima is now much richer and cover most of the allowed region. Interestingly enough, along the Δ_T direction we find that there is a clear tendency of the minima to cluster around $\Delta_T \approx 2\Delta_\sigma + 2$, see figure 5.19 (a) for $d = 2$ (a similar phenomenon occurs in $d = 3$ and $d = 4$), where we report the distribution of the end-minima in the $(\Delta_\sigma, \Delta_T)$ plane. As can be seen, we have many more end-minima with respect to those found when $\Delta_T = d$ and $\Delta_{T'} > d + 1$ were imposed. Interestingly enough, most end-minima have $d \leq \Delta_T \leq d + 2\Delta_\sigma$. Note that only for a limited range in Δ_σ, end-minima with $\Delta_T = d$ are found. This is particularly evident in $d = 2$, where an end-minimum at $\Delta_T = 2$ is found only at $\Delta_\sigma = 1/8$. This signals the fact that the extremal end-minima associated to the (generalized) minimal models with $m > 3$ found in subsection 5.3.3 become unstable when we relax Δ_T and move towards the GFT region. In panel (a) of figure 5.19 two specific end-minima points have been singled out at $\Delta_\sigma = 1/8$ (green circle) and at $\Delta_\sigma = 3/10$ (red circle). They have been selected as those resembling most closely the GFT conformal data using (5.3.20) as criterion. The truncated spectrum

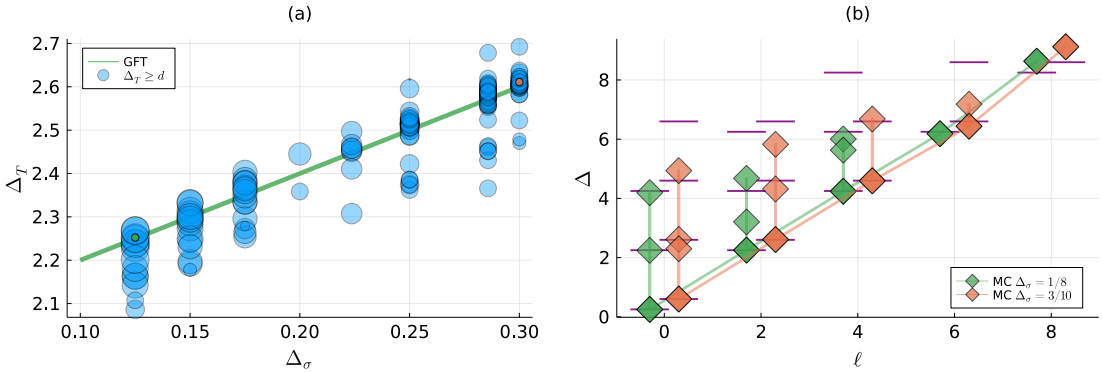

Figure 5.19: (a): End-minima in $d = 2$ with no condition on Δ_T besides unitarity. (b): Spectra for the closest match to the GFT for $\Delta_\sigma = 1/8, 3/10$. The colors and the lines connect operators within the same end-minimum. Purple lines represent the theoretical values of the GFT at that Δ_σ.

at those points is reported in panel (b) of figure 5.19. Note the good agreement beyond the first Regge trajectory, in particular in the scalar sector where the first three scalars are well reproduced in both theories.

We have also explored the effect of fixing the scaling dimension of the first spin 2 operator at the exact GFT value, still assuming $\Delta_{T'} \geq d + 1$. This is useful to understand whether minima at fixed Δ_T are "harder" to reach than similar points when Δ_T is allowed to vary. We show these results in figure 5.20 for the $d = 3$ case, where the blue circles are obtained at $\Delta_T = 3$ and are the same as in figure 5.13, while the red ones are those arising at $\Delta_T = 2\Delta_\sigma + 2$. The red end-minima align along the GFT line, as expected, but they spread a wider area, which however does not include the extremality region. Similar considerations apply also in $d = 2$ and $d = 4$.

We saw in figure 5.19 (a) that some of the minima found by our protocol at $\Delta_\sigma = 1/8$ do resemble local theories, although they are clearly disfavoured in front of the GFT-like ones. We would like to determine more precisely how well we reproduce local theories when no constraint on Δ_T is imposed. This can be attained by taking the 2d Ising theory and the GFT as reference points and defining a distance measure between our minima and these exactly known CFTs. We will here take the scaling dimensions of the first scalar and first spin-2 operators and their associated OPEs coefficients, and compute the average relative error with respect to those of the known theory:

$$Q(\mathbf{v}_{min}, \mathbf{v}_{exact}) = \frac{1}{4}\sqrt{\sum_{i=1}^{4}\left(\frac{v^i_{min} - v^i_{exact}}{v^i_{exact}}\right)^2}. \tag{5.3.20}$$

where $\mathbf{v} = (\Delta_\epsilon, \Delta_T, \lambda^2_{\sigma\sigma\epsilon}, \lambda^2_{\sigma\sigma T})$.

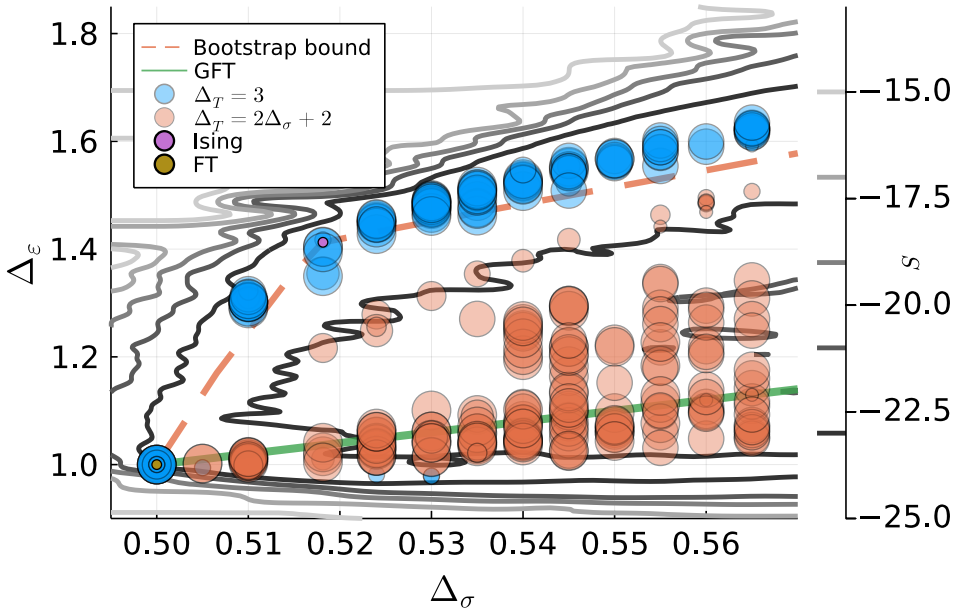

Figure 5.20: $d = 3$. Same as figure 5.13 but we also show with red circles the minima found by fixing Δ_T to the GFT value. Note that we show here in blue all the end-minima that in figure 5.13 were reported in blue and green.

In figure 5.21 we show how the blue circles reach configurations that are not too far away from the 2d Ising theory (roughly 10% mean relative error) but also cover configurations which reproduce the leading conformal data of the GFT even better than the MC which had $\Delta_T = 2 + 2\Delta_\sigma$ to begin with. Finally, figure 5.21 supports the interpretation of the green minima in figure 5.9 to be "images" of the GFT, since we can appreciate that they correspond to solutions which reproduce the Conformal Data of this theory with an error of less than 10%.

5.3.5 A taste of non-unitarity: The 2d Yang-Lee Model

The MC search protocol of section 5.2 does not rely on unitarity. Although we mostly focus on unitary models in this paper, we would like to briefly show here a proof of concept of its use in the non-unitary realm, by checking that the $d = 2$ Yang-Lee (YL) model can easily be found using our method. Non-unitary theories have received less attention from the bootstrap community due to their non tractability with linear or positive semidefinite programming methods. The best approach so far to solve non-unitary theories with the conformal bootstrap is given by [20, 54], which also severely truncates the crossing equations (as we do). As well-known, the $d = 2$ YL model can be described by the non-unitary minimal model $\mathcal{M}(5, 2)$, which contain only two Virasoro primaries related by the following fusion rule:

$$\Phi \times \Phi \sim 1 + \Phi. \tag{5.3.21}$$

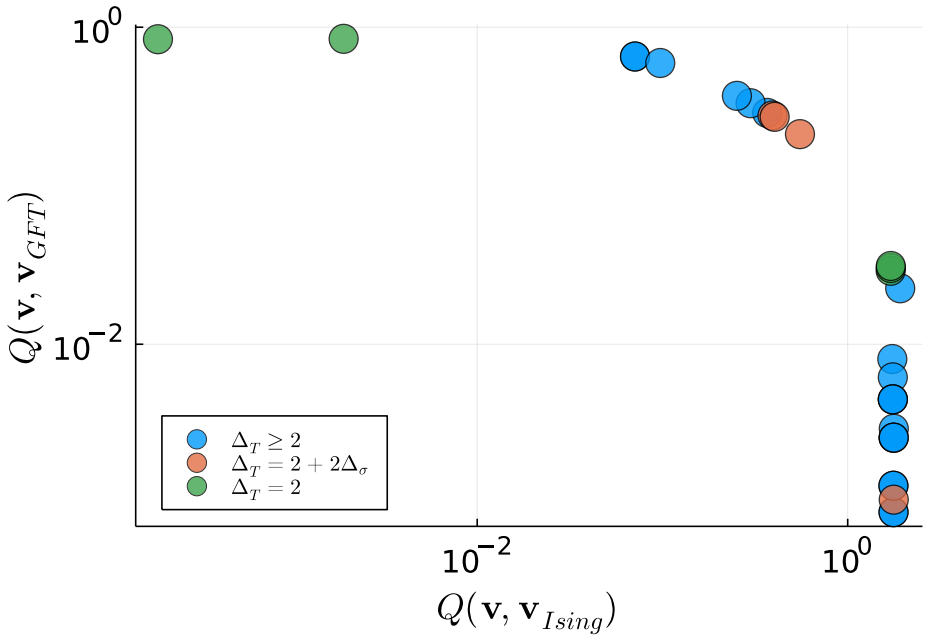

Figure 5.21: Distance of different end-minima to the $d = 2$ Ising and the GFT with $\Delta_\sigma = 1/8$. The quantity Q is computed according to (5.3.20) for end-minima with $\Delta_T = 2, 2 + 2\Delta_\sigma$ and those in which Δ_T is determined dynamically.

This means in practice that the external dimension Δ_ϕ will also be the scaling dimension of the first exchanged scalar and that we must not impose positivity of the OPE coefficients.

We launched a Metropolis Monte Carlo search with $T = 0.5$ and a spectrum 3_1_2_1 ($\Delta^* = 9$) to sample a parameter space close to the one containing the exact CFT data of the $2d$ YL model. We find that the global minimum is compatible with the exact values, as can be seen in figure 5.22 for Δ_ϕ and Δ_4 (the first spin 4 operator). At the global minimum the other operators show also similar agreements with the exact values.

We note in passing that in $d = 3$, if we relax the positivity constraint on the OPE coefficients, a search with a 1_1_1_1 spectrum shows another basin of attraction besides those discussed in section 5.3.2. The basin is in a region well below the unitarity bounds for Δ_σ and lies roughly along the line $\Delta_\sigma = \Delta_\epsilon$. Besides being an interesting feature of the landscape in itself, we consider this to be an indication that the $d = 3$ YL model should also appear as a minimum if investigated with our method.

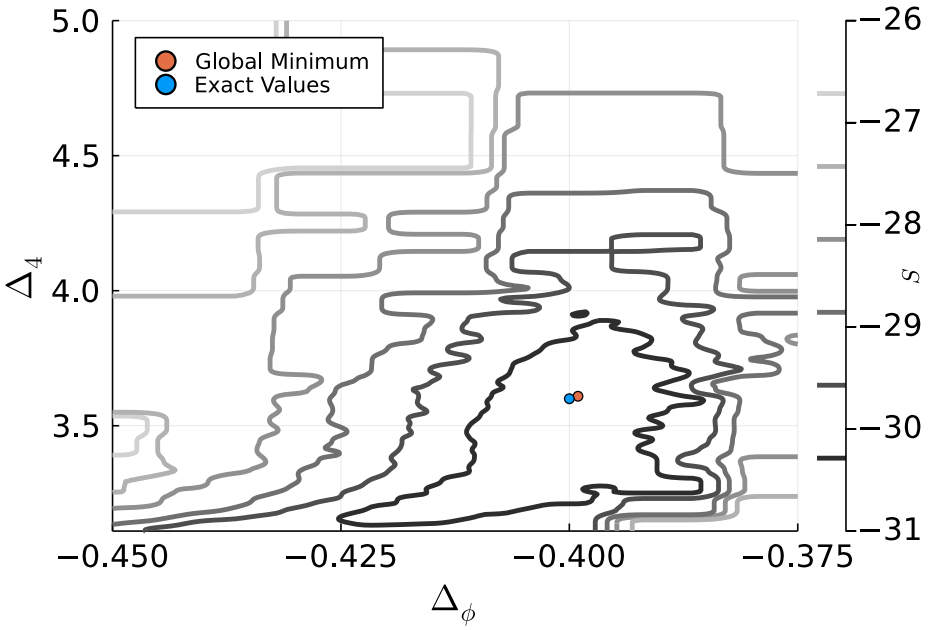

Figure 5.22: Projection of the value of the action S on the (Δ_ϕ, Δ_4)- plane. The lowest-action point visited by the MC at $T = 0.5$ and the exact values are shown as red and blue circles, respectively.

5.4 Outlook

Motivated by the pressing need of a tool to explore the inner part of the allowed space of CFTs, we have introduced in this section a method based on a stochastic minimization via a Metropolis algorithm to find approximate numerical solutions with a sufficiently sparse spectrum of operators to truncated bootstrap equations for CFTs in arbitrary dimensions. Given an initial value of scaling dimensions for a reduced set of primary operators up to some scaling dimension Δ^*, the action (5.1.6) is minimized and an approximate set of CFT data found.

While for all physical CFTs we should eventually have $F = e^S \to 0$ in the limit when all operators are taken into account, at fixed operator truncation the rate in which this limit is reached does matter. For instance, we have seen that for arbitrary severe truncations of the operator spectrum, the free theory minimum dominates over all and no other theory can be found, see e.g. figure 5.5. In order to find other theories, extra conditions, such as fixing the external operator dimension, have to be imposed. It is clear that, at fixed truncation, not all CFTs are equally accessible, even assuming the same sparsity of spectrum. We expect that richer set of solutions can be found by generalizing our method to multiple correlators and by imposing further constraints that would halt the MC evolution towards specific attractors (e.g. the extremality line or the GFT line in $d = 2$). Though we mostly focused on unitary theories, the method does not rely on it and can efficiently be used in the

non-unitary realm. This is particularly important considering that for non-unitary theories we still do not have rigorous numerical protocols. It would be interesting to see how our numerical method performs with respect to Gliozzi's method [20, 54] and its subsequent versions [106, 107]. The aim of this work is very similar to that of [57, 56], where approximate solutions to crossing have been achieved using a similar logic but a different technique (reinforcement learning instead of MC techniques). It would be interesting to systematically compare the two approaches.

The `FORTRAN`-code used in this work is limited to machine-like precision. While this allowed us to perform extensive MC searches at little cost, limited precision does not allow us to systematically increase the value of Δ^* and N_{Ops}. For example we do not have enough accuracy to understand the nature of the green end-minima we found in $2d$ (figure 5.9), whether they are unidentified local CFTs of some kind or some sort of numerical artifacts resembling GFT theories. For $d > 2$ the accuracy is even less and the nature of the found end-minima is yet to be understood. Despite the limited accuracy of the algorithm, we think the results of this paper have shown that the method works. Upgrading the current code to arbitrary precision will be the key for a fully working program and is the most important thing to do in the near future. We believe this is feasible, given the ample room for improvement of the code performance in terms of speed.

In summary, we hope that the non-rigorous approach initiated in this work, properly extended and improved, might be a useful tool to navigate in the space of allowed CFT and guide subsequent analysis performed using more rigorous numerical algorithms.

Chapter 6

Conclusions and outlook

Stochastic minimization algorithms are a natural choice whenever the parameter space of an optimization problem is high dimensional and several minima are present. In this dissertation we have shown the usefulness of Metropolis Monte Carlo as an optimizer for a function that characterizes approximate solutions to the crossing equations of identical scalars in conformal field theories. This problem requires in principle an optimization in an infinite parameter space, where each theory corresponds to a different local minimum of a function that vanishes for configurations that satisfy the crossing equations. Therefore, so the use of these methods is more than justified.

In practice, we find that this approach enables us to find local minima in which the leading operators of several known theories are reproduced with a good degree of accuracy (as high as one per mil error for certain scaling dimensions). Although most of these cases are along the extremal lines determined in previous bootstrap approaches, we find that our analysis does sample the interior of the allowed region. In particular, we identify in $d = 3, 4$ a locus of minima at fixed external dimension has no clear physical candidate that we know of. Our analysis gives as a side-product the evolution of certain minima for different truncations, allowing us to analyze the trends of certain physical quantities as a function of Δ^*.

Regarding the caveats, this method has several "hyperparameters" that need to be tuned in order to obtain results in an efficient manner. The most immediate one is the Metropolis temperature T which was fixed by inspection in this work. This is not optimal, but the range of T for which the MC behaved efficiently was large enough that we did not need at this stage to try more advanced approaches (e.g. *replica exchange*[95]). A more determinant one is the distribution sampled in the space of cross ratios. So far we have worked with points z_i sampled from a grid of fixed spacing and constrained to $\lambda(z) < \lambda_0$. Thus, λ_0 defines the size of the

region where the crossing equations are analyzed and consequently influences which operators contribute in greater measure to them.

Although in this work we attained consistent results with a fixed value of $\lambda_0 = 0.42$, it is clear that this cannot be the case for more general searches. We entertain three possible improvements that will be explored in further work. One approach would be to make λ_0 scale automatically with Δ^*. In principle several analytical results should be of help (e.g. the convergence estimate of [98]). However, we have not found an effective prescription yet. Another interesting improvement would be to integrate the crossing equations over a region of the $z-$plane with an appropriate measure. This should reduce the numerical noise due to the choice of the grid, but it is not clear how to choose the measure in order not to include big devations from crossing that occur near $z = 0, 1$. Finally, using derivatives would be most in line with other technical developments in the bootstrap, but as we noted in section 5.1.3 computing the residuals numerically for derivatives of the crossing equations requires a more delicate weighting of the errors.

Another interesting direction that could be pursued with our approach is that of considering simultaneously several correlators. To do this we foresee two considerable hurdles. The more complicated dependence on the OPE coefficients would make their straightforward minimization impossible. We can always leave the OPE coefficients as parameters to be optimized, but the wide range of orders of magnitude that they span would make the approach numerically challenging. Most importantly, the tabulation that we performed in order to approximate the conformal block would not work any more due to their dependence on the external scaling dimensions. This can circumvented by working at fixed external dimensions, but then, scanning in a traditional way these scaling dimensions we would be giving up some of the power of Monte Carlo Methods.

Concerning physics there remain two main open questions after the conclusion of this work:

1. What is the physical meaning of the minima found with our method away from the allowed region?

2. Are there other minima that we have so far overlooked?

The answer to the first question lies in exploring higher values of Δ^* in order to determine whether these minima are artefacts or instead belong to physical theories. One could, for example, consider a minimum found with our method at a low value of Δ^* and then add higher Δ operators one by one, optimizing the spectrum at each step with some deterministic method in a language with arbitrary precision (e.g. `Mathematica`). To answer the second one we also need higher N_{Ops} so that the

inner region of the landscape thus explored is sampled in a more systematic way. This introduces operators with very small OPE coefficients that require more than double precision in order to be properly resolved. Thus, we see that both questions require increasing the working precision of our algorithm.

The implementation of this method in arbitrary precision is far from trivial. As we showed in 5.1.4, a straightforward implementation is prohibitively slow. Our current implementation in `FORTRAN` would need to be fundamentally overhauled or maybe migrated to another programming languages where Multiple Precision Arithmetic Libraries are available (e.g. `C` or `Julia`). Fortunately, recent developments in the technology for computing the conformal blocks (see, e.g. [108]) seem to indicate that this approach might become tractable. In any case, such a project would go beyond the power of a desktop computer and go into the realm of High Performance Computing.

Summarizing, this work shows that using Metropolis Monte Carlo with a double precision approximation to the crossing equations is a promising method to identify salient features of the landscape. However, determining the physical significance of some results might require an upgrade to higher precision machinery.

Bibliography

[1] Alessandro Laio, Uriel Luviano Valenzuela, and Marco Serone. Monte carlo approach to the conformal bootstrap. *Phys. Rev. D*, 106:025019, Jul 2022.

[2] G. Mack and Abdus Salam. Finite component field representations of the conformal group. *Annals Phys.*, 53:174–202, 1969.

[3] S. Ferrara, A. F. Grillo, and R. Gatto. Manifestly conformal covariant operator-product expansion. *Lett. Nuovo Cim.*, 2S2:1363–1369, 1971.

[4] S. Ferrara and G. Parisi. Conformal covariant correlation functions. *Nucl. Phys. B*, 42:281–290, 1972.

[5] Joseph Polchinski. *String Theory.* Cambridge University Press, 1 edition, October 1998.

[6] Juan Martin Maldacena. The Large N limit of superconformal field theories and supergravity. *Adv. Theor. Math. Phys.*, 2:231–252, 1998.

[7] Kenneth G. Wilson. Renormalization group and critical phenomena. 1. Renormalization group and the Kadanoff scaling picture. *Phys. Rev. B*, 4:3174–3183, 1971.

[8] Alexander M. Polyakov. Conformal symmetry of critical fluctuations. *JETP Lett.*, 12:381–383, 1970.

[9] A. B. Zamolodchikov. Renormalization Group and Perturbation Theory Near Fixed Points in Two-Dimensional Field Theory. *Sov. J. Nucl. Phys.*, 46:1090, 1987.

[10] Kenneth G. Wilson. The renormalization group and critical phenomena. *Rev. Mod. Phys.*, 55:583–600, Jul 1983.

[11] Riccardo Rattazzi, Vyacheslav S. Rychkov, Erik Tonni, and Alessandro Vichi. Bounding scalar operator dimensions in 4D CFT. *JHEP*, 12:031, 2008.

[12] Filip Kos, David Poland, David Simmons-Duffin, and Alessandro Vichi. Precision Islands in the Ising and $O(N)$ Models. *JHEP*, 08:036, 2016.

[13] Filip Kos, David Poland, David Simmons-Duffin, and Alessandro Vichi. Bootstrapping the O(N) Archipelago. *JHEP*, 11:106, 2015.

[14] Nikolay Bobev, Sheer El-Showk, Dalimil Mazac, and Miguel F. Paulos. Bootstrapping the Three-Dimensional Supersymmetric Ising Model. *Phys. Rev. Lett.*, 115(5):051601, 2015.

[15] Denis Karateev, Petr Kravchuk, Marco Serone, and Alessandro Vichi. Fermion Conformal Bootstrap in 4d. *JHEP*, 06:088, 2019.

[16] David Simmons-Duffin. A Semidefinite Program Solver for the Conformal Bootstrap. *JHEP*, 06:174, 2015.

[17] Walter Landry and David Simmons-Duffin. Scaling the semidefinite program solver SDPB. 9 2019.

[18] Sheer El-Showk and Miguel F. Paulos. Bootstrapping Conformal Field Theories with the Extremal Functional Method. *Phys. Rev. Lett.*, 111(24):241601, 2013.

[19] Marten Reehorst, Slava Rychkov, David Simmons-Duffin, Benoit Sirois, Ning Su, and Balt van Rees. Navigator Function for the Conformal Bootstrap. *SciPost Phys.*, 11:072, 2021.

[20] Ferdinando Gliozzi. More constraining conformal bootstrap. *Phys. Rev. Lett.*, 111:161602, 2013.

[21] Philippe Di Francesco, Mathieu, Pierre, and Sénéchal, David. *Conformal field theory*. Graduate texts in contemporary physics. Springer, New York, NY, 1997.

[22] Miguel S. Costa, Joao Penedones, David Poland, and Slava Rychkov. Spinning Conformal Correlators. *JHEP*, 11:071, 2011.

[23] F. A. Dolan and H. Osborn. Conformal four point functions and the operator product expansion. *Nucl. Phys. B*, 599:459–496, 2001.

[24] F. A. Dolan and H. Osborn. Conformal partial waves and the operator product expansion. *Nucl. Phys. B*, 678:491–507, 2004.

[25] Al. B. Zamolodchikov. Conformal symmetry in two-dimensional space: Recursion representation of conformal block. *Theoretical and Mathematical Physics*,

73(1):1088–1093, October 1987.

[26] A. B. Zamolodchikov. CONFORMAL SYMMETRY IN TWO-DIMENSIONS: AN EXPLICIT RECURRENCE FORMULA FOR THE CONFORMAL PARTIAL WAVE AMPLITUDE. *Commun. Math. Phys.*, 96:419–422, 1984.

[27] Filip Kos, David Poland, and David Simmons-Duffin. Bootstrapping Mixed Correlators in the 3D Ising Model. *JHEP*, 11:109, 2014.

[28] A. A. Belavin, A. M. Polyakov, and A. B. Zamolodchikov. Infinite conformal symmetry in two-dimensional quantum field theory. *Nuclear Physics B*, 241(2):333–380, 1984.

[29] G. Mussardo. *Statistical field theory: an introduction to exactly solved models in statistical physics*. Oxford graduate texts. Oxford University Press, Oxford ; New York, 2010. OCLC: ocn359673689.

[30] Pedro Liendo, Leonardo Rastelli, and Balt C. van Rees. The Bootstrap Program for Boundary CFT$_d$. *JHEP*, 07:113, 2013.

[31] Connor Behan. Unitary subsector of generalized minimal models. *Phys. Rev. D*, 97(9):094020, 2018.

[32] Lars Brink, John H. Schwarz, and J. Scherk. Supersymmetric Yang-Mills theories. *Nuclear Physics B*, 121(1):77–92, 1977.

[33] Eric D'Hoker and Daniel Z. Freedman. Supersymmetric gauge theories and the AdS / CFT correspondence. In *Theoretical Advanced Study Institute in Elementary Particle Physics (TASI 2001): Strings, Branes and EXTRA Dimensions*, pages 3–158, 1 2002.

[34] William E. Caswell. Asymptotic Behavior of Non-Abelian Gauge Theories to Two-Loop Order. *Physical Review Letters*, 33(4):244–246, July 1974.

[35] T. Banks and A. Zaks. On the phase structure of vector-like gauge theories with massless fermions. *Nuclear Physics B*, 196(2):189–204, March 1982.

[36] Lars Onsager. Crystal Statistics. I. A Two-Dimensional Model with an Order-Disorder Transition. *Physical Review*, 65(3-4):117–149, February 1944.

[37] Mikhail V. Kompaniets and Erik Panzer. Minimally subtracted six-loop renormalization of O (n) -symmetric ϕ 4 theory and critical exponents. *Physical Review D*, 96(3):036016, August 2017.

[38] Matthijs Hogervorst, Slava Rychkov, and Balt C. van Rees. Unitarity violation

at the Wilson-Fisher fixed point in $4 - \epsilon$ dimensions. *Physical Review D*, 93(12):125025, June 2016.

[39] Moshe Moshe and Jean Zinn-Justin. Quantum Field Theory in the Large N Limit: a review. *Physics Reports*, 385(3-6):69–228, October 2003. arXiv:hep-th/0306133.

[40] O. F. de Alcantara Bonfirm, J. E. Kirkham, and A. J. McKane. Critical exponents for the percolation problem and the Yang-Lee edge singularity. *Journal of Physics A: Mathematical and General*, 14(9):2391–2413, September 1981.

[41] Michael E. Fisher. Yang-Lee Edge Singularity and ${\ensuremath{\phi}}ˆ{3}$ Field Theory. *Physical Review Letters*, 40(25):1610–1613, June 1978. Publisher: American Physical Society.

[42] C. N. Yang and T. D. Lee. Statistical theory of equations of state and phase transitions. i. theory of condensation. *Phys. Rev.*, 87:404–409, Aug 1952.

[43] Giorgio Parisi and Nicolas Sourlas. Critical Behavior of Branched Polymers and the Lee-Yang Edge Singularity. *Phys. Rev. Lett.*, 46:871, 1981.

[44] Youngah Park and Michael E. Fisher. Identity of the universal repulsive-core singularity with Yang-Lee edge criticality. *Physical Review E*, 60(6):6323–6328, December 1999.

[45] Brian P. Flannery, Saul A. Teukolsky, William H. Press, and William T. Vetterling. *Numerical recipes: the art of scientific computing*. Cambridge University Press, 3rd ed edition, 2007.

[46] Riccardo Rattazzi, Slava Rychkov, and Alessandro Vichi. Bounds in 4D Conformal Field Theories with Global Symmetry. *Journal of Physics A: Mathematical and Theoretical*, 44(3):035402, January 2011. arXiv: 1009.5985.

[47] David Poland, David Simmons-Duffin, and Alessandro Vichi. Carving Out the Space of 4D CFTs. *JHEP*, 05:110, 2012.

[48] Sheer El-Showk, Miguel F. Paulos, David Poland, Slava Rychkov, David Simmons-Duffin, and Alessandro Vichi. Solving the 3D Ising Model with the Conformal Bootstrap. *Phys. Rev. D*, 86:025022, 2012.

[49] Filip Kos, David Poland, and David Simmons-Duffin. Bootstrapping the $O(N)$ vector models. *JHEP*, 06:091, 2014.

[50] David Poland, David Simmons-Duffin, and Alessandro Vichi. Carving Out the Space of 4D CFTs. *Journal of High Energy Physics*, 2012(5):110, May 2012.

arXiv: 1109.5176.

[51] Cumrun Vafa. Toward classification of conformal theories. *Physics Letters B*, 206(3):421–426, May 1988.

[52] S. Hikami. Conformal Bootstrap Analysis for Yang-Lee Edge Singularity. *Progress of Theoretical and Experimental Physics*, 2018(5), May 2018. arXiv: 1707.04813.

[53] F. Gliozzi, P. Liendo, M. Meineri, and A. Rago. Boundary and Interface CFTs from the Conformal Bootstrap. *Journal of High Energy Physics*, 2015(5):36, May 2015. arXiv: 1502.07217.

[54] Ferdinando Gliozzi and Antonio Rago. Critical exponents of the 3d Ising and related models from Conformal Bootstrap. *JHEP*, 10:042, 2014.

[55] Andre LeClair and Joshua Squires. Conformal bootstrap for percolation and polymers. *Journal of Statistical Mechanics: Theory and Experiment*, 2018(12):123105, December 2018. arXiv: 1802.08911.

[56] Gergely Kántor, Vasilis Niarchos, and Constantinos Papageorgakis. Conformal bootstrap with reinforcement learning. *Phys. Rev. D*, 105(2):025018, 2022.

[57] Gergely Kántor, Vasilis Niarchos, and Constantinos Papageorgakis. Solving Conformal Field Theories with Artificial Intelligence. *Phys. Rev. Lett.*, 128(4):041601, 2022.

[58] Sheer El-Showk, Miguel F. Paulos, David Poland, Slava Rychkov, David Simmons-Duffin, and Alessandro Vichi. Solving the 3d Ising Model with the Conformal Bootstrap II. c-Minimization and Precise Critical Exponents. *J. Stat. Phys.*, 157:869, 2014.

[59] David Simmons-Duffin. The Lightcone Bootstrap and the Spectrum of the 3d Ising CFT. *Journal of High Energy Physics*, 2017(3):86, March 2017. arXiv: 1612.08471.

[60] Marten Reehorst. Rigorous bounds on irrelevant operators in the 3d Ising model CFT. *arXiv:2111.12093 [cond-mat, physics:hep-th]*, November 2021. arXiv: 2111.12093.

[61] Shai M. Chester, Walter Landry, Junyu Liu, David Poland, David Simmons-Duffin, Ning Su, and Alessandro Vichi. Carving out OPE space and precise $O(2)$ model critical exponents. *arXiv:1912.03324 [cond-mat, physics:hep-lat, physics:hep-th]*, December 2019. arXiv: 1912.03324.

[62] Shai M. Chester, Walter Landry, Junyu Liu, David Poland, David Simmons-Duffin, Ning Su, and Alessandro Vichi. Bootstrapping Heisenberg magnets and their cubic instability. *Physical Review D*, 104(10):105013, November 2021.

[63] Marten Reehorst, Maria Refinetti, and Alessandro Vichi. Bootstrapping traceless symmetric $O(N)$ scalars. *arXiv:2012.08533 [cond-mat, physics:hep-lat, physics:hep-th]*, December 2020. arXiv: 2012.08533.

[64] Benoit Sirois. Navigating through the O(N) archipelago. *arXiv:2203.11597 [cond-mat, physics:hep-th]*, March 2022. arXiv: 2203.11597.

[65] Johan Henriksson, Stefanos R. Kousvos, and Andreas Stergiou. Analytic and Numerical Bootstrap of CFTs with $O(m)\times O(n)$ Global Symmetry in 3D. *arXiv:2004.14388 [cond-mat, physics:hep-th]*, April 2020. arXiv: 2004.14388.

[66] Luca Iliesiu, Filip Kos, David Poland, Silviu S. Pufu, David Simmons-Duffin, and Ran Yacoby. Bootstrapping 3D Fermions. *JHEP*, 03:120, 2016.

[67] Shai M. Chester and Silviu S. Pufu. Towards Bootstrapping QED$_3$. *Journal of High Energy Physics*, 2016(8):19, August 2016. arXiv: 1601.03476.

[68] Anatoly Dymarsky, Joao Penedones, Emilio Trevisani, and Alessandro Vichi. Charting the space of 3D CFTs with a continuous global symmetry. *JHEP*, 05:098, 2019.

[69] Anatoly Dymarsky, Filip Kos, Petr Kravchuk, David Poland, and David Simmons-Duffin. The 3d Stress-Tensor Bootstrap. *JHEP*, 02:164, 2018.

[70] Riccardo Rattazzi, Slava Rychkov, and Alessandro Vichi. Bounds in 4D Conformal Field Theories with Global Symmetry. *J. Phys. A*, 44:035402, 2011.

[71] Francesco Caracciolo, Alejandro Castedo Echeverri, Benedict von Harling, and Marco Serone. Bounds on OPE Coefficients in 4D Conformal Field Theories. *Journal of High Energy Physics*, 2014(10):20, October 2014. arXiv: 1406.7845.

[72] Yu Nakayama. Bootstrap bound for conformal multi-flavor QCD on lattice. *Journal of High Energy Physics*, 2016(7):38, July 2016. arXiv:1605.04052 [hep-lat, physics:hep-th].

[73] Yu Nakayama. Exclusion Inside or at the Border of Conformal Bootstrap Continent. *arXiv:1912.11748 [hep-th]*, December 2019. arXiv: 1912.11748.

[74] Andrea Cappelli, Lorenzo Maffi, and Satoshi Okuda. Critical Ising Model in Varying Dimension by Conformal Bootstrap. *Journal of High Energy Physics*,

2019(1):161, January 2019. arXiv:1811.07751 [cond-mat, physics:hep-th].

[75] Shai M. Chester, Silviu S. Pufu, and Ran Yacoby. Bootstrapping O (N) vector models in 4 < d < 6. *Physical Review D*, 91(8):086014, April 2015.

[76] Jin-Beom Bae and Soo-Jong Rey. Conformal Bootstrap Approach to O(N) Fixed Points in Five Dimensions, December 2014. arXiv:1412.6549 [hep-th].

[77] Yu Nakayama and Tomoki Ohtsuki. Five dimensional $O(N)$-symmetric CFTs from conformal bootstrap. *Physics Letters B*, 734:193–197, June 2014. arXiv:1404.5201 [hep-th].

[78] Yin-Chen He, Junchen Rong, and Ning Su. Non-Wilson-Fisher kinks of $O(N)$ numerical bootstrap: from the deconfined phase transition to a putative new family of CFTs. *arXiv:2005.04250 [cond-mat, physics:hep-th]*, May 2020. arXiv: 2005.04250.

[79] Junchen Rong and Jierong Zhu. On ϕ^3 Theory Above Six Dimensions. *arXiv:2001.10864 [hep-th]*, January 2020. arXiv: 2001.10864.

[80] Ying-Hsuan Lin, Shu-Heng Shao, Yifan Wang, and Xi Yin. (2,2) Superconformal Bootstrap in Two Dimensions. *Journal of High Energy Physics*, 2017(5):112, May 2017. arXiv: 1610.05371.

[81] Ying-Hsuan Lin, Shu-Heng Shao, David Simmons-Duffin, Yifan Wang, and Xi Yin. N=4 Superconformal Bootstrap of the K3 CFT, November 2015. Number: arXiv:1511.04065 arXiv:1511.04065 [hep-th].

[82] Aleix Gimenez-Grau and Pedro Liendo. Bootstrapping Coulomb and Higgs branch operators. *arXiv:2006.01847 [hep-th]*, June 2020. arXiv: 2006.01847.

[83] Yu Nakayama. Is there supersymmetric Lee-Yang fixed point in three dimensions? *arXiv:2104.13570 [hep-th]*, April 2021. arXiv: 2104.13570.

[84] Joao Penedones, Joao A. Silva, and Alexander Zhiboedov. Nonperturbative Mellin Amplitudes: Existence, Properties, Applications. *arXiv:1912.11100 [hep-th]*, December 2019. arXiv: 1912.11100.

[85] Andrea Guerrieri, Joao Penedones, and Pedro Vieira. S-matrix Bootstrap for Effective Field Theories: Massless Pions. *arXiv:2011.02802 [hep-th]*, November 2020. arXiv: 2011.02802.

[86] Denis Karateev, Simon Kuhn, and Joao Penedones. Bootstrapping Massive Quantum Field Theories. *arXiv:1912.08940 [hep-th]*, December 2019. arXiv: 1912.08940.

[87] Denis Karateev, Jan Marucha, João Penedones, and Biswajit Sahoo. Bootstrapping the a-anomaly in $4d$ QFTs. *arXiv:2204.01786 [hep-th]*, April 2022. arXiv: 2204.01786.

[88] Nima Afkhami-Jeddi, Thomas Hartman, and Amirhossein Tajdini. Fast Conformal Bootstrap and Constraints on 3d Gravity. *JHEP*, 05:087, 2019.

[89] Nima Afkhami-Jeddi, Henry Cohn, Thomas Hartman, David de Laat, and Amirhossein Tajdini. High-dimensional sphere packing and the modular bootstrap. *arXiv:2006.02560 [hep-th]*, June 2020. arXiv: 2006.02560.

[90] Nima Afkhami-Jeddi. Conformal Bootstrap Deformations. *arXiv:2111.01799 [hep-th]*, November 2021. arXiv: 2111.01799.

[91] Kenneth Levenberg. A method for the solution of certain non-linear problems in least squares. *Quarterly of Applied Mathematics*, 2(2):164–168, 1944.

[92] Donald W. Marquardt. An Algorithm for Least-Squares Estimation of Nonlinear Parameters. *Journal of the Society for Industrial and Applied Mathematics*, 11(2):431–441, June 1963.

[93] Mark K. Transtrum, Benjamin B. Machta, and James P. Sethna. The geometry of nonlinear least squares with applications to sloppy models and optimization. *Physical Review E*, 83(3):036701, March 2011. arXiv:1010.1449 [cond-mat, physics:physics].

[94] Christian P. Robert and George Casella. *Monte Carlo Statistical Methods*. Springer Texts in Statistics. Springer New York, New York, NY, 2004.

[95] Robert Swendsen and Jian-Sheng Wang. Replica monte carlo simulation of spin-glasses. *Physical review letters*, 57:2607–2609, 12 1986.

[96] Alex Rodriguez and Alessandro Laio. Clustering by fast search and find of density peaks. *Science*, 344(6191):1492–1496, June 2014.

[97] Sheer El-Showk and Miguel F. Paulos. Extremal bootstrapping: go with the flow. *JHEP*, 03:148, 2018.

[98] Duccio Pappadopulo, Slava Rychkov, Johnny Espin, and Riccardo Rattazzi. OPE Convergence in Conformal Field Theory. *Physical Review D*, 86(10):105043, November 2012. arXiv: 1208.6449.

[99] Alejandro Castedo Echeverri, Benedict von Harling, and Marco Serone. The Effective Bootstrap. *JHEP*, 09:097, 2016.

[100] Simon Caron-Huot. Analyticity in Spin in Conformal Theories. *JHEP*, 09:078, 2017.

[101] Paul H. Ginsparg. APPLIED CONFORMAL FIELD THEORY. In *Les Houches Summer School in Theoretical Physics: Fields, Strings, Critical Phenomena*, 9 1988.

[102] Vyacheslav S. Rychkov and Alessandro Vichi. Universal Constraints on Conformal Operator Dimensions. *Phys. Rev. D*, 80:045006, 2009.

[103] Al. B. Zamolodchikov. Two-dimensional conformal symmetry and critical four-spin correlation functions in the Ashkin-Teller model. *Soviet Journal of Experimental and Theoretical Physics*, 63:1061, May 1986. ADS Bibcode: 1986JETP...63.1061Z.

[104] Lance J. Dixon, Daniel Friedan, Emil J. Martinec, and Stephen H. Shenker. The Conformal Field Theory of Orbifolds. *Nucl. Phys. B*, 282:13–73, 1987.

[105] David Simmons-Duffin. The Lightcone Bootstrap and the Spectrum of the 3d Ising CFT. *JHEP*, 03:086, 2017.

[106] Ilya Esterlis, A. Liam Fitzpatrick, and David Ramirez. Closure of the Operator Product Expansion in the Non-Unitary Bootstrap. *JHEP*, 11:030, 2016.

[107] Wenliang Li. New method for the conformal bootstrap with OPE truncations. 11 2017.

[108] Rajeev S. Erramilli, Luca V. Iliesiu, Petr Kravchuk, Walter Landry, David Poland, and David Simmons-Duffin. blocks_3d: software for general 3d conformal blocks. *JHEP*, 11:006, 2021.